Understanding the morphological development of the Oesterdam nourishment

MSc thesis

Michiel Pezij
21-Aug-15

UNIVERSITY OF TWENTE.

Deltares
Enabling Delta Life

Understanding the morphological development of the Oesterdam nourishment

Submitted to acquire the degree of Master of Science
To be presented in public
On August 28 2015 at 15.00 hours
At University of Twente, Enschede, The Netherlands

Author information:
Michiel Pezij
University of Twente
Faculty of Engineering Technology
Student number: s1109278
E-mail: m.pezij@student.utwente.nl

Supervisors:

Prof. Dr. S.J.M.H. Hulscher	[University of Twente]
Dr. Ir. P.C. Roos	[University of Twente]
Dr. Ir. J.J. van der Werf	[Deltares]
Ir. P.L.M. de Vet	[Deltares]

Project:
1210607-Oesterdam

Abstract

The construction of the storm surge barrier in 1986 has led to a strong decrease of flow velocities and consequently in sediment transport in the Dutch Eastern Scheldt basin, while the magnitude of locally-generated erosive wind waves has not changed. Therefore, the intertidal areas in the basin receive less sediment and experience net erosion. Intertidal areas damp waves and erosion of those areas leads to a reduction of coastal safety, as the wave attack on the dams in the basin increases. The height of the tidal flat near the Oesterdam has decreased by 25 to 50 cm since 1986. A nourishment, placed in front of the dam in November 2013, should mitigate the erosion of the flat and extend the life span of the dam and surrounding levees with 25 to 30 years.

The effect of the nourishment on currents and waves is poorly understood and it is not clear which processes drive sediment transport. Data retrieved during a monitoring campaign are used in the present work to set-up a numerical model (Delft3D) in depth-averaged mode that is able to simulate the evolution of the nourishment. Wave behaviour is simulated using the SWAN-model. The goal of this study is to identify the mechanisms that control the morphodynamic impact of the nourishment on the intertidal area. This thesis reveals the accuracy of the model, the effect of the nourishment on hydro- and morphodynamic processes and the drivers of morphological changes near the nourishment.

Two models that simulate flow, wave behaviour, sediment transport and morphological changes are set-up. The simulation of flow and waves is coupled, as they interact with each other. A large-scale model of the Eastern Scheldt model (Scaloost) generates the hydraulic boundary conditions for a model covering the back of the basin (Oesterdam). It was concluded, after calibration and validation, that the model is accurately enough to study the evolution of the nourishment. It should however be noted that although the simulation of wave heights in deeper parts like near the Marollegat measuring station is correct, an overestimation of 20 to 40 cm near the intertidal area is observed. A manual calculation using the Brettschneider method showed that the model results are more plausible than the observed values. The quality of the measurements is thus questionable. Also, the model cannot be used for assessing the durability of the nourishment, because bed level changes are significantly overestimated.

Analysis of model results indeed showed that tidal currents are the main drivers of sediment transport towards the tidal flat and waves form the erosive forces of intertidal areas. A long-term simulation showed that the tidal flat would continue to erode if the nourishment was not performed. Hydrodynamics are significantly affected by the nourishment: a zone of flow convergence is observed directly east of the nourishment, increased energy dissipation by the breaking of waves on the nourishment leads to more wave damping as well as sediment transport rates increased on top of the nourishment and decreased in the sheltered area behind the hook. The elevated nourishment is from a morphological point of view the most active zone, while the sheltered area hardly shows any morphological changes. In general, sediment is eroded from the top of the nourishment and deposited near its edges. Suspended sediment transport is dominant on the tidal flat, but became subordinate to bed load transport on the elevated parts of the coarser grained nourishment.

The morphodynamics are mainly controlled by waves and indirectly by wind as correlations between wind and wave conditions were found. Breaking of waves on top of the nourishment causes sediment stirring, which leads to sediment transport. Wind-driven and wave-induced currents transport the sand towards the edges of the nourishment, where sediment accretes. The impact of tidal currents is limited, although they are responsible for the development of a channel east of the nourishment hook. Eventually, the Delft3D-model proved its value as it allowed for area-wide analyses of the different phenomena. Finally, it was recommended to focus on the quality of wave measurements in future monitoring campaigns and investigate the accuracy of wave simulations using SWAN.

Preface and acknowledgments

This thesis is the last part of completing my Master's programme Civil Engineering & Management at the University of Twente. I had a great time in Enschede, learned a lot and experienced some great things, such as an internship at the National Institute of Water and Atmospheric Research in New Zealand. Therefore, I am very happy that I can continue my stay at the University of Twente as a PhD-candidate.

The problems concerning the erosion of tidal flats in the Eastern Scheldt is a hot topic at the moment. Several nourishment projects are seen as the solution to mitigate solution, although their impact is poorly understood. The findings in this work can hopefully be used in the analysis of future projects. For example, also the Roggenplaat will be nourished. Especially the findings concerning local wave height measurements can contribute to this new project.

I want to express some final words. I would like to thank Jebbe van der Werf for being my supervisor at Deltares, I enjoyed working with you! Furthermore, I would like to thank Lodewijk de Vet for being my second supervisor, but more importantly helping me with modelling issues and analysis of results. Also, I want to thank Suzanne Hulscher en Pieter Roos from the University of Twente for supporting me during this graduation project.

Lastly, many thanks to all the people at Deltares who helped me; especially I want to thank my fellow students at Deltares for all the lunches, coffee breaks and good conversations. I hope that at least most of them now know that the world does not end after Amersfoort and that Enschede is a great city to live and study!

Michiel Pezij
Almelo, August 2015

Table of Contents

1 Introduction

This chapter provides an introduction into the topic, followed by the problem definition, objective and research questions. Furthermore, an overview of the research method is given. The chapter ends with an outline of this thesis.

1.1 Research background

The Eastern Scheldt (Dutch: Oosterschelde) is a large basin in the province of Zeeland in the Netherlands. Its location in the Netherlands can be seen in Figure 1. Historically being an estuary, the Eastern Scheldt is now considered as a tidal inlet/basin. There are a lot of intertidal areas such as shoals and tidal flats present, acting as a unique habitat for species like for example birds.

FIGURE 1: LOCATION OF EASTERN SCHELDT IN THE NETHERLANDS (PINK SHAPE).

According to Van Zanten & Adriaanse (2008), the intertidal areas are built up by tidal currents and eroded by wind waves. The construction of the Eastern Scheldt storm surge barrier in 1986 decreased the tidal dynamics in the basin significantly. The magnitude of the wind waves did not change however, leading to large scale erosion of the intertidal areas (Figure 2). This process is referred to as the 'Sand Hunger' of the Eastern Scheldt, as the eroded sand is transported to the deep channels in the basin. These channels are out of morphological equilibrium because of the decreased tidal dynamics and therefore 'consume' large amounts of sediment. Van Zanten & Schaap (2012) state that of the 11.000 hectare of intertidal area present in 1986, approximately 1.500 hectare will remain in 2100 if no measures are performed to mitigate the undesired erosion. For example, the height of the tidal flat near the Oesterdam has decreased by 25 to 50 cm since 1986.

1.2 Problem definition

Since the shoals are important for coastal safety, local ecology, shipping, recreation and (shell-) fishery, the erosion of the tidal flats is undesirable. The intertidal areas act as wave damping buffers for dams and levees, thereby decreasing the load on those coastal protection systems. Tidal flats thus extend the lifespan of hydraulic structures such as dams and levees (Van Zanten & Schaap, 2012).

The project 'Verkenning Zandhonger' was set-up by the Dutch Ministry of Infrastructure and the Environment and the Ministry of Economic Affairs to investigate the effects of the Sand Hunger with respect to the long term and to come up with potential interventions. One of the eroding tidal flats, the

Galgeplaat, was nourished in 2008. Das (2010), Van der Werf et al. (2013) and Van der Werf et al. (2015) studied the effects of this nourishment. These studies confirmed that waves are the driving force behind the erosion of the Galgeplaat. Another conclusion was that the tide in the Eastern Scheldt is indeed not strong enough anymore to build up the Galgeplaat. Most importantly, nourishments were identified as possible measures to mitigate the erosion of the shoals.

FIGURE 2: EMPLOYEES OF RIJKSWATERSTAAT INDICATING THE ORIGINAL HEIGHT OF THE ROGGENPLAAT IN THE EASTERN SCHELDT (RIJKSWATERSTAAT, 2013).

A new nourishment project started close to the eroding tidal flat near the Oesterdam in 2013 (Boersema, et al., 2014), see Figure 3. 350,000 m^3 of sand were nourished in front of this dam over a length of approximately 2 km and a width of 200 to 800 m. The nourishment height varied between 0.5 and 1 m. Goal of the project is to mitigate the erosion of the tidal flat and extend the life span of the dam and levees with 25 to 30 years. This project is initiated and executed by Rijkswaterstaat Zeeland.

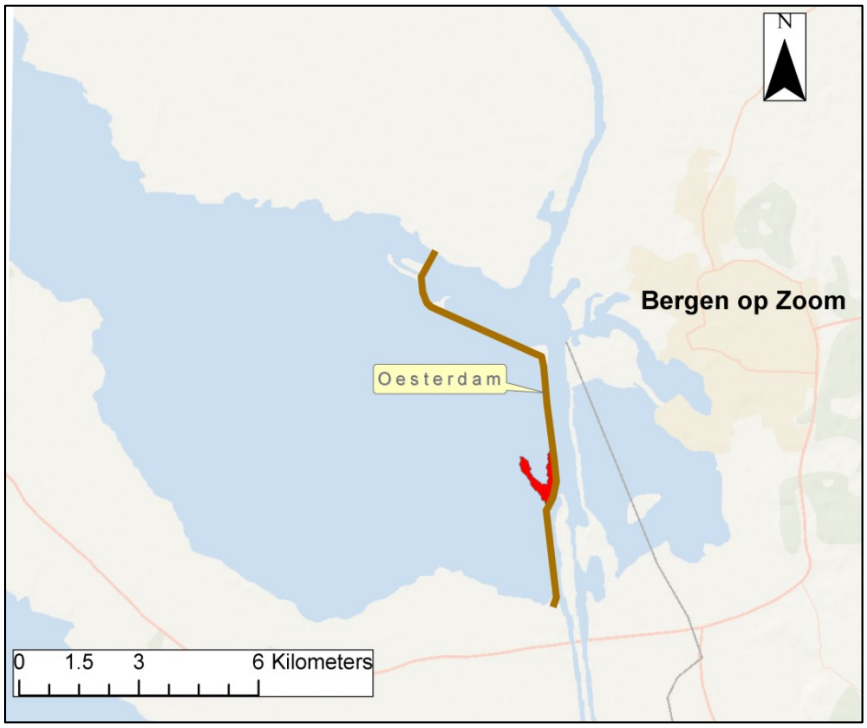

FIGURE 3: OVERVIEW OF THE AREA. NOURISHMENT IS VISUALIZED BY RED HOOK SHAPE.

However, it is not known how the nourishment will develop. After a year, a shift of sediment transport towards the north is observed during a first evaluation (Boersema, et al., 2015). Nevertheless many

questions remain. For example, it is still unknown whether a decrease in wave energy can be observed. Also, the long term development of the nourishment is an important aspect which should be investigated. A monitoring program was set up to be able to address these questions. A model could improve the knowledge gained by analysing the monitoring data, as much longer time periods can be covered if the model simulations are of sufficient quality. The use of a depth-averaged Delft3D-model could have great potential, because it allows for analysing hydro- and morphodynamics in a systematic and controlled way. Also, the hydraulic conditions vary significantly in the Eastern Scheldt basin. A model can give insight in these conditions near the Oesterdam area.

Besides that, general knowledge about modelling nourishments near intertidal areas will be extended. Das (2010) modelled the hydrodynamics near the Galgeplaat using Delft3D. Cronin (2012) and Zhang (2012) extended this research by including morphodynamics. The present project continues their work on modelling such areas. Both hydrodynamics and morphodynamics will be included. The focus of this work will be identifying the important processes that affect such nourishments. This is done in cooperation with Deltares, an institute for applied research in the field of water, subsurface and infrastructure.

1.3 Objective and research questions

The subject and problem definition have been introduced in the previous section. Next, the objective and research questions are introduced.

The main objective of this study is:

> *To identify the mechanisms that control the morphodynamic impact of the 2013 nourishment in an intertidal area near the Oesterdam in the Eastern Scheldt.*

In order to achieve this goal, the hydro- and morphodynamic processes in the Eastern Scheldt should be investigated in both time and space. This includes the influences of waves, winds and tidal currents on the Oesterdam nourishment. Linked to this is the impact of the nourishment on these processes.

This objective leads to the following research questions:

> *Q1: How well can Delft3D simulate the hydrodynamic processes and morphological developments near the nourishment?*

A numerical model simulating the hydro- and morphodynamics near the nourishment is only useful if the simulation is accurate. Therefore, criteria have to be defined concerning model accuracy which should be used to assess the model.

> *Q2: What are the flow, wave, sediment transport and morphodynamic patterns in the area before and after construction of the nourishment?*

Firstly, the hydro- and morphodynamic behaviour of the area before and after construction of the nourishment should be understood. Flow patterns, wave behaviour and sediment transport patterns will be described. These physical quantities experience relatively quickly the effects of an anthropogenic modification of a coastal system. Therefore it is important to study the initial changes in hydrodynamics and sediment transport after construction of the nourishment. The new conditions should be compared to the old conditions to see whether significant changes have occurred.

> *Q3: What processes drive the morphodynamics of the nourished Oesterdam tidal flat?*

The morphodynamics are driven by currents and waves, leading to sediment transport. Changes in morphology also lead to changes in hydrodynamics like waves and currents. A feedback mechanism is

thus present. The important processes that cause morphological changes should be identified. Knowledge about these processes contributes to the knowledge of the system, as the Oesterdam tidal flat is not the only intertidal area in the Eastern Scheldt that shows large erosion problems.

1.4 Methodology

Field data obtained from the monitoring campaign are used in present work to set-up and validate a numerical model. Different types of field data are used for analysis. Among others bathymetric, water level, wave, wind, flow velocity, and grain size data are used.

The simulations are performed using the numerical process-based model Delft3D in order to gain insight in the hydro- and morphodynamic processes present in the Eastern Scheldt and how these processes changed in response to the nourishment. Das (2010), De Bruijn (2012) and Eelkema (2013) used Delft3D in depth-averaged mode for modelling of hydro- and morphodynamics inside the Eastern Scheldt and found satisfying results. It is assumed that the physical processes as present in the Eastern Scheldt can indeed be modelled using Delft3D in depth-averaged mode (Deltares, 2014). The equations used in Delft3D are described and discussed more detailed in chapter 3 and in Lesser et al. (2004).

Within Delft3D, two models are created to achieve the required level of simulation accuracy: one overall coarser gridded model (Scaloost) covering the entire Eastern Scheldt and a finer gridded model (Oesterdam) covering a smaller area that is nested in the coarser model. The Scaloost-model generates the hydraulic boundary conditions for the Oesterdam-model. The models will be calibrated in order to be able to simulate physical process accurately. Subsequently, the models are validated using a hydrodynamic and morphodynamic approach. This will answer the first research question.

Short-term and long-term hydro- and morphodynamics are investigated using various time periods to answer the second research question. Initial effects are explored by running the model for one tidal cycle. Boersema et al. (2015) identify a period of 3 months after construction of the nourishment with significant morphological changes. After this period, the morphological developments become much less distinct. Short-term dynamics are therefore examined by running the model for a period of three months. Longer-term dynamics are identified by running the model for a longer period, for example 6 months.

The results are analysed as follows: flow patterns, wave behaviour and sediment transport patterns are compared with their behaviour in the situation before the construction of the nourishment. The change in bed level is visually compared by means of sedimentation/erosion patterns. Both observed data and model output will be used. Also bed shear stresses are investigated and the influence of both bed load and suspended load is discussed.

Finally, the importance of tidal, wave and wind forcing is investigated to answer the third research question. Simulations with/without waves and with/without wind input will lead to an increase of knowledge about the contribution of these processes to sediment transport and morphological changes in an intertidal area.

1.5 Outline

This thesis is organized as follows: first an in-depth description of the study area is presented in chapter 2, including the history of the basin. Then the set-up of the Delft3D-models is elaborated in chapter 3. Chapter 4 describes the validation of the model using observed and simulated data. The impact of the nourishment on hydrodynamics is investigated in Chapter 5 and the drivers of morphological changes are studied in Chapter 6. Furthermore, a discussion can be found in chapter 7. The conclusions with respect to the research questions and recommendations are presented in chapter 8.

2 Description of the study area

The Eastern Scheldt basin is geographically part of the delta region in the Netherlands. This chapter elaborates on the hydro- and morphodynamics of this system and describes the human interventions in the past and present. Furthermore the problem as described in section 1.2 as well as the motivation for the 2013 Oesterdam nourishment is discussed in more detail. Last, a provisional overview of direct impacts of this nourishment is given.

2.1 Estuaries/tidal basins

Often, the Eastern Scheldt is referred to as an estuary. However, this statement is not true, as will be discussed in this section. It is helpful to first focus on the general characteristics of such areas. In the broadest sense, an estuary is a zone where salt- and freshwater derived from catchments merge (Rogers & Woodroffe, 2012). Pritchard (1967) defined an estuary as:

> *An estuary is a semi-enclosed coastal body of water which has a free connection with the open sea and within which sea water is measurably diluted with freshwater derived from land drainage.*

Estuaries are usually found where rivers meet seas or oceans. They contain brackish water, a mixture between fresh- and saltwater. The hydro- and morphodynamics of estuaries are more complicated than for a normal river or coastal system because of the complex interaction between salt water from the sea and freshwater from the river, sediment exchange and biological activities. Often they are very dynamic areas due to the daily rise and fall of the tides and because of water density differences in the basin. These features make estuaries ideal habitats for species like birds and therefore these systems accommodate some of the most valuable ecosystems in the world (Eelkema, 2013).

Some of these properties can be observed when looking at the Eastern Scheldt. These properties are described in the remainder of this chapter.

2.1.1 Important dynamics near estuaries/tidal basins

The most important processes that occur in and near basins such as the Eastern Scheldt are described in this section. These include forcing, roughness characteristics and sediment transport processes. Three main forcing principles can be found within the system; tides, wind and waves. These principles do not only act individually, they also interact with each other.

Tides

The tide is an important driver and leads to large scale water level differences (Das, 2010). The tidal wave originates from the Atlantic Ocean and propagates across the coasts of the North Sea. The Eastern Scheldt basin will be filled with water from sea during flood and water levels decrease during ebb within a tidal cycle.

The differences in water levels lead to currents and subsequently to sediment transport. Also, the tidal flats are flooding and drying. The tidal asymmetry (faster rise/fall of the tide) controls whether there is net deposition or erosion of the tidal flats. The shape of the tidal wave in the Eastern Scheldt is determined by several factors, including basin geometry, ocean tide characteristics, bed roughness characteristics and freshwater flow (De Bok, 2001).

Wind

Wind can result in water level set-up and locally generated waves. The set-up causes a water level gradient which leads to wind-induced currents. Wind-driven currents tend to become more important for a decreasing water depth, because the velocity profile can adapt more easily. Because water depth is significantly decreasing near intertidal areas, wind-driven currents have a strong influence on the resultant currents near those areas. This also affects sediment transport. Jacobse (2005) found that wind-

driven currents have a large impact on the Galgeplaat with respect to sediment transport. Therefore, it can be expected that wind is important when considering the Oesterdam nourishment.

Waves

Waves originating from the North Sea hardly enter the basin (Louters et al., 1998; Das, 2010). Only near the storm surge barrier, offshore waves may be important. For areas deep within the basin, only locally generated wind-waves are significant.

Wave (inter)action becomes more important in shallow regions. For example, shoaling will occur when waves propagate into shallower water, resulting in larger wave heights. The wave height will become larger until waves become too steep, after which wave breaking occurs. Wave breaking brings a lot of sediment into suspension as bed shear stresses increase. Thus bed load as well as suspended sediment transport will be important when looking at the intertidal areas. More sediment in suspension increases bed friction which in turn results in more flow resistance.

Roughness characteristics

Flow resistance is partly caused by bed roughness; an increasing roughness causes more resistance. Bed roughness in turn is a combined effect of roughness caused by individual sediment grains and bed forms. So, roughness and flow regime are coupled, they form a feedback mechanism. Mussels and oysters, common organisms in the Eastern Scheldt, can also affect bed roughness (Das, 2010). The bed roughness varies in space and time: grain sizes are not uniformly distributed and bed form characteristics depend on local flow conditions.

Sediment transport processes

Currents and waves lead to transport of sediment. When flow forces exceed a critical value, sediment will start to move. A distinction can be made between bed load and suspended load transport. Bed load is the transport of bed material, while suspended load is sediment that is suspended in the fluid for some time (Van Rijn, 2007). Aeolian sediment might be of importance, as the tidal flats can become dry. This last process will not be included in the present study due to model limitations.

Estuaries (and tidal basins) are important contributors to the sediment budget of coastal zones. These systems either act as a source or sink of sediment (Rogers & Woodroffe, 2012). Waves tend to move sediment towards the basin, while the tidal motion tends to move the sediment offshore of the basin. It is the competition between these processes that determines whether such a system acts as a source or sink of sediment. The inlets and estuaries in the Netherlands are mostly tide-dominated and relatively stable in their location. A disturbance in the form of human interventions can bring the system out of morphological equilibrium. The system then typically evolves towards an equilibrium state by redistributing sediment (Eelkema, 2013).

The net sediment transport in the channels of such a basin is the result of asymmetries in tidal currents and waves. The propagation speed of a tidal wave depends on the local water depth and thus the crest of such a wave can propagate at a different speed than the through. Therefore, the duration of the flood and ebb tides is different. However, an equal amount of water has to be transported, leading to differences in flood and ebb currents. At sea the crest of the tidal wave will propagate faster, leading to flood-asymmetry and flood-directed net sediment transports. However, in estuaries, the presence of intertidal areas can cause the flood tide to propagate slower than the ebb tide, caused by the smaller cross-sectional area. This leads to ebb-asymmetry and ebb-directed transport as was found by Friedrichs & Aubrey (1988).

2.2 Eastern Scheldt basin

The Eastern Scheldt basin has an open connection with the North Sea, is approximately 50 km long and has a surface area of 351 km^2 as can be found in Eelkema (2013). A lot of geomorphological features can be observed within the estuary: meandering tidal channels, tidal flats, mud shoals and salt marshes. Most of them form the lateral boundaries of the basin.

The Eastern Scheldt is a meso-tidal estuary, which means that the estuary is characterized by a tidal range of 2 to 4 m (Davies, 1964). The mean tidal range at the inlet is 2.9 m while the tidal range increases to 3.5 m during spring tide and decreases to 2.3 m during neap tide. Also the estuary mouth shows the formation of a composite delta on the seaward side, known as an ebb-tidal delta.

Human interventions and extreme events significantly changed the shape of the Eastern Scheldt in the past, also affecting neighbouring estuaries (Eelkema, 2013). Historically the Eastern Scheldt was an eroding basin. However, since 1986 the Eastern Scheldt is considered as a sedimentation basin with channels in demand of sediment and degrading tidal flats (Mulder & Louters, 1994). Among others, the construction of the storm surge barrier in 1986 is responsible for this change. The basin however experienced more human influences in the past and present. An overview of the human interventions in the Eastern Scheldt basin can be found in Figure 4. Most of these interventions are part of the Delta Works.

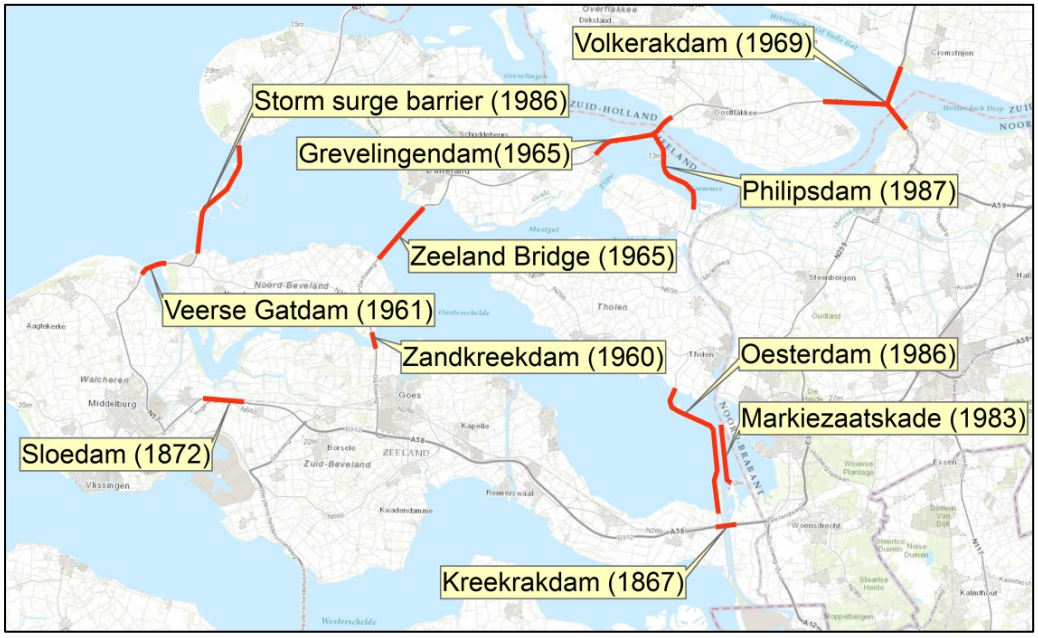

FIGURE 4: DAMS AND OTHER HYDRAULIC STRUCTURES IN THE EASTERN SCHELDT

Due to these interventions, the basin can no longer be considered as an estuary. Since the completion of the Kreekrakdam in 1867 and the closure of the Sloe in 1872 the Scheldt River does not discharge anymore in the Eastern Scheldt. The discharges from the Rhine and Meuse rivers are controlled since the completion of the Volkerak dam. Once in a while, freshwater from the Rhine and Maas passes through sluices in this dam. However, this discharge is only 20 m^3/s (De Bok, 2001), resulting in hardly any inflow into the basin. Therefore, the Eastern Scheldt should be referred to as a tidal basin nowadays.

2.2.1 Hydrodynamic development of the Eastern Scheldt basin

As discussed in the previous section, the construction of the storm surge barrier and other compartment dams affected the tidal dynamics in the basin. This change in hydrodynamics is described in this section.

History of the Eastern Scheldt basin

After the large 1953 flood in Zeeland, the Netherlands, a decision was made by the Dutch government to separate all inlets and estuaries in Zeeland from the sea. This plan is worldwide known as the Delta plan (Eelkema, 2013). Because of public concern, the Eastern Scheldt was not fully dammed. Ecologists predicted that the ecology in the basin would seriously degrade after separating this estuary from the sea by means of a dam. The importance of the Eastern Scheldt was considered large for local wildlife and fishery due to its saltwater environment.

FIGURE 5: THE EASTERN SCHELDT STORM SURGE BARRIER (FLETCHER, 2012)

Instead of fully damming the Eastern Scheldt, a storm surge barrier was built, see Figure 5. Construction finished in 1986. In this way, the safety of Zeeland against floods was guaranteed and the original environment could be maintained as the barrier would only close during severe storm conditions. An expected seaward water level of 3.0 m +NAP leads to closure of the barrier (Willems & Webbers, 2003). Although the environment is much less damaged, the impact of such a barrier is still significant (Van Zanten & Adriaanse, 2008).

The construction of the barrier is not the only modification of the basin. As stated earlier, the freshwater supply was already cut off in 1969 due to the completion of the Volkerak dam. Also, the Oesterdam (1986) and Philipsdam (1987) were constructed in the basin. The aim of the latter two dams was to preserve the tidal range inside the Eastern Scheldt (Mulder & Louters, 1994). The Delta project changed the hydrodynamic processes within the Eastern Scheldt as follows (Vroon, 1994):

1958-1964: Grevelingendam
The construction of the Grevelingendam was finished in 1964. The entire northern branch of the Eastern Scheldt was cut off from the Grevelingen estuary.

1964-1969: Volkerakdam
The Volkerakdam was completed in 1969. The freshwater inflow of the Eastern Scheldt was limited to a minimum at this time. Sluices were incorporated in this dam to regulate river flow.

1969-1985: Storm surge barrier part I
The first phase of the Eastern Scheldt project started. Work islands were constructed in the mouth (e.g. Neeltje Jans) and in the eastern part of the basin (e.g. near the Oesterdam).

1985-1986: Storm surge barrier part II and compartment dams
The storm surge barrier was finished in 1986. This barrier was constructed in the mouth of the Eastern Scheldt. Two compartmentalisation dams (Philips- and Oesterdam) were built in the eastern parts to restore part of the original hydrodynamics.

Change in tidal prism, tidal range and flow velocities
De Bok (2001) showed that originally the Eastern Scheldt was limited by land boundaries and by two tidal divides. These divides were situated near the transition of the Eastern Scheldt and the Haringvliet and the Eastern Scheldt and the Grevelingen.

The completion of the Grevelingen dam increased the tidal volume of the basin by 8%. Also, a small decrease in tidal range was observed. De Bok (2001) and Eelkema (2013) state that the effects of the Grevelingen dam were small because this dam was built on the tidal watershed between the Grevelingen and Volkerak. The construction of the Volkerakdam amplified the tidal wave in the northern branch of the Eastern Scheldt due to resonance, increasing the tidal range of the Eastern Scheldt and Volkerak (De Bok, 2001). The construction of the storm surge barrier significantly changed the hydrodynamic characteristics of the basin. For example, the tidal volume decreased with 29% and average current velocities were reduced by 33% (Eelkema, 2013). Also, the tidal range was considerably decreased. A timeline of these events is presented in Figure 6.

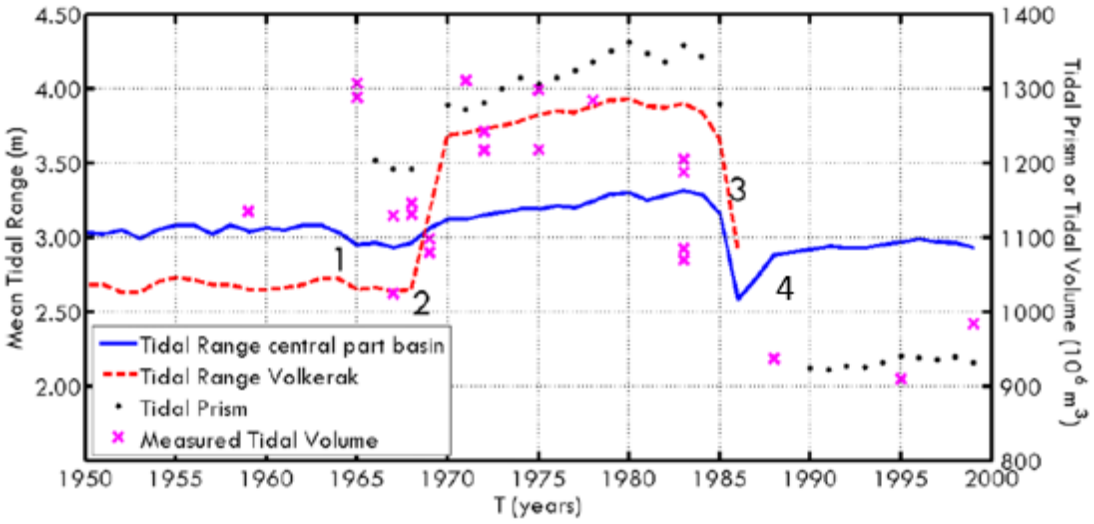

FIGURE 6: CHANGE IN MEAN TIDAL RANGE AND PRISM IN TIME. NUMBERS INDICATE COMPLETION OF (1) GREVELINGEN DAM (2) VOLKERAK DAM (3) STORM SURGE BARRIER AND (4) OESTER- AND PHILIPSDAM (DE BOK, 2001).

An important cause of the changes due to the barrier was the reduction of the effective cross-sectional area of the Eastern Scheldt inlet (Vroon, 1994). The original cross-sectional area of 80.000 m^2 was reduced to 17.900 m^2. According to Eelkema (2013), this constriction causes large amounts of local turbulence and a large loss in the energy head over the barrier. This might explain the large decrease in tidal prism after the construction of the barrier. Indeed a linear relationship between the cross-sectional area of the inlet and the tidal prism was found by Mulder & Louters (1994). The loss is visible as a decrease of the tidal range within the basin and is accompanied by a shift in the phase of the tidal wave (Vroon, 1994).

Research has already been done on the behaviour of the tidal inlet and ebb-tidal delta of the Eastern Scheldt. This can be found in Mulder & Louters (1994) and Eelkema (2013). The present study, however, will not focus on the dynamics concerning the inlet, but on the dynamics near the Oesterdam tidal flat.

Oester- and Philipsdam

Within a couple of years after completion of the storm surge barrier, an increase of tidal range can be observed in Figure 6. Figure 7 zooms in on this period. This figure shows the average tidal range in the basin during the period 1980-1998. The completion of the barrier reduced the range by about 20 to 30%. This reduction is partly mitigated by the construction of the Philips- and Oesterdam. They were built in the back of the basin.

These compartment dams served two purposes. First, the area of the tidal basin behind the barrier was reduced. The dams enlarged the reflection and amplification of the tidal wave, effectively increasing the tidal range at Yerseke to 3.00 m (Eelkema, 2013). At that time (1986), it was assumed that this tidal range was sufficiently large to maintain natural values in the basin as can be found in Mulder & Louters (1994). By reducing the basin length the loss in tidal range was reduced by 10% (Eelkema, 2013). However, they also caused a decrease of the basin area from 452 km^2 to 351 km^2. The second purpose of the dams was the emergence of a tide-free shipping route between Antwerpen and the Rhine.

Before the construction of the Oesterdam, the Markiezaatskade was constructed in 1983 near Bergen op Zoom. This dam is situated to the east of the Oesterdam. The Markiezaatskade simplified the closure of the Oesterdam. Furthermore, current velocities in the channel that served as the Scheldt-Rhine connections were kept within limits by this dam.

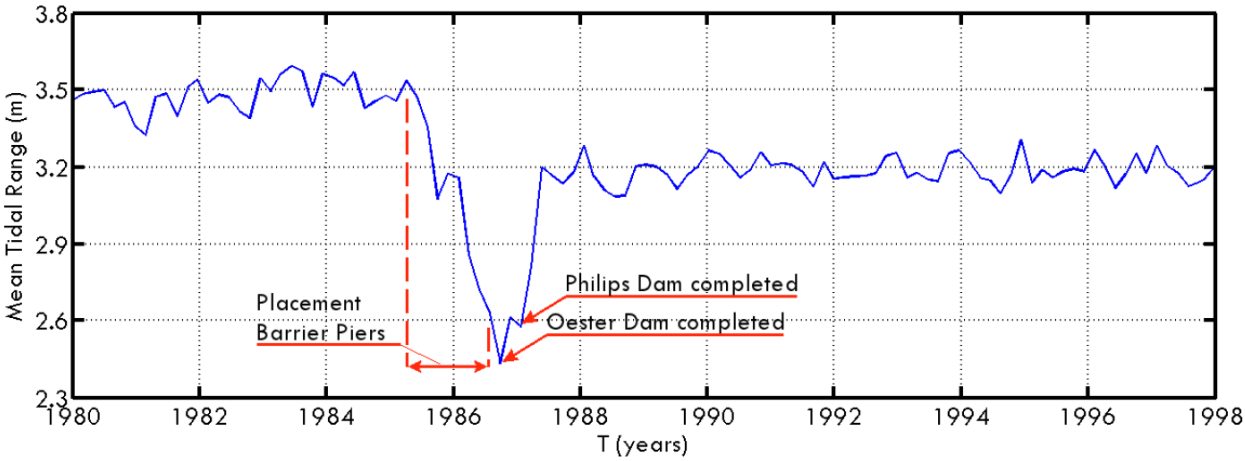

FIGURE 7: AVERAGE TIDAL RANGE AS OBSERVED IN THE CENTRAL PART OF THE EASTERN SCHELDT (DE BOK, 2001)

Change in current velocities

According to Louters et al. (1998), the significant decrease in tidal range is not the only undesirable effect of the storm surge barrier. Also tidal current velocities are affected. This can be seen in Figure 8. Measurements of flow velocities and sediment transport rates are shown for the Galgeplaat, an intertidal area situated in the Eastern Scheldt. Both flood and ebb tide velocities as well as sediment transport rates are visualized.

It can be observed that both flow velocities and sediment transport rates significantly decreased after construction of the barrier. Especially the velocities during flood tide show a reduction in magnitude. Because sediment transport depends faster than linear on flow velocities, sediment transport decreases significantly when flow velocities reduce. Das (2010) and Eelkema (2013) modelled parts of the Eastern Scheldt and reproduced the reduction of flow velocities and sediment transport.

Concluding, the combination of the storm surge barrier and the back-barrier dams resulted in a decrease of tidal prism in the basin. De Bok (2001) found that the tidal prism was reduced by approximately 25%

from 1200 Mm^3 per tide to 900 Mm^3 per tide. Vroon (1994) stated that the maximum flow velocities in the western part of the basin were reduced by roughly the same percentage.

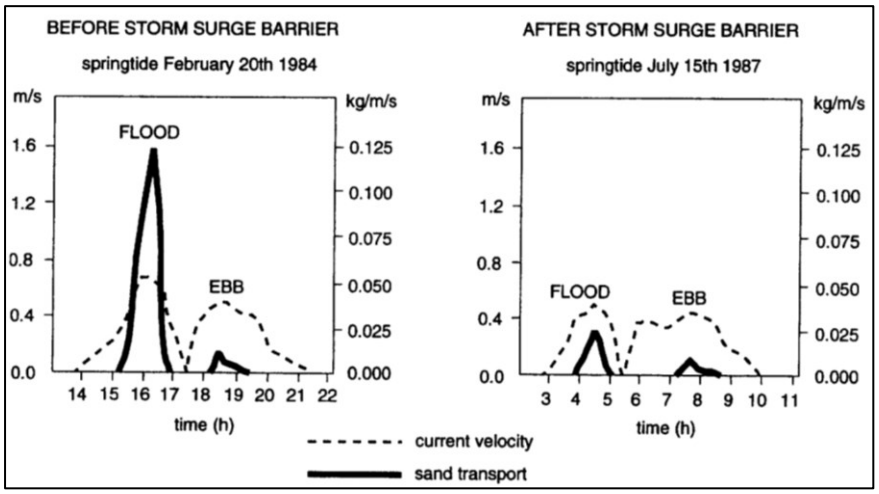

FIGURE 8: FLOW VELOCITIES AND SEDIMENT TRANSPORT MEASUREMENTS DURING AVERAGE WEATHER CONDITIONS ON THE GALGEPLAAT BEFORE AND AFTER CONSTRUCTION OF THE STORM SURGE BARRIER (LOUTERS ET AL., 1998).

2.2.2 Morphodynamic development of the Eastern Scheldt basin

Historically, sediment was supplied by the North Sea and the river discharges into the basin. The sediment budget of the basin was negative while the budget of the ebb-tidal delta was positive (Louters et al., 1998). The Eastern Scheldt is nowadays a basin that is out of morphological equilibrium since the construction of the Delta works.

In its evolution towards an equilibrium, the tidal channels need to become smaller and therefore additional sediment is required (Van Zanten & Adriaanse, 2008; Das, 2010). The sediment required for the adaptation of these channels is eroded from the intertidal areas inside the basin, as visualized in Figure 9. These intertidal areas are thus significantly decreasing in volume. This phenomenon, known as the Sand Hunger of the Eastern Scheldt, was already predicted by Kohsiek et al. (1987).

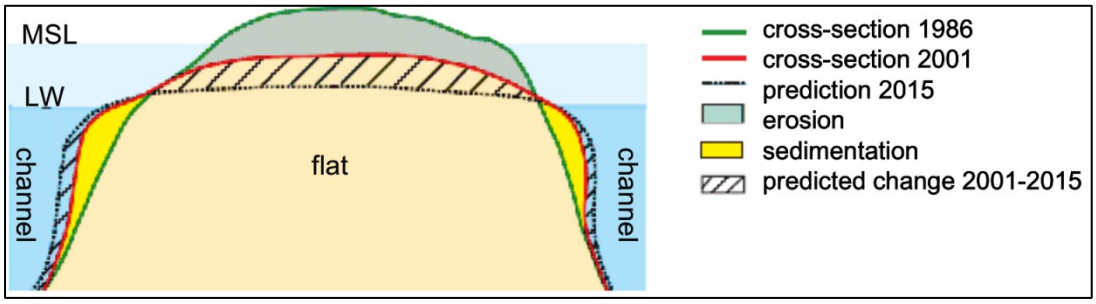

FIGURE 9: DEVELOPMENT OF A SHOAL IN THE EASTERN SCHELDT AFTER 1986 (BOSBOOM & STIVE, 2015).

As mentioned before, Das (2010) and Eelkema (2013) modelled the behaviour of hydro- and morphodynamics in the Eastern Scheldt. They both found that tidal currents form the main processes that cause sediment transport towards intertidal areas. Because the magnitude of the tidal currents decreased after 1986, also sediment transport towards the intertidal areas decreased, as was already observed in Figure 8.

The tidal flats also experience erosive processes. Locally generated wind waves are the main drivers of erosion of the intertidal areas (Van Zanten & Adriaanse, 2008; Das, 2010; Eelkema, 2013). These waves are generated within the basin by wind stresses and are not affected by the sluices of the storm surge barrier. Therefore, the magnitude of the erosion due to waves has not changed after the construction of

the barrier. Tidal flats experience more erosion by wind waves than deposition by the tidal currents. The result is a net erosion of the intertidal areas in the basin.

2.2.3 Comparison with other basins

It is useful to see if the same processes can be observed in other estuaries or tidal basins worldwide. However, the conditions as present in the Eastern Scheldt are unique. There is no basin in the world where the construction of a barrier has led to eroding intertidal areas. Probably, the Afsluitdijk also caused degradation of such areas in the former Zuider Sea. However, no details can be found in literature.

The closure of the Lauwers Sea in the northern part of the Netherlands also shows some similarities. Since the separation of the sea in 1969, the area is known as Lake Lauwers. The closure led to elimination of tidal prism in the basin and thus to the reduction of the tidal flat building force as stated by Wang et al. (2009). Also the eroding forces (wave action) did not decrease in this case. Intertidal areas in the region are therefore reducing in size, in particular the Engelsmanplaat. However, the Lauwers Sea was fully closed, so the tidal influence in the area has disappeared completely. This makes a direct comparison with the problems occurring in the Eastern Scheldt difficult. Besides that, no attempts have been made to mitigate this erosion yet.

2.3 Problems caused by Sand Hunger

As outlined in section 2.2, the shoal-building force has decreased dramatically while erosion of the intertidal areas by waves has not changed in magnitude. Therefore, net erosion of the intertidal areas in the Eastern Scheldt takes place. The development of those areas in the period 1990-2010 is visualized in Figure 49 in appendix II. Large amounts of erosion can be observed. The 'Kom'-region in the back of the basin is one of the areas that is eroding. The intertidal area near the Oesterdam is situated here.

Not only is the morphological development of the basin affected; an important side-effect is the decrease of coastal safety. Intertidal areas, such as the area in front of the Oesterdam, cause wave damping, thereby decreasing the wave attack on the revetment of the dam. The erosion of shoals and flats in front of the dam thus increases the wave attack on the dam; see Figure 50 in appendix II for more detail. The dam and levees have to be reinforced earlier due to this phenomenon. The costs of strengthening dams and levees as well as renewing their revetments are high, which makes it an undesirable operation.

Other aspects influenced are the reduction in habitat of benthic organisms and the decrease of available food for birds. Furthermore, the scenic values and socio-economic interests of the region are negatively influenced. These indirect effects are undesirable as well because the Eastern Scheldt is part of a Natura 2000-area according to Boersema et al. (2014). The Natura 2000-legislation imposes strict requirements on the local environment in the Eastern Scheldt.

2.3.1 Outline of measures: nourishments

To increase coastal safety and improve ecology, measures have to be implemented. The recovery of the original morphological equilibrium in the basin is probably the most sustainable solution. However, this measure is not realistic as one required action is the removal of the barrier and the compartment dams in the Eastern Scheldt as found by De Ronde et al. (2013). The most promising intervention is the use of nourishments, where large volumes of sediment are artificially deposited. This is a measure that tries to mitigate erosion rather than to restore the morphological equilibrium.

The shoal 'Galgeplaat' in the Eastern Scheldt was nourished in 2008. Das (2010) and Van der Werf et al. (2013) evaluated this project and found that nourishments can lead to mitigation of the large-scale erosion. The deposited sand did not erode immediately and ecological recovery was observed. A first estimation of the lifespan of the nourishment is 30 to 40 years, although this value is quite uncertain.

It was not confirmed that the nourishment led to more damping of wave energy due to dataset limitations. However it became clear that nourishments would be suitable measures against the erosion of intertidal areas. More nourishments were already planned at that time, thus the amount of data is going to increase and so is probably the understanding of these phenomena (Van Zanten & Adriaanse, 2008). One of those projects is the nourishment near the tidal flat in front of the Oesterdam, where the 'Safety Buffer Oesterdam'-project is performed in 2013.

2.4 Nourishment and monitoring at the Safety Buffer Oesterdam

Rijkswaterstaat Zee & Delta started the project in 2013 concerning the tidal flat near the Oesterdam to decrease wave load to such an extent that the dam will meet the assessment in 2060 (Van Zanten & Provoost, 2013). Concretely this means that the life time of the dam has to be extended by 25 to 30 years. Also, the nourishment should mitigate the erosion of the adjacent tidal flat area (Ikeya, 2014). The relevant objectives as defined by Boersema et al. (2014) are:

1. Development of a sustainable and safe solution for the Oesterdam, such that the Oesterdam is free of excessive wave attack and major investments in strengthening the stone revetment due to the Sand Hunger can be delayed by at least 25 years.
2. Development of a solution that tackles the problem of the Sand Hunger near the Oesterdam in such a way that the valuable landscape with intertidal areas and its ecological functions can be maintained in the next 50 years.
3. Contribute to knowledge about processes concerning the Sand Hunger and contribute to the development of flexible, climate-proof and cost-effective coastal management through a full-scale pilot project.

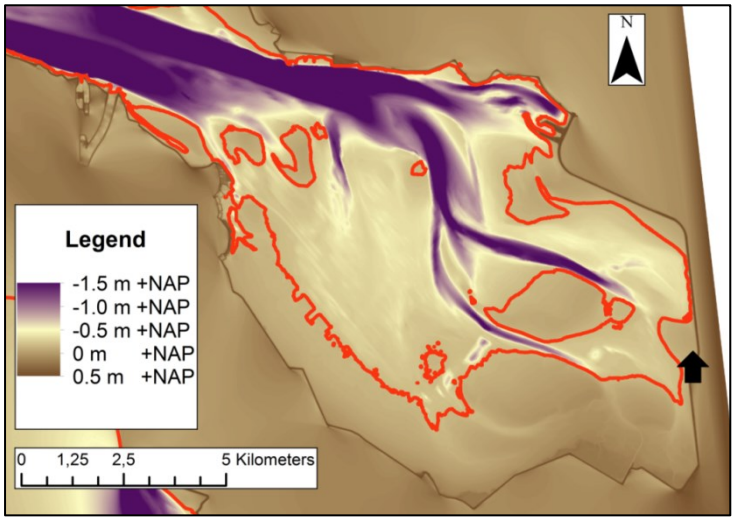

FIGURE 10: AVERAGE LOW WATER LINE (RED) IN OESTERDAM AREA. THE OESTERDAM TIDAL FLAT IS INDICATED BY THE BLACK ARROW.

The average low water line of the Oesterdam region is visualized in Figure 10. The areas that are always flooded and the areas that dry and flood can be distinguished in this figure. Some large intertidal areas can be observed. The Oesterdam tidal flat is indicated by the black arrow. To the west of this area, a much larger tidal flat can be seen. This is the 'Hooge Kraaijer'. Also the breakwaters of the 'Bergsediep'-sluice can be clearly identified in the northern parts of the area.

The plan consists of a 350,000 m^3 hook-shaped nourishment in front of the dam and near the edge of the tidal flat, see Figure 11. Part of the sand was placed directly near the Oesterdam as additional protection. Construction finished in the last week of November 2013. The construction time was 6 weeks. The hook is approximately 2 km long and has a width of 200 to 800 m. The height varies between 0.5 and 1 m. A large

monitoring campaign was set-up to gather field data. These data can be used for implementation in a model. The locations where measurements were gathered are indicated in Figure 11.

The hook is flooded during high tide. A lowering is applied (near MP22) in the middle of the hook to permit flow of water and restricted flow of sand from the south to the north on the existing flat. Artificial oyster reefs have been constructed to decrease the erosion of the intertidal area even more.

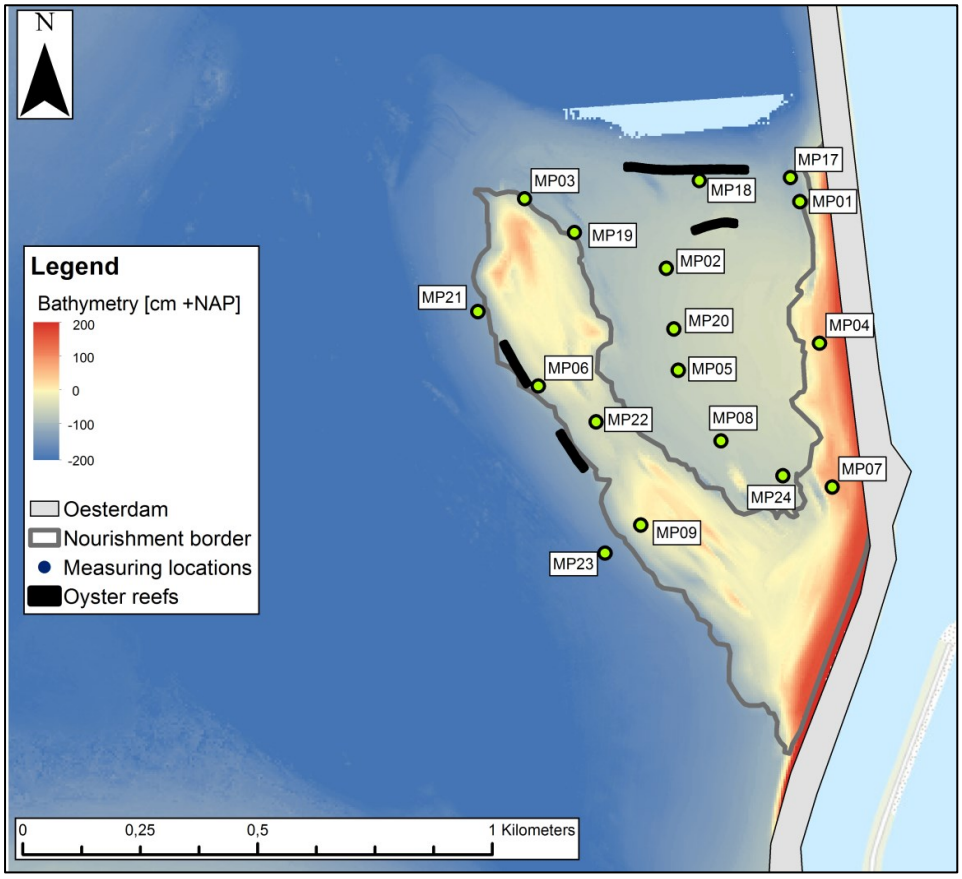

FIGURE 11: SPATIAL LAYOUT OESTERDAM NOURISHMENT.

The choice of a so-called soft intervention is in line with the 'Building with nature'-programme (De Vriend & Van Koningsveld, 2012). According to this programme, it is crucial to design infrastructure that serves more than one purpose, is aligned with natural processes instead of working against them and is able to cope with sea level rise. Nourishments satisfy these criteria. The Oesterdam nourishment is innovative because the tidal flat is not covered entirely, thereby limiting the negative effects on nature.

Van der Werf et al. (2013) state that the results of the Galgeplaat nourishment evaluation cannot be directly extrapolated to other nourishments in the Eastern Scheldt, as the hydraulic conditions and sediment properties vary greatly in the basin. Therefore the Oesterdam nourishment should be analysed independently, e.g. using a numerical model to increase the understanding of the nourishment development as was described by Boersema et al. (2014).

2.4.1 Evaluation of nourishment impact

Boersema et al. (2015) evaluated the development of the nourishment after one year. A lot of morphological developments have taken place during the first half year after the nourishment. When looking at the hook, an adjustment period can be identified in which significant changes can be observed. This period (November 2013 to February 2014) is shown in Figure 12. Overall, erosion can be observed on top of the nourishment, while deposition can be seen near the edges of the nourishment. The tidal flat

itself is rather stable and no significant bed changes can be observed in the sheltered area east of the hook. Furthermore, aeolian transport was observed near the Oesterdam, resulting in deposition of sand near the dam. A re-profiling of the nourishment section close to the dam was executed during March 2014 in order to reduce the aeolian transport. Last, the areas near the oyster reefs show local morphological changes.

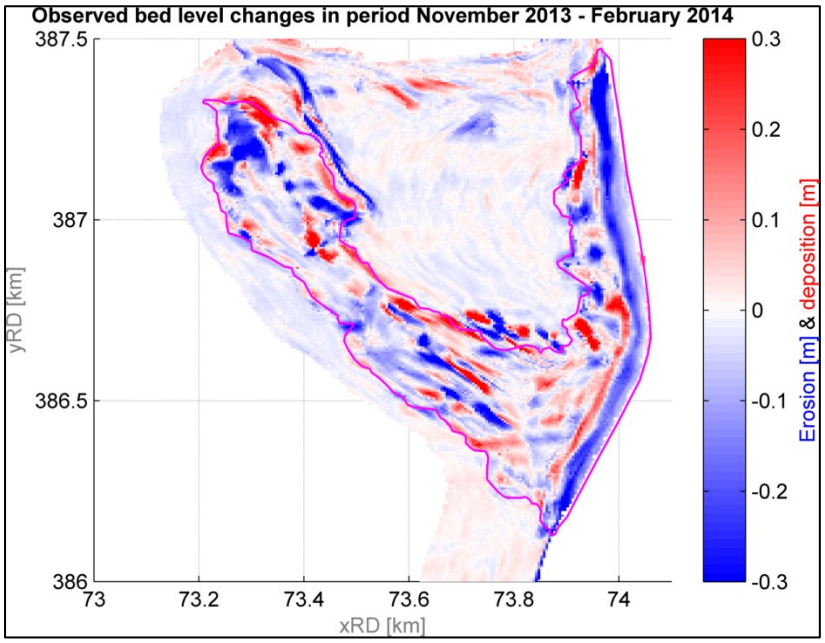

FIGURE 12: SEDIMENTATION AND EROSION OF THE BED IN PERIOD NOVEMBER 2013 AND FEBRUARY 2014. PURPLE LINE INDICATES NOURISHMENT CONTOUR.

5% of the nourished sand volume has moved from the nourishment between November 2013 and February 2014. Transport from the intertidal area is only observed at one location (Figure 12); a relatively large area with deposition can be seen to the north of the hook. Also a channel has formed near the nourishment. The large area to the north of the hook probably exists due to the relatively large ebb flow velocities in the channel. Therefore, Boersema et al. (2015) identify this area as an 'ebb-tidal delta'.

Another important observation is that the influence of wind on the magnitude and direction of currents towards and on the tidal flat seems to be quite large. This is confirmed by observations of the measured direction of sediment transport. Last, the wave attack is observed to be larger near the dam. However it is too early to ascribe these effects to the nourishment. Available data is not sufficient to make a proper comparison. Therefore, additional research is required.

2.5 Synthesis

This chapter elaborated on the processes that occur in the Eastern Scheldt. Large-scale erosion of intertidal areas is observed due to decreased tidal dynamics caused by the storm surge barrier and other compartment dams. Nourishments are identified as measures to mitigate this erosion. A nourishment project has been performed near the eroding Oesterdam tidal flat. The first evaluation of the developments of this nourishment is promising. However, the use of a numerical model should increase the knowledge about the nourishment development. In the next chapter, the set-up of this model can be found.

3 Modelling the Eastern Scheldt and Oesterdam area

This chapter describes the set-up of two models that are used in this study. A process-based model is used to assess the development of the nourishment in space and time. First, an introduction is given of the modelling method. Then the set-up of the Scaloost- and Oesterdam-models is presented.

3.1 Introduction

The main focus of this work is the area near the Oesterdam. The simulation of the processes in this region should therefore be of sufficient quality. The resolution of the model is one of the main factors that determine the simulation accuracy. In order to reach a sufficient resolution, model trains are often used. In such a train, a coarse-gridded model generates the boundary conditions for a model with a finer resolution. This is also known as nesting.

A train of three models is used in this work, see Figure 13. First, the output (water levels) of an overall North Sea model (DCSMv6-ZUNOv4) is used to create the offshore boundary conditions for a large-scale model of the Eastern Scheldt. This Scaloost-model is used to generate the hydraulic boundary conditions for a finer gridded model representing the area near the Oesterdam. This Oesterdam-model is used to investigate the development of the nourishment. Also data obtained from measuring stations is used.

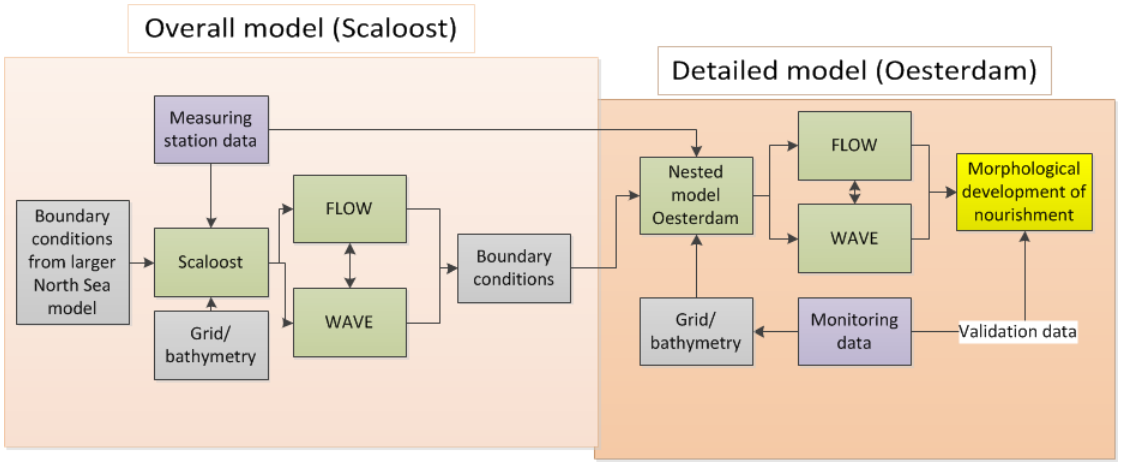

FIGURE 13: MODELLING APPROACH

It should be noted that although output from the overall North Sea model is used in this work, operating the model was not part of this project. This model is an operational model of Rijkswaterstaat. Deltares used this model to generate boundary conditions for the Scaloost-model and provided this data to the author. The Scaloost- and Oesterdam- models are created and used by the author of this work. Therefore only these two models are described in Figure 13 and in sections 3.2 and 3.3.

3.1.1 Delft3D and model assumptions

The modelling package Delft3D (version 4.01.00) is used to simulate hydro- and morphodynamics. Delft3D is a numerical process-based model environment developed by Deltares, formerly known as WL | Delft Hydraulics. It solves the non-linear shallow water equations derived from the three-dimensional Navier-Stokes equations for incompressible free surface flow. Delft3D consists of two modules: FLOW and WAVE. The first simulates both non-steady flow and sediment transport, while the latter simulates wave behavior. The WAVE-module makes use of the wave-model SWAN (Booij, Ris, & Holthuijsen, 1999). An online coupling between the FLOW- and WAVE-module ensures that every half hour the FLOW-module receives new information about waves from the WAVE-module. A more comprehensive description of Delft3D can be found in appendix III.1 as well as in Lesser et al. (2004) and Deltares (2014).

There is hardly any freshwater inflow in the basin as described earlier in this work, thus density-driven currents do hardly exists. Also, three-dimensional processes such as spiral flow are assumed to be of minor importance when looking at the spatial scales in this work. Das (2010) found that secondary currents do not have to be considered when modelling the behaviour of tidal flats in the Eastern Scheldt. Therefore, a two-dimensional depth-averaged (2DH) approach is chosen. Only flow and variations in x- and y-direction are thus considered. In this way, the model is simplified and calculation times can be significantly reduced. This approach is supported by Dissanayake et al. (2012); They state that a 2DH-version of Delft3D is able to simulate major channel/shoal patterns and development of intertidal area in the Wadden Sea tidal basin. The processes in this basin are comparable to the processes occurring in the Eastern Scheldt basin.

3.2 Hydraulic boundary conditions: Scaloost-model

As mentioned, the Scaloost-model generates the hydraulic boundary conditions for the Oesterdam-model. Therefore, Scaloost does not allow bed level changes. Originally, Scaloost is a SIMONA-concept (SImulatie MOdellen NAtte waterstaat) of Rijkswaterstaat, which means that a WAQUA-model simulates hydrodynamics. This model did not include a wave-model. Scaloost is converted to a Delft3D-model for this project. The reason for this decision is that the knowledge of the author about Delft3D is larger than the knowledge about SIMONA. Also it is more straightforward to make a wave model in Delft3D.

Permission was granted by Rijkswaterstaat to use the original SIMONA-grid of the Scaloost-model. The set-up of the Delft3D-version of Scaloost will be elaborated in this section. Among others the grid, bathymetry and time frame will be discussed.

3.2.1 Grid and bathymetry

The grid of the Scaloost-model can be found in Figure 14. It includes the Eastern Scheldt and part of the Dutch coast (from the Brouwersdam to the most western point of Walcheren). The latter is required in order to ensure model stability; the model boundaries should be situated far from the area of interest.

The grid is curvilinear and uses the so-called Dutch Rijksdriehoekstelstel coordinate projection (RD-projection). It extends 30 km into the sea and connects here to the grid of the Kuststrook-model. The number of grid cells is 244 by 579; approximately 89000 cells are active. The grid is derived from the original SIMONA-grid. The resolution varies between 250 by 450 m near open sea and 150 by 250 m in the back of the Eastern Scheldt. The finest resolution is found in the middle of the basin near Colijnsplaat; 30x50 m. 62 sluices of the storm surge barrier are included. All thin dams and dry points are adopted from the SIMONA-version of Scaloost. The wave module uses a grid of the same spatial scale as the Scaloost FLOW-module. The resolution is a factor three coarser.

The bathymetry is constructed using two datasets. The first and most detailed set of measurements of the bed is known as vaklodingen, consisting of 20x20 m measurements. The data are measured along transects of 100 to 200 m. This dataset originates from Rijkswaterstaat and is described by Wiegmann et al. (2005). The bathymetry of the Eastern Scheldt is measured with an interval of a couple of years. The last measurements were done in 2013, so the 2013 bathymetry of the Eastern Scheldt is implemented in the model.

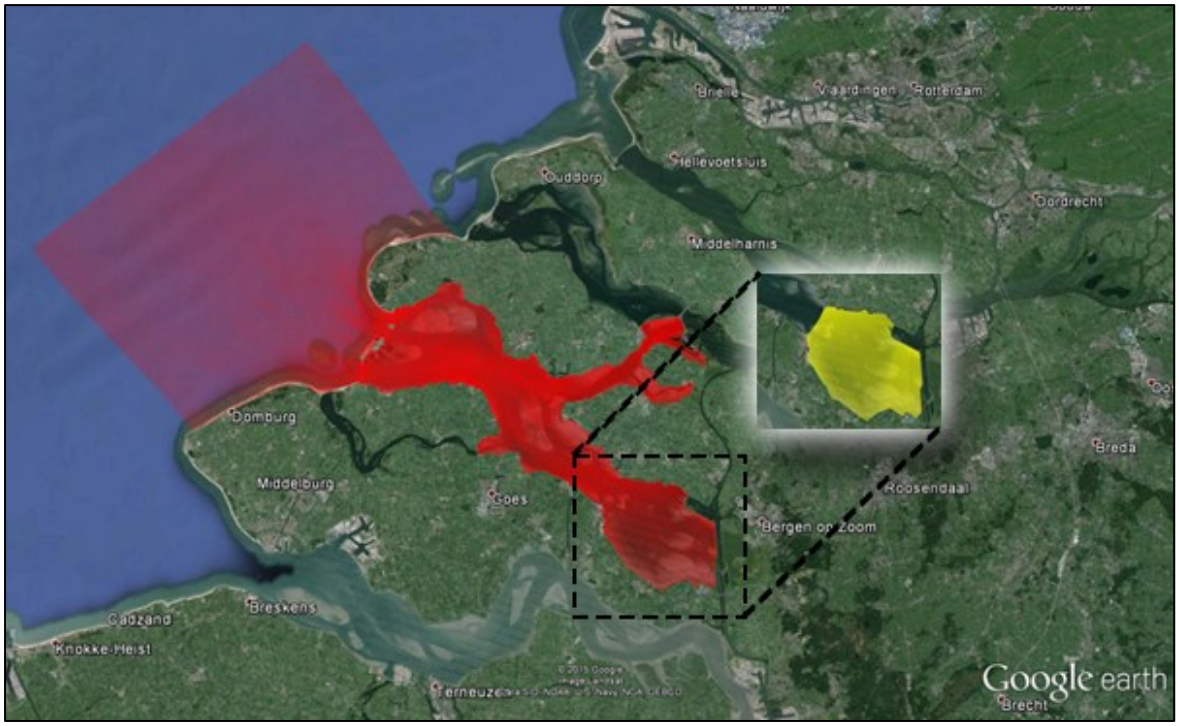

FIGURE 14: GRIDS OF: SCALOOST-MODEL (RED) AND OESTERDAM-MODEL (YELLOW) (GOOGLE EARTH, 2013).

Part of the bathymetry offshore is derived from the bathymetry used in the KustZuid-model, as the vaklodingen do not contain data about bed elevation at these locations. The bathymetry of the KustZuid-model represents the 2004 situation (Das, 2010). This data has a resolution of 2000 by 400 m. A visualization of the bathymetry of the Scaloost-model can be found in Figure 15.

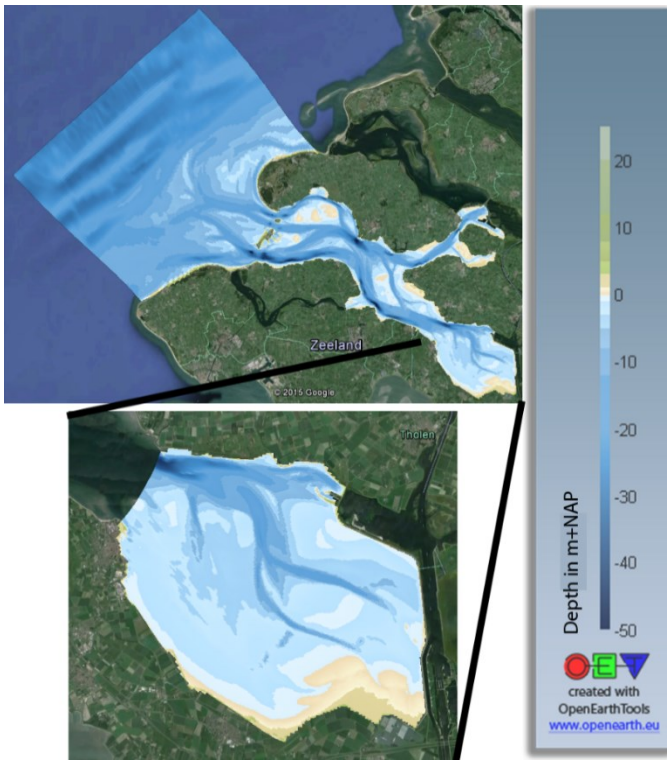

FIGURE 15: BATHYMETRY OF: SCALOOST-(UPPER) AND OESTERDAM-MODEL (LOWER) (GOOGLE EARTH, 2013).

3.2.2 Time frame

Although the numerical scheme adopted in Delft3D is unconditionally stable, the choice of a specific time step should be made on basis of accuracy demands (Deltares, 2014). The time step can be assessed using the Courant number. This coefficient is defined as equation 1:

$$C = \frac{\Delta t \sqrt{gh}}{\{\Delta x, \Delta y\}} \quad (1)$$

With Δt the time step in s, g the gravitational acceleration constant in m/s and h the local water depth in m. $\{\Delta x, \Delta y\}$ represents the minimal value of the grid spacing in either direction in m. The Courant number should generally not exceed a value of 10, although for modelling small variations in space and time the number is allowed to be substantially larger (Deltares, 2014).

A time step of 15 seconds is sufficient for Courant numbers below 15 according to the description of the original Scaloost-model. Courant numbers of 25-30 can occur locally in deep and small cells, for example near Colijnsplaat and Zierikzee. These relatively large values can also be observed for the Delft3D-version of the model using a time step of 15 s. A simulation with an online coupling of FLOW and WAVE using a time step of 15 s becomes inaccurate after simulating 3-4 days in the model. A reduction of the time step to 7.5 s was required to reduce the Courant numbers in the domain to approximately 10.

3.2.3 Additional parameters and settings

The model parameters and settings that are not covered in this chapter are summarized in Table 1. They are not discussed in this work because they are either default or trivial values. A more detailed description can be found in appendix III.2.

TABLE 1: MODEL SETTINGS

Parameter/setting	**Value**
Latitude	52 [degrees]
Reference date	25 12 2012 [dd mm yyyy]
Bed roughness (Manning's n)	0.029 [s/m$^{1/3}$]
Initial water level in whole domain	1.5 [m]
Wind drag coefficient (default values)	
Breakpoint 1 (wind speed of 0 m/s)	0.00063 [-]
Breakpoint 2 (wind speed of 100 m/s)	0.00723 [-]
Breakpoint 3 (wind speed of 100 m/s)	0.00723 [-]
Horizontal eddy viscosity (default value)	1 [m^2/s]
Additional keywords used:	
Upwppl = #Y#	Applies an upwind calculation scheme close to the storm surge barrier to avoid instabilities.
Cstbnd = #yes#	Allows non-perpendicular flow near boundaries.

3.3 Oesterdam-model

In this section, the Oesterdam-model is described. The set-up of the Oesterdam-model is similar to the set-up of the Scaloost-model. The same physical processes are implemented. Also, a lot of data is retrieved from the same source. Therefore, only the aspects that deviate will be discussed in this section.

3.3.1 Grid and bathymetry

Figure 14 also shows the Oesterdam-model grid. The spatial extent of both the Scaloost- and Oesterdam grids can be compared in this figure. The grid used in the FLOW-module of the Oesterdam-model consists of more than 88000 active cells. A large grid resolution is achieved due to this number of grid cells. Two reasons exist to use a large grid resolution. First, there are variations in bed level at very small spatial

scales. For example, small channels exist on the tidal flats. Due to these small variations, locally differences in hydro- and morphodynamics exist. Secondly, the drying and flooding of the intertidal areas is represented more accurately with a smaller grid cell size, as a cell is either dry or flooded (Das, 2010).

The ideal grid size would be approximately 15 by 15 m, as there are features visible on the tidal flat of order of magnitude 10-20 m. However, calculation times were too large when using this resolution as the required time step also decreases. Therefore, a coarser grid was used; the grid size varies from 50 by 20 m in the western parts to 30 by 30 m in the area containing the Oesterdam tidal flat. The grid used by the WAVE-module covers the same spatial scale. Again, an online coupling between both modules is included.

The bathymetry of the Oesterdam-model can be found in Figure 15. The bathymetry is derived from the vaklodingen-dataset and is therefore equal to the bathymetry used in the Scaloost-model except for the area near the nourishment. Data concerning the initial height of the nourishment are collected using a RTK-GPS at November 20 2013. The measuring error of this method is 10 cm (Boersema, et al., 2015). The dataset is used to implement the nourishment in the bathymetry.

The oyster reefs were constructed because of their possible function to hinder sediment transport and mitigate erosion. These reefs are modelled using three assumptions. First, the bathymetry is locally heightened. Oyster reefs in the Eastern Scheldt have approximately a height of 0.4 m (Walles, 2015). Also, the reefs cause increased bed roughness, see appendix III.2 for more details. Last, the sediment layer of the model has been set to zero at the location of the reefs to prevent unrealistic erosion of these objects.

3.3.2 Time frame

Again, the criterion of Courant numbers smaller than 10 should be satisfied. Locally, larger values can be allowed. It is found that a time step of 7.5 s is sufficient for a stable online coupling of the FLOW- and WAVE-module. Although the Courant numbers for wave propagation become larger than 10 near the open boundary, they vary from 1 to 5 near the Oesterdam. Therefore, although the grid is finer than the grid of the Scaloost-model, the same time step is used. In order to improve the simulation of waves near the boundary, the time step could be reduced to 3 s to ensure Courant numbers lower than 10. This would however increase computational time too much.

3.3.3 Grain sizes

The simulations are performed using two different grain sizes. Before the nourishment was constructed, the median grain size of the intertidal area varied between 165 and 187 µm (Boersema, et al., 2015). This is in line with other observations; Huisman & Luijendijk (2009) state that the bottom of the Eastern Scheldt mainly consists of fine sand with a median grain diameter of 150-200 µm.

After construction, median grain sizes on top of the nourishment varied between 276 and 290 µm, with outliers to 320 µm (Boersema, et al., 2015). The nourishment was constructed of coarser sand, obtained from a channel in the Eastern Scheldt. Therefore, a uniform median grain size of 180 µm was assigned to the domain, except for the location of the nourishment, where a grain size of 285 µm is used. These grain sizes are assumed to represent average values. Sediment measurements near the oyster reefs support these assumptions. The median grain size near the oyster reefs east of the nourishment ranges from 186 to 189 µm, while the median grain size near the oyster reef on top of the nourishment varies between 249 and 306 µm. These measurements were executed in May 2015. Other important parameters used are the specific density (2650 kg/m^3) and the dry bed density (1600 kg/m^3). Last, the morphological acceleration factor MorFac is applied. More details about this method can be found in appendix III.2.

3.4 Synthesis

This chapter introduced the Scaloost- and Oesterdam-models. The next chapter will elaborate on the question whether the models can accurately simulate hydro- and morphodynamics.

4 Validation of the Scaloost- and Oesterdam-models

The accuracy of the Scaloost- and Oesterdam-models will be assessed in this chapter. The goal is to see if the morphological development of the nourishment can be simulated accurately. First, a calibration is performed. Then, a hydrodynamic validation method is used. Bed level changes are not allowed then, thus morphology is not taken into account. In this way, the hydrodynamic simulation can be assessed. Thereafter, bed level changes are allowed and a morphodynamic validation is performed. Obviously, the morphodynamic validation is not performed for the Scaloost-model, as there are only morphological changes allowed in the Oesterdam-model.

Data retrieved from measuring stations and from a measuring campaign are used to calibrate the model. The validation is performed by using another period of the datasets. These data are described in the next section.

4.1 Description of calibration and validation data

Several measuring stations that are present in the Eastern Scheldt are implemented in the model. In this way, a comparison can easily be made between observed and simulated data. The location of these stations can be seen in Figure 16. The stations are managed by the Hydro Meteo Centra Zeeland (HMCZ) of Rijkswaterstaat. They provide data about water levels, wind and waves. Measurements are performed every 10 minutes. An overview of which data are measured per station can be found in Table 15 of appendix IV.

FIGURE 16: OBSERVATION STATIONS OF SCALOOST-MODEL, LIGHTER LINE SHOWS THALWEG.

The accuracy of the Scaloost-model will be assessed by using the following stations: Oosterschelde 11 (OS11), Oosterschelde 4 (OS4), Stavenisse (STAV) and Yerseke (YE); OS11 is representative for the offshore behavior, OS4 for the behavior in the neighborhood of the storm surge barrier, STAV for the middle of the basin and YE for the region where the boundary conditions for the Oesterdam model are generated. These stations are situated along the thalweg of the Eastern Scheldt. The accuracy of the Oesterdam-model is assessed using the stations Yerseke, Bergsediepsluice West and Marollegat, as only they are situated in the domain of this model.

Furthermore, data obtained during the monitoring campaign is used for validation; significant wave height and current velocity measurements are compared with simulated values close to and on the nourishment. The monitoring data that are used in this work are presented in Table 2.

TABLE 2: DATA RETRIEVED DURING MONITORING CAMPAIGN (BOERSEMA, ET AL., 2014).

Measured variable	Measuring location	Measurement instrument
Bed levels	Intertidal area	RTK-dGPS
Significant wave height	Intertidal area	Pressure box
Flow velocities	Intertidal area	Aquadopps
Grain sizes	Intertidal area	Tubes

The measurements of the monitoring campaign were not performed at the same time. Therefore, it is not possible to select one distinct period for validation. Consequently, it is difficult to relate observations of different variables with each other.

4.2 Calibration

The set-up of the Scaloost- and Oesterdam-models is similar. Errors in the Scaloost-model will continue in the Oesterdam-model because the boundary of the latter model retrieves its imposed conditions from the Scaloost-model. Only the Scaloost-model is therefore calibrated. Two calibration parameters are defined for the FLOW-module: the energy loss coefficient and the bottom roughness coefficient. The transmission coefficient is defined as the calibration parameter for the WAVE-module. The motivation to use these parameters is described in the next section. The calibration period is September 1 2013 to September 30 2013. The calibrated values of the energy loss and the bottom roughness coefficients are respectively 2.6 [-] and 0.029 $s/m^{1/3}$. A more extensive description of the calibration can be found in appendix V.1.

Energy loss coefficient

The Eastern Scheldt storm surge barrier sluices are modelled in the FLOW-module as porous plates. The thickness of such a plate is much smaller than the grid size. Due to their partial transparency mass and momentum can be exchanged through the plates. The porosity of the plate is controlled by a quadratic friction term: the energy loss coefficient. The constriction of flow by the barrier is realistically represented by these plates. A value of zero means that all the energy is blocked by the plates, while a value of one does not block energy at all. This approach has been adopted from Hoogduin (2009), Das (2010) and De Bruijn (2012). Although this approach may not properly simulate processes close to the barrier, it does not affect simulated water levels in the Eastern Scheldt as was found by De Bruijn (2012).

The storm surge barrier sluices are modeled in the WAVE-module as sheet obstacles, because porous plates cannot not implemented in this module. The transmission coefficient of these sheets is analogous to the energy loss coefficient used in the FLOW-module.

The value of this coefficient does not matter as can be seen in Figure 17. The results of a sensitivity analysis performed during calibration can be seen in this figure. The amount of energy transmitted through the barrier does not have any effect on the simulation of wave in the back of the Eastern Scheldt (station Marollegat). Also, offshore wave heights are not affected by this transmission coefficient when looking at the Schouwenbank and Oosterschelde 4 stations. It can be concluded that waves originating from the open sea are not important for Oesterdam-area. Only locally generated wind waves are important in the back as was already found by Louters et al. (1998) and Das (2010). It is important to note that it cannot be stated that wave heights directly east of the barrier are independent of this coefficient.

Bottom roughness coefficient

The bottom roughness coefficient is chosen for calibration as this coefficient has been identified as highly sensitive for sediment transport applications by Van Rijn (2007). Among others Das (2010), Eelkema (2013) and Zijl et al. (2013) used this approach to calibrate their models.

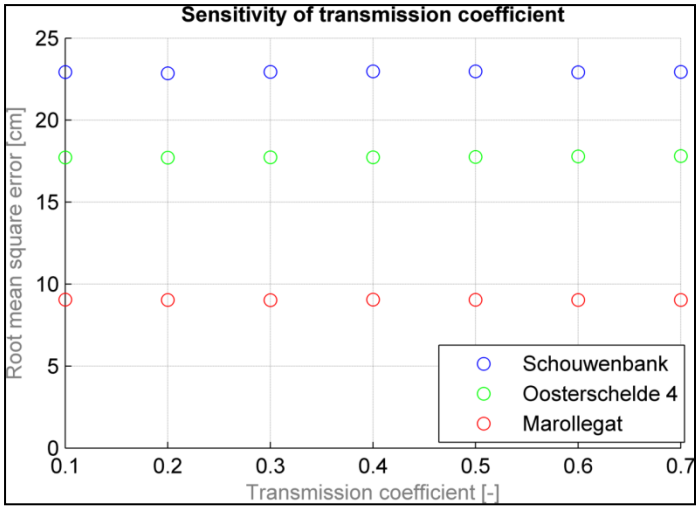

FIGURE 17: SENSITIVITY ANALYSIS TRANSMISSION COEFFICIENT. THE ROOT MEAN SQUARE ERROR DESCRIBES THE DEVIATION BETWEEN SIMULATED AND OBSERVED WAVE HEIGHT.

4.3 Validation

The calibrated model can then be validated using another part of the observed dataset. The validation is described in this section. Both the Scaloost- and Oesterdam-models are assessed.

4.3.1 Scaloost-model

The Scaloost-model is validated by looking at the simulation of different tidal constituents, water levels and significant wave heights. Flow velocities are not considered, as the observations stations do not measure velocities.

Tidal components and asymmetry

A first assessment of model accuracy is done by looking at the simulation of the change in amplitude and phase of different tidal components along the basin. A definition of the amplitude and phase of tidal components is given in appendix V.2. The tidal components are derived from the tidal signal using a harmonic analysis performed by the MATLAB-package T_tide. A comprehensive description of this program can be found in Pawlowicz et al. (2002). Both the observed and simulated water levels at different measuring stations are split up in different tidal constituents. In this work, the M2-, M4- and S2-amplitudes and phases are investigated. The M2- and S2-signals are taken into account because they are main contributors to the full tidal signal; the M4-signal indicates tidal asymmetry. The entire year 2013 is used for the harmonic analysis to maximize the number of recognized tidal constituents.

The spatial change in amplitude along the basin can be seen in the upper part of Figure 18. The behaviour of the simulated M2-, M4- and S2-amplitudes is comparable with the behaviour of the observed amplitudes. An increase of M2-amplitude can be observed throughout the basin, while the M4-amplitude slightly decreases. The S2-amplitude is relatively constant throughout the basin.

The simulated phase of tidal components in the Scaloost-model is consistent with the observed phase, as can be seen in the lower part of Figure 18. The phase of every constituent is increasing in the basin. Remarkable is the relatively large increase of M4-phase directly beyond the storm surge barrier (near OS4). The tidal wave is deformed near the inlet of the Eastern Scheldt, which can be concluded due to the large increase in M4-phase directly after OS4. This was already found in 2.2.1.

Furthermore, some small deviations can be found. For example, the M2-amplitude is slightly underestimated, while the M2-phase is slightly overestimated. This can also be observed for the S2-component. A possible explanation is that the roughness is not yet optimally calibrated.

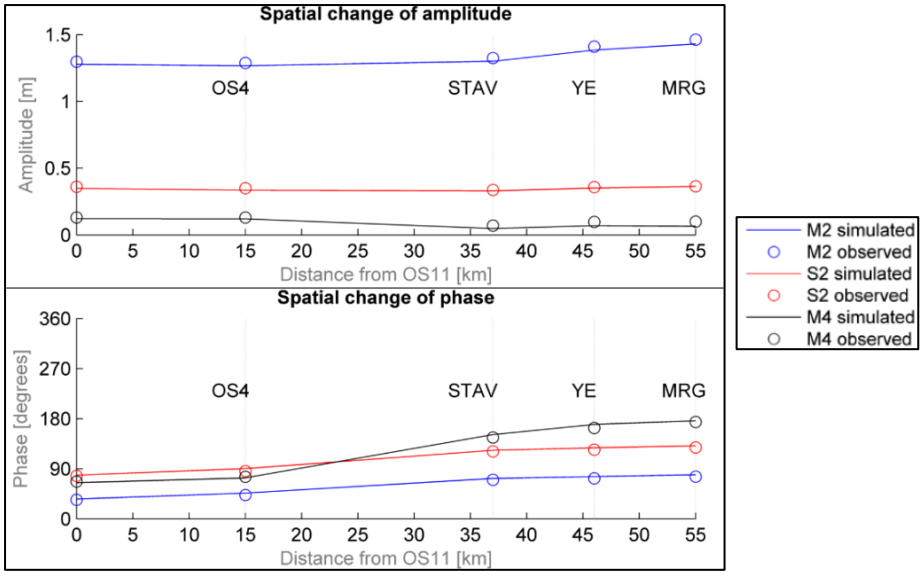

FIGURE 18: CHANGE OF TIDAL COMPONENT AMPLITUDE AND PHASE ALONG THALWEG; (OS11) IS OFFSHORE.

The relative phase difference (2M2-M4) and the M4/M2-amplitude ratio indicate tidal asymmetry. Friedrichs & Aubrey (1988) state that a phase difference of 0 to 180 degrees indicate flood-dominant flow, while a phase difference of -180 to 0 degrees indicate ebb-dominant flow. The M4/M2-amplitude ratio shows the strength of flood/ebb dominance. Table 3 shows that flow is flood-dominant offshore of the barrier, while inside the Eastern Scheldt basin ebb-dominant flow is observed. The presence of intertidal areas in the basin causes this effect, as was already explained in section 2.1.

TABLE 3: TIDAL DISTORTION OF FLOW

	OS11	OS4	STAV	YE	MRG
Relative phase difference 2M2-M4 [degrees]	6.4	19.2	-6.2	-17.8	-17.8
M4/M2-amplitude ratio [-]	0.095	0.095	0.037	0.050	0.046

Water levels

As shown in the previous section, the spatial variation of the tidal components is simulated in an accurate way. Next, the simulation of the full tidal signal is assessed. Three coefficients are defined that indicate model accuracy; the unbiased root mean square error, the bias and the Nash-Sutcliffe coefficient. These coefficients will first be introduced.

The unbiased Root Mean Square Error (uRMSE) describes how large the error is between observed and simulated values and is defined as equation 2:

$$uRMSE = sign(\sigma_{observed} - \sigma_{simulated}) \sqrt{\frac{1}{n}\sum_{i=1}^{n}(y_{observed} - y_{simulated})^2} \quad (2)$$

With $sign(\sigma_{observed} - \sigma_{simulated})$ the sign of the standard deviation of the observed variable minus the simulated variable, n the number of measurements and y either the observed or simulated variable value. Furthermore, the bias of the simulated variable is calculated using equation (3.

$$Bias = \frac{1}{n}\sum_{i=1}^{n} y_{observed} - \frac{1}{n}\sum_{i=1}^{n} y_{simulated} \quad (3)$$

A positive bias indicates that the average of for example simulated water levels is larger than the observed water levels. Also, the Nash-Sutcliffe coefficient is used to assess the simulation quality (Nash & Sutcliffe, 1970). This coefficient is a non-dimensional coefficient describing the squared difference between simulated and observed values. If this coefficient is 0 or larger, the model has predictive capabilities. When the Nash-Sutcliffe coefficient is 1, the model results match the observed measurements exactly. Values between 0 and 1 are generally accepted as good levels of performance. The coefficient is defined as equation 4:

$$NS = 1 - \frac{\sum_{i=1}^{n}(y_{observed} - y_{simulated})^2}{\sum_{i=1}^{n}\left(y_{observed} - y_{average\ observed}\right)^2} \quad (4)$$

The uRMSE is a coefficient that indicates absolute errors, while the NS-coefficient indicates relative errors. Both coefficients are required as the tidal range varies along the basin. The use of the uRMSE does not tell the whole story in that case. For example, the simulation of water levels at stations A and B leads to an uRMSE of 10 cm. It might be concluded that the accuracy of the simulation at both stations is similar. The relative error will then be much larger for station A if the tidal range is much larger at station B. The uRMSE and NS-coefficient thus complement each other.

The boundary conditions used in the Scaloost-model originate from the DCSMv6-ZUNOv4-model. The performance of this model is assessed by Zijl et al. (2013). They consider model performance as excellent when the uRMSE has a value of 5 to 10 cm. Therefore, the Scaloost-model is considered to be of good quality when the uRMSE of the simulated water levels has a value of 5 to 10 cm.

Two validation periods are selected; the first period is December 1 2013 to December 31 2013. This is during the winter season when more storms occur. The response of the system to extreme events can then be measured. The second validation period, March 1 2014 to March 31 2014, is a period with calmer meteorological conditions. For simplicity, only part of the validation series is visualized in the next figures.

Figure 19 shows the water levels during validation period 1. Water levels (the full tidal signal) are predicted well, although low waters are underestimated. The peak at December 5 2013 is also overestimated. Offshore water levels of more than 3.5 m +NAP can be found during this day. This is the infamous ‘Sinterklaasstorm’ of 2013. On this day, large deviations between the simulated and observed water levels can be found for measuring stations within the basin (e.g. Stavenisse and Yerseke). The storm surge barrier closes when offshore water levels exceed 3 m +NAP, which was the case on this day. This effect is not included in the model due to time limitations. Therefore, this day will not be included in the validation.

Overall, the phase of the tidal wave is simulated very accurately, while the simulation of the amplitude shows some deviations as seen in Figure 19. Remarkable is the difference in waveform between stations offshore and on the basin-side of the storm surge barrier. The offshore tidal wave shows a much larger asymmetry. This effect was already observed, as the M4-phase is increasing east of the storm surge barrier.

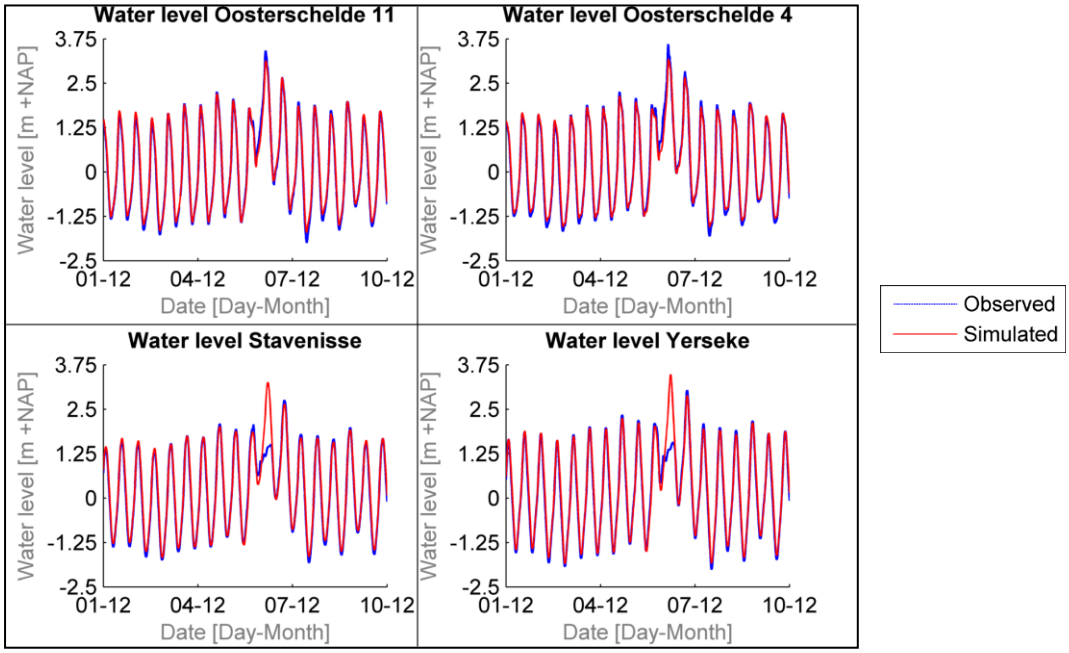

FIGURE 19: OBSERVED AND SIMULATED WATER LEVELS AT DIFFERENT STATIONS DURING PERIOD DECEMBER 1 2013- DECEMBER 10 2013.

The second validation period is visualized in Figure 20. The conditions during this period were much calmer and no large peaks can be seen. Flood tide is simulated very well. However, again a slight underestimation of the ebb tide can be seen.

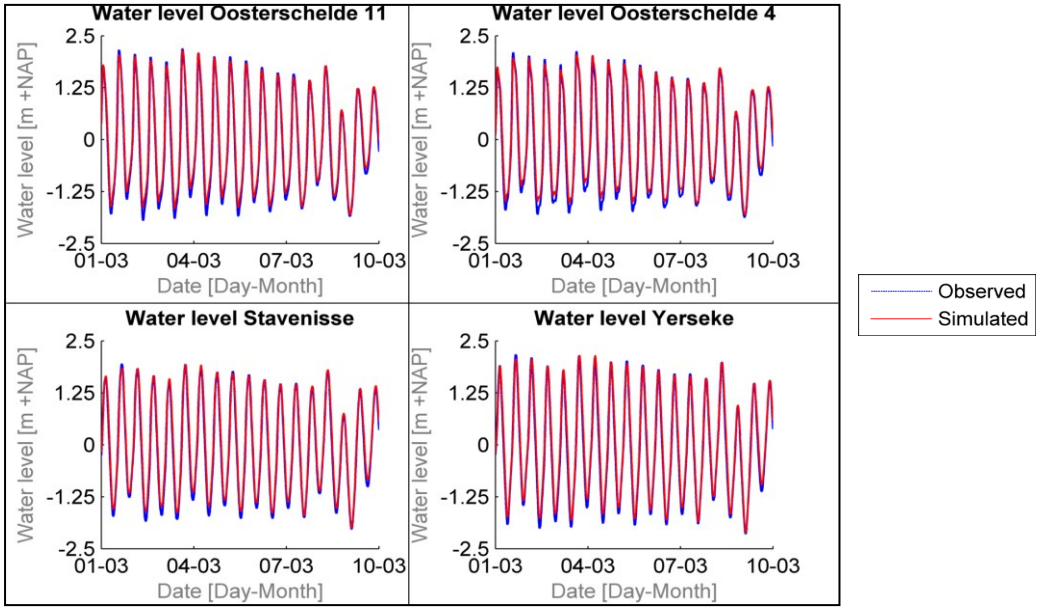

FIGURE 20: OBSERVED AND SIMULATED WATER LEVELS AT DIFFERENT STATIONS DURING PERIOD MARCH 1 2014 - MARCH 10 2014.

The model overestimates the low waters by 5-10 cm. A possible explanation is the absence of small channels in the model. The intertidal areas are easily drained through the small branches of the channel system. However, these small channels cannot be simulated due to the limited grid resolution. Thus, water has to leave the intertidal areas by flowing over the flats. The water tends to be flowing over the intertidal areas for a longer period, causing the low water peak to decrease. This modelling issue was also

found by Borsje et al. (2008), who modelled the Dutch Wadden Sea, a similar area with a lot of intertidal areas. It was not possible to eliminate this underestimation by calibrating model parameters.

The uRMSE- and NS-coefficient-values are presented in Table 4. For each station, the uRMSE is slightly above the acceptable limit of 5-10 cm. The preferred accuracy is thus not reached. However, the uRMSE still indicates good model accuracy. The indeed bias shows a small overestimation. The NS-value of each station is close to 1. The model is performing best offshore from the barrier, while the accuracy inside the basin is less. Presumably, this is caused by the assumption of a constant energy loss coefficient used for simulating processes near the storm surge barrier.

TABLE 4: WATER LEVEL ANALYSIS: RMSE- AND NS-VALUES FOR EACH STATION.

	Validation period 1			Validation period 2		
Station	**uRMSE [cm]**	**Bias [cm]**	**NS [-]**	**uRMSE [cm]**	**Bias [cm]**	**NS [-]**
Oosterschelde 11	--8	4	0.99	-8	5	0.98
Oosterschelde 4	-10	5	0.99	-10	6	0.98
Stavenisse	-9	6	0.97	-9	7	0.99
Yerseke	-11	6	0.97	-11	6	0.99

Significant wave height

A common indicator for wave model validation is the scatter index (SI) as described by Clancy et al. (1986). This index is obtained by dividing the standard deviation of the difference between simulated and observed wave heights by the mean observed wave height (equation (5):

$$SI = \frac{standard\ deviation\ of\ errors}{average\ observed\ wave\ height} \quad (5)$$

The closer this value is to zero, the more accurate the model. Common SI-values range between 0.2 for detailed models with high quality wind fields and 0.6 for less complex models with less accurate wind fields (Howard, et al., 2009). Simulated significant wave height values will be validated using this coefficient instead of the NS-coefficient. The simulated significant wave height is assessed during the defined validation periods. Again, two snapshots are shown; December 1 2013 to December 10 2013 and March 1 2014 to March 10 2014.

Overall the prediction of the wave height during storm conditions corresponds with observed values as can be seen in the left part of Figure 21. Large peaks are simulated well. The wave height at the Schouwenbank, Oosterschelde 4 and Marollegat stations is simulated accurately. The right part of Figure 21 shows the significant wave height during calm conditions. The behaviour of the model is good in such a case. Simulated peak values slightly differ from observed values.

Small waves with heights of 5-6 cm are not simulated in a correct way. Significant wave heights tend to become zero. Possible explanations are that wind conditions are not well represented at those moments in time or the grid cell where the station is located becomes dry at such a moment. In the latter case the model does not calculate wave conditions in a grid cell. Also there could be an error in the observed values. Furthermore, the Schouwenbank station did not measure wave height in the first days of March. The wave heights occurring between 7 and 10 March are however correctly simulated.

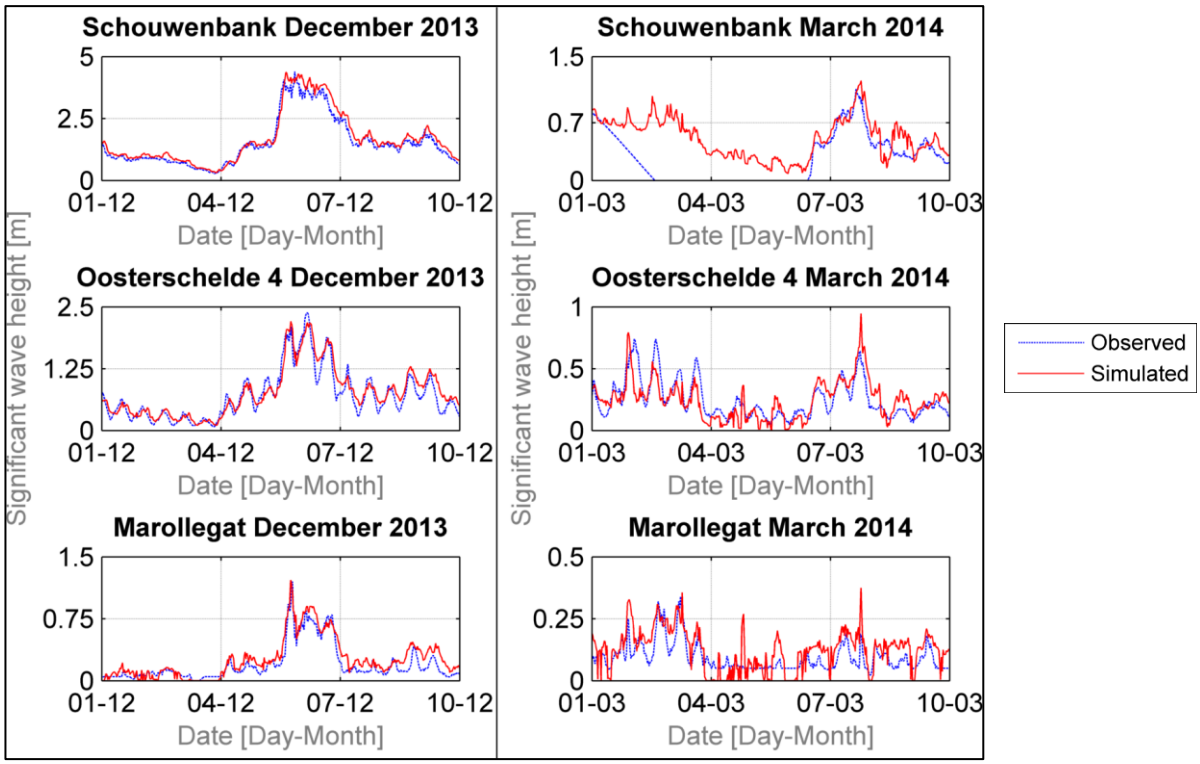

FIGURE 21: OBSERVED AND SIMULATED SIGNIFICANT WAVE HEIGHTS AT DIFFERENT STATIONS DURING DECEMBER 2013 AND MARCH 2014. NOTE THAT NO DATA IS AVAILABLE FOR SCHOUWENBANK STATION IN PERIOD MARCH 3 MARCH 6 2014.

uRMSE-, bias- and SI- values can be found in Table 5. Conditions about the maximum error in significant wave height simulation have not been set on forehand. Overall, uRMSE-values are slightly larger than values found when validating water levels. The uRMSE for the offshore station is higher than the uRMSE for stations situated in the Eastern Scheldt basin. Also, the bias is larger offshore, while the bias is low in the back of the basin. Also, maximum conditions were not set for the SI beforehand. However, it was mentioned that simulations of significant wave height using detailed state-of-the-art models normally lead to SI-values of 0.2. SI-values as presented in Table 5 indicate that the accuracy of wave simulation in the Scaloost-model is comparable to the performance of such detailed models. Last, the accuracy of the stormy period is comparable with the accuracy of the calm period. The wave heights at the Marollegat station are simulated best, while the Schouwenbank station shows the least accurate results.

TABLE 5: ASSESSMENT OF SIGNIFICANT WAVE HEIGHT SIMULATION SCALOOST-MODEL.

	Validation period 1			Validation period 2		
Station	**uRMSE [cm]**	**Bias [cm]**	**SI [-]**	**uRMSE [cm]**	**Bias [cm]**	**SI [-]**
Schouwenbank	20	11	0.11	16	12	0.08
Oosterschelde 4	12	9	0.05	15	4	0.06
Marollegat	8	3	0.01	7	3	0.01

Synthesis

Concluding, the accuracy of the Scaloost-model is good. The behaviour of the model in terms of tidal constituents is good, while water levels and significant wave heights are simulated correctly. Scaloost can thus be used to generate the hydraulic boundary conditions for the Oesterdam-model. The validation of that model can be found in the next section.

4.3.2 Oesterdam-model

The Scaloost-model is validated by looking at the simulation of water levels, significant wave heights and flow velocities. Both data obtained from measuring stations and the monitoring campaign are used.

Water level

The Oesterdam model is validated using the same validation periods as introduced in section 4.3.1. Water levels during these periods are shown in Figure 22. The left part of this figure represents the stormy period. The prediction of this period is good. Again water levels during ebb tide are underestimated while water levels during flood tide are represented in an accurate way. Also, the effect of closure of the storm surge barrier is visible. The same holds for the second validation period as can be seen in the right part of Figure 22.

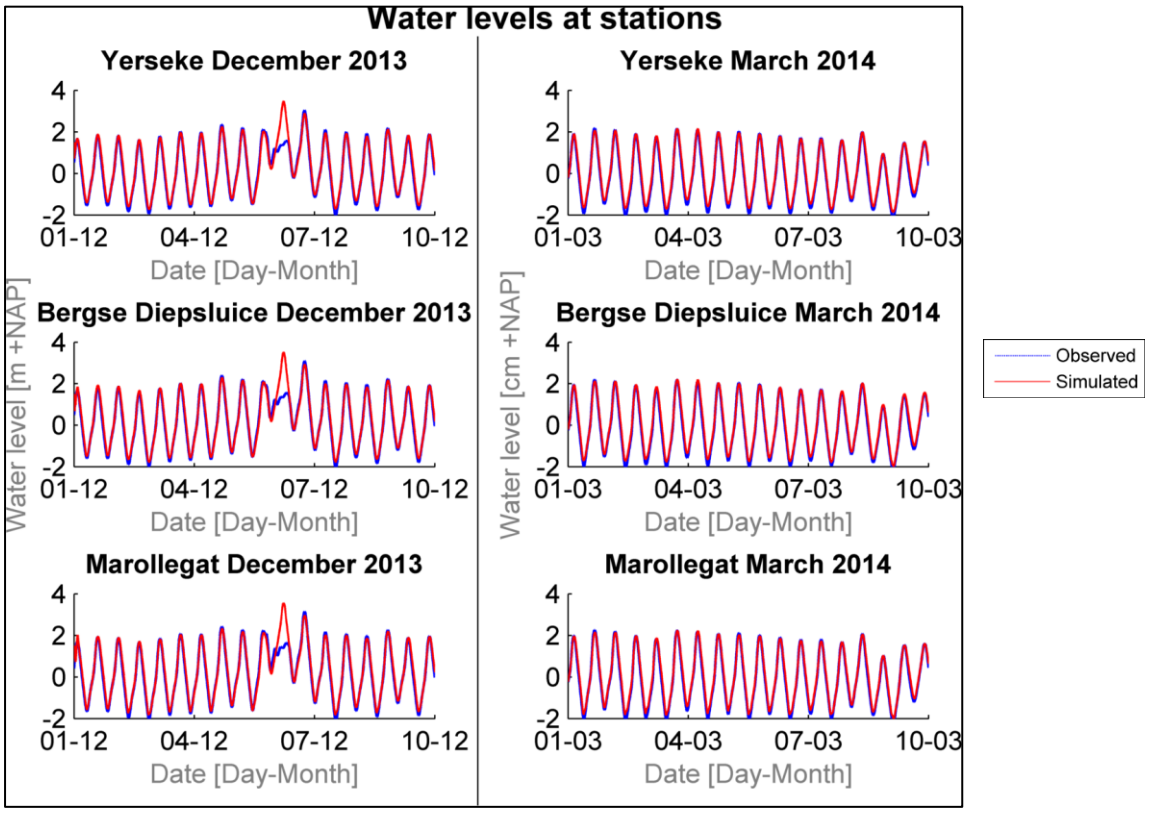

FIGURE 22: OBSERVED AND SIMULATED WATER LEVELS AT DIFFERENT STATIONS DURING PERIODS DECEMBER 1 2013 - DECEMBER 10 2013 (LEFT) AND MARCH 1 2014 - MARCH 10 2014 (RIGHT).

The quantitative assessment of the Oesterdam model can be found in Table 6. Values of the uRMSE and NS-coefficient as well as the bias are similar to the values obtained during validation of the Scaloost-model. The accuracy of the Oesterdam-model is thus comparable to that of the Scaloost-model. Water levels are represented in a correct way and the accuracy of the prediction is suitable for simulating the spatial and temporal behaviour of the nourishment.

TABLE 6: WATER LEVEL ANALYSIS: URMSE- AND NS-VALUES FOR EACH STATION.

	Validation period 1			Validation period 2		
Station	**uRMSE [cm]**	**Bias [cm]**	**NS [-]**	**uRMSE [cm]**	**Bias [cm]**	**NS [-]**
Yerseke	-12	7	0.99	-9.2	11	0.99
Bergse Diepsluis West	-12	6.6	0.99	-8.6	11	0.99
Marollegat	-12	7	0.99	-7.2	9	0.99

Significant wave height

One measuring station that measures wave height is located in the Oesterdam-model domain; station Marollegat. The observed and simulated significant wave heights for this station are found in Figure 23.

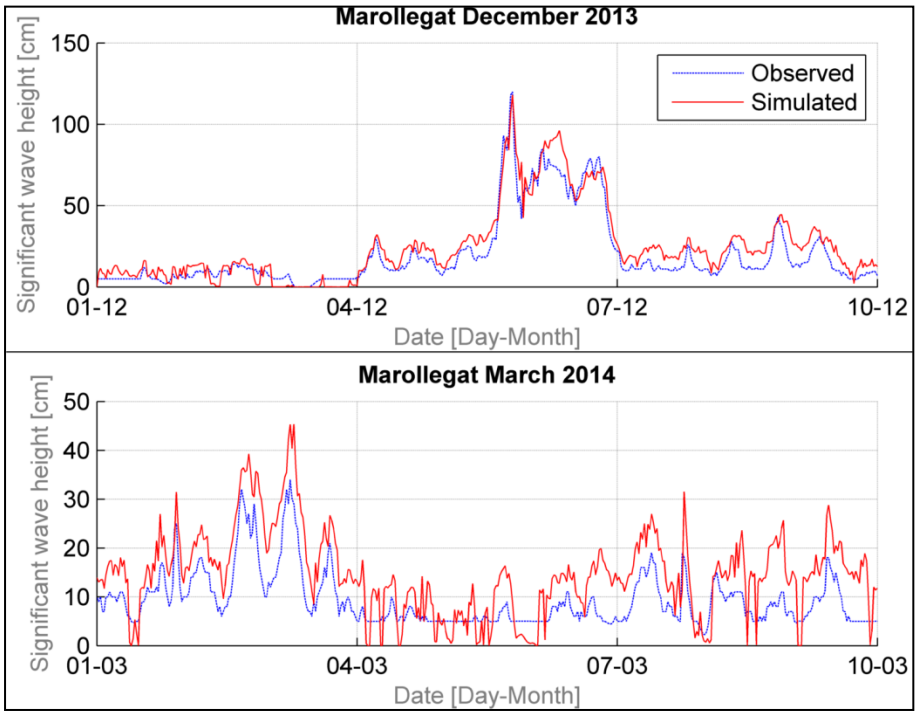

FIGURE 23: OBSERVED AND SIMULATED SIGNIFICANT WAVE HEIGHT AT DIFFERENT STATIONS DURING PERIOD DECEMBER 1 2013 - DECEMBER 10 2013 (TOP) AND MARCH 1 2014 - MARCH 10 2014 (BOTTOM).

The simulation of significant wave heights is consistent with observed values, although a systematic overestimation of 5-10 cm can be observed. The timing of peaks is predicted well. Again, the significant wave height tends to become zero for low wave heights. This effect is however much smaller than it was in the Scaloost-model. This is properly due to the increased grid resolution; the location of the Marollegat station is represented more realistically in the Oesterdam-model. Probably the grid cell that contains this station does not dry as much as the grid cell containing the station in the Scaloost-model.

The model accuracy when looking at the simulation of significant wave heights is comparable to the accuracy of the Scaloost-model as can be seen in Table 7. RMSE- and SI-values as well as the bias are within acceptable ranges and indicate good model performance. Indeed an overestimation of a couple of centimetres is found.

TABLE 7: SIGNIFICANT WAVE HEIGHT ANALYSIS: URMSE-, NS- AND SI-VALUES FOR MAROLLEGAT STATION.

	Validation period 1			Validation period 2		
Station	**uRMSE [cm]**	**Bias [cm]**	**SI [-]**	**uRMSE [cm]**	**Bias [cm]**	**SI [-]**
Marollegat	-6	4	0.01	6	4	0.01

The monitoring campaign provided both local measurements of significant wave height and current velocities on the tidal flat and nourishment. The accuracy of the Oesterdam-model near the intertidal area can therefore be validated. The measurements locations were already visualized in Figure 11.

The wave height data however do not match with simulated values as can be seen in Figure 24. A constant overestimation of 20-30 cm can be observed. In deeper water (for example near the Marollegat station), the simulation of waves is much better. The occurring wind speeds are also plotted. They however do not show behaviour that can explain the low observed wave heights.

Das (2010) also found a large overestimation of wave height when simulating waves at the Galgeplaat with Delft3D-WAVE (SWAN). The overestimation in that research was in general 20-25 cm. It was recommended that the SWAN-model should be re-calibrated. For the present work, re-calibration did not result in satisfactory results. An overview of this re-calibration can be found in appendix V.3. But, when looking at the model results from a theoretical point of view, the quality of the measurements might also be questionable. Measured wave heights hardly exceed values of 5-6 cm.

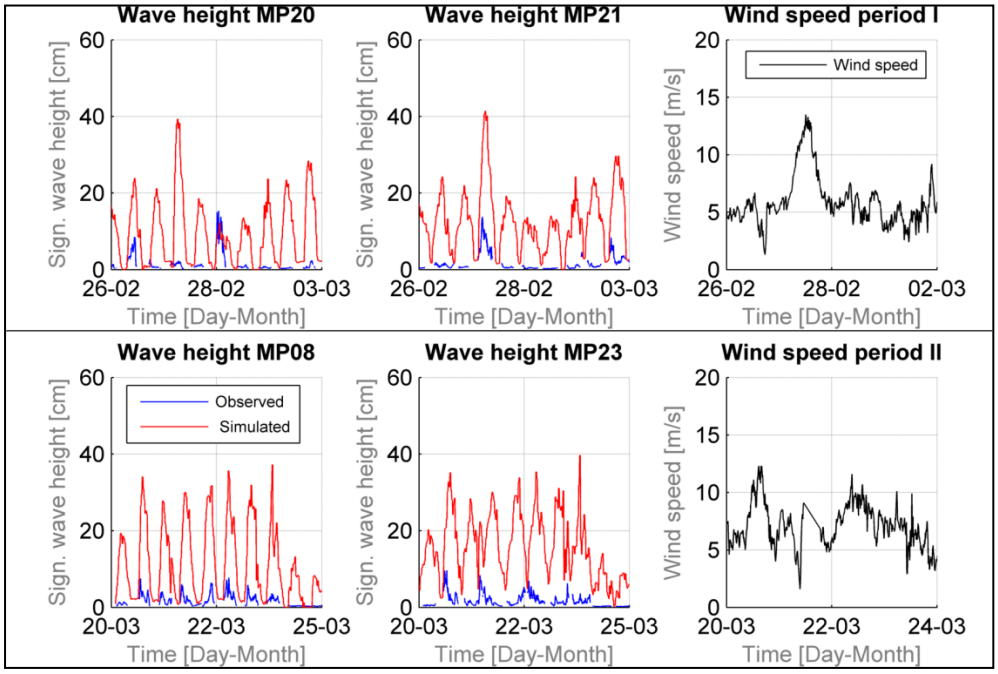

FIGURE 24: OBSERVED (BLUE) AND SIMULATED (RED) SIGNIFICANT WAVE HEIGHT AT MEASURING LOCATIONS NEAR NOURISHMENT.

The correctness of the measurements are verified by a manual calculation of the wave height. There are several methods to calculate the height of wind waves, one of them is the Brettschneider-method (Nederpel & Van Balen, 2012). This method is discussed in appendix V.4. The results can be found in Table 8. The southern direction is not considered, as waves hardly originate from that direction. It can be observed that the simulated wave heights are more realistic than the observed wave heights according to Brettschneider. Furthermore, the raw measurement data was inspected to no prevail. A spectral analysis

of the raw measurement data would clarify whether the measurement data are reliable. However, due to time limitations, it was not possible to do this analysis within this project.

Therefore, the quality of the wave height measurements is questionable and it was not possible to use the monitoring data to validate the accuracy of the wave simulation near the intertidal area.

TABLE 8: RESULTS MANUAL CALCULATION SIGNIFICANT WAVE HEIGHT USING BRETTSCHNEIDER METHOD.

Date	Direction of wind	Observed wave height [cm]	Simulated wave height [cm]	Wave height Brettschneider [cm]
March 3 2014 06:00	South	8	31	32
February 28 2014 13:00	West	5	12	9
February 25 2014 16:30	East	6	14	19

Flow velocities

As sediment transport is directly related and non-linearly related to current velocities, it is important to validate the simulation of flow velocities near and on top of the nourishment. Local flow measurements are available for the period February 21 2014 to March 19 2014. The measured flow velocities can be found in Figure 25. The corresponding location of the measuring instruments was already visualized in Figure 11. The data of other measuring points that are shown in Figure 11 but not in Figure 25 were not available and therefore are not used. Also, this monitoring campaign was done independently of the local wave measures and the measurement period therefore deviates. The corresponding uRMSE-, bias- and NS-values can be found in Table 19 of appendix V.5.

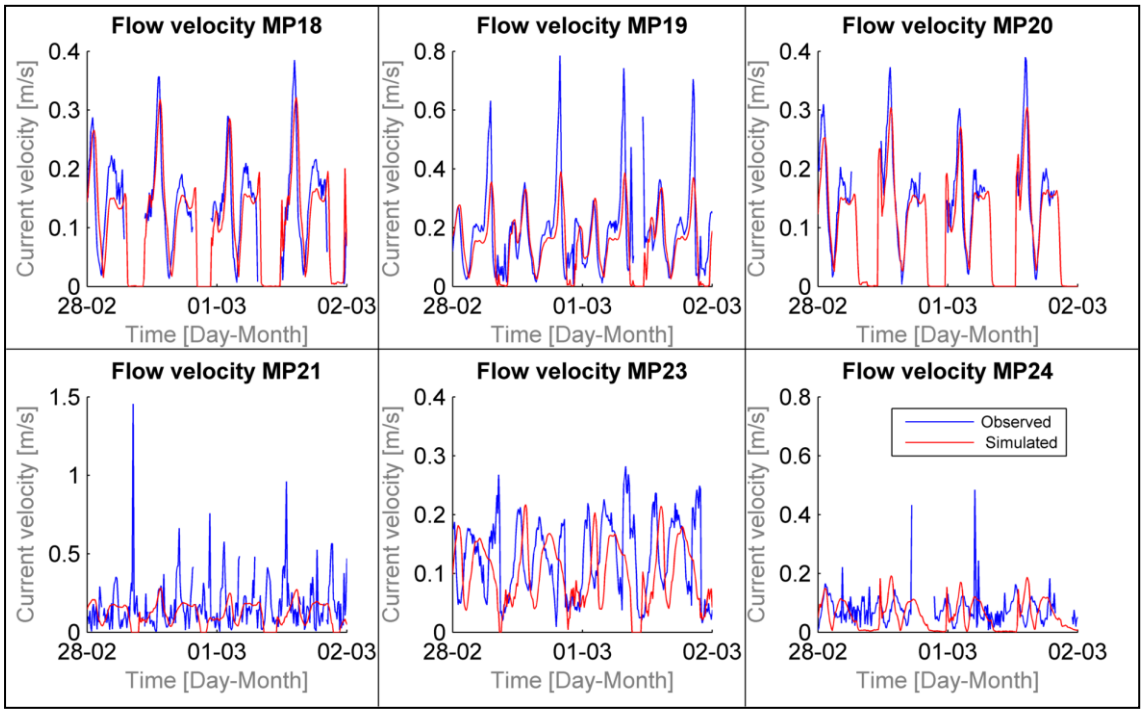

FIGURE 25: OBSERVED AND SIMULATED FLOW VELOCITIES NEAR OESTERDAM IN PERIOD FEBRUARY 28 2014 AND MARCH 2 2014.

Overall, the current velocities are simulated well. MP18 and MP20 show the best prediction, whereas MP23 shows a small phase lag in simulated values. Their amplitudes are also slightly underestimated by the model. The phase lag was not observed when looking at the water level data. Three distinct velocity peaks are not simulated at all at MP23. A possible explanation is that the corresponding grid cell becomes

dry at this moment. Likely, in reality the measuring device was still flooded and flow was registered. The same can be observed for measuring locations 21 and 24.

MP19 is consistent with observed values; however the peaks are significantly underestimated. This measuring point is situated in the deep channel directly east to the nourishment. The depth of this channel is not well represented due to the grid size resolution. Also, it was already noted that low tide is underestimated. The water level gradients are thus less, leading to smaller peaks in flow velocities.

Flow velocities at MP21 and MP24 are not well simulated. Large peaks can be found in the observed dataset. It is therefore questionable if the data obtained from these locations are useful for validation. MP18, MP19 and MP20 represent velocities in the sheltered area behind the nourishment hook. Velocities are simulated well at the tidal flat. MP21 and MP23 are situated west of the hook. Velocities are simulated less accurate here. An explanation for the large deviations is the grid resolution. The nourishment slope is quite steep here. Therefore, the depth at the measuring location can easily be over- or underestimated. This problem is less distinct on the east side of the flat, where the slope is gentler. Also, the dataset used for creating the bathymetry of the Oesterdam-model has an error of 10 cm. This leads to a less representative depth. Smoothing of the bathymetry did not solve this problem.

It should be noted that the velocities show cyclic behaviour. Every tidal cycle a larger and smaller peak can be observed. Ebb and flood tides alternate, thereby flooding and drying the intertidal areas. Current velocities become zero when the intertidal area is dry, as there is no flow in that case. However, velocities are smaller during ebb than during flood tide. The statement that the area is ebb-dominant (section 4.3.1) is thus not reflected by the Oesterdam-model, except for measuring location MP19.

Bed levels

Next, the morphological behaviour of the Oesterdam-model is assessed. Simulated and observed sedimentation/erosion-patterns are compared. The validation period is from November 20 2013 to February 18 2014. The bed of the tidal flat was monitored in this period and observation data is available. The data is collected by means of a RTK-GPS and have a resolution of 5 by5 m. Bed level changes were modelled by simulating 1 month of hydrodynamics and using a MorFac of 3. Some areas are defined that represent distinct features. These areas can be found in Figure 26. Areas I, II, III and IV are important for model validation, as the monitoring campaign included these locations.

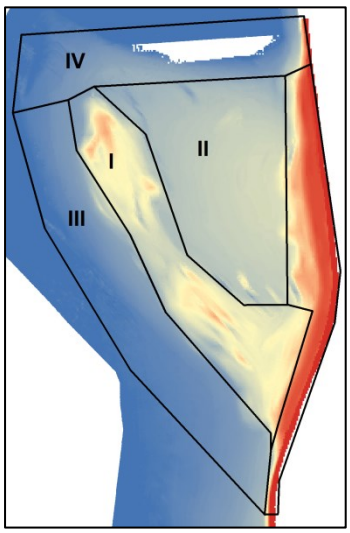

I:	**Hook of nourishment**
II:	**Sheltered area of tidal flat**
III:	**Lower elevated area west of flat**
IV:	**Lower elevated area north of flat**

FIGURE 26: DEFINITION OF AREAS ON TIDAL FLAT.

Observed sedimentation/erosion-patterns were already visualized in Figure 12. To facilitate visual comparison, this map is reprinted in the left part of Figure 27. Simulated bed level changes are shown in the right part of this figure.

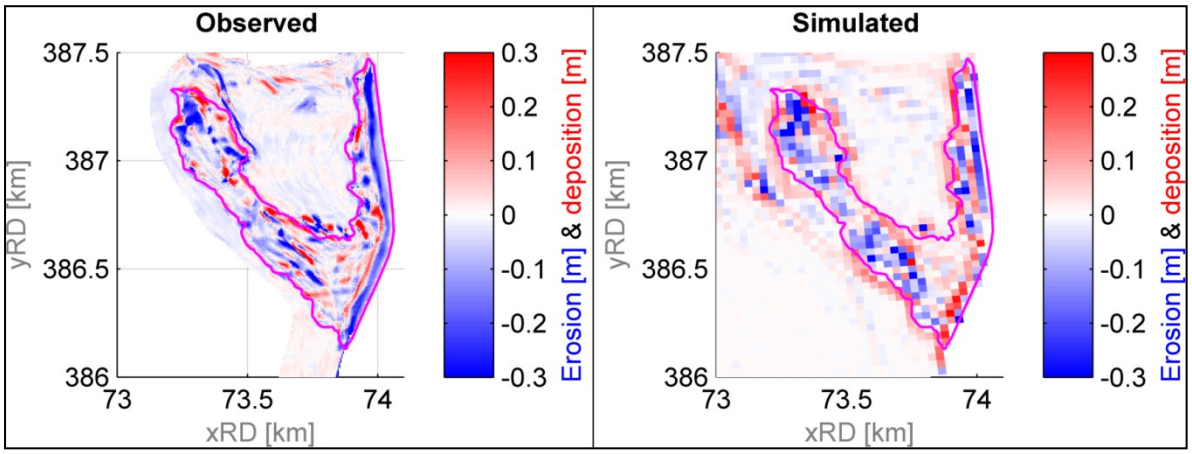

FIGURE 27: OBSERVED AND SIMULATED SEDIMENTATION- AND EROSION-PATTERNS BETWEEN NOVEMBER 2013 AND FEBRUARY 2014. NOTE THAT OBSERVED RTK-DATA DOES NOT COVER AREA WEST OF TIDAL FLAT. THE PURPLE LINE INDICATES NOURISHMENT CONTOUR.

In general, the hook (area I) is eroding. The eastern edge of the hook is accreting when looking at both the observed and simulated patterns. Especially for the most dynamic part of the nourishment, which is the top of the hook, the patterns are similar. There are hardly any changes visible in the sheltered region (area II) for both the measurements and the model results.

The oyster reefs do not erode, although close to their location distinct erosion and deposition patterns can be observed. This shows that the oysters are modelled in a correct way. The distinct gully that in reality develops east of the hook is not present in the model output. The grid size of the model is the origin of this discrepancy. The channel has a width of a few meters, while the grid size of one cell is 30 m. This makes it impossible to correctly represent the depth of the channel and has the consequence that velocities cannot fully develop. The flow is then not strong enough to move sediment from this location.

Close to the Oesterdam the patterns are consistent. Directly near the dam a zone of erosion is observed in both observed and simulated values. A quantitative method (Brier skill scores) of assessing the bed level predictions by the model can be found in appendix V.6. Furthermore, bed level predictions were also assessed by looking at the morphological development of cross-sections. It was concluded that the model roughly identifies the regions with large-scale erosion and deposition rates in a correct way, although their magnitude is overestimated by approximately 20 cm. A description of the validation of the cross-section's development can be found as well in appendix V.6.

4.4 Synthesis

Concluding, the hydrodynamic validation shows that the Scaloost-model as well as the Oesterdam-model show good simulation behaviour. The accuracy of water levels and significant wave heights is good, while current velocities are predicted well. Though, the simulation of significant wave height near the tidal flat shows large deviations. However, the quality of the observed data is questionable. The morphodynamic behaviour of the model is reasonable, as large-scale patterns are correctly simulated. However, the magnitude of the bed level changes is strongly overestimated. Although the model is not suitable to simulate detailed morphological changes, it is able to simulate hydrodynamic processes and large-scale morphological developments. Therefore, model simulations are used in the next chapter to investigate the hydro- and morphodynamic processes occurring before and after construction of the nourishment.

5 Impact on hydro- and morphodynamics

The models and their output have been validated in the previous chapter. In this chapter, first the hydro- and then the morphodynamic impact of the nourishment is presented by means of model results. Different model cases are created to investigate the impact, see Table 9.

TABLE 9: MODEL CASES USED TO INVESTIGATE IMPACT ON DYNAMICS.

Case	Morphological time period	MorFac
A.1	24 hours	1
A.2	3 months	3
A.3	6 months	6

The initial effects of the nourishment are covered by case A.1. The time period is one tidal cycle. A MorFac of 1 is used, so no morphological acceleration is present. The short-term impact of the nourishment is investigated using case A.2, where a MorFac of 3 is used to simulate 3 months of morphological developments. Last, the long-term developments are studied using case A.3 where 6 months of morphological developments are simulated.

Both the situation before and after construction of the nourishment are taken into account. The first is referred to as the autonomous situation and the second as the situation in presence of nourishment. Also, the cross-sections that are defined in Figure 28 will be used for analysis.

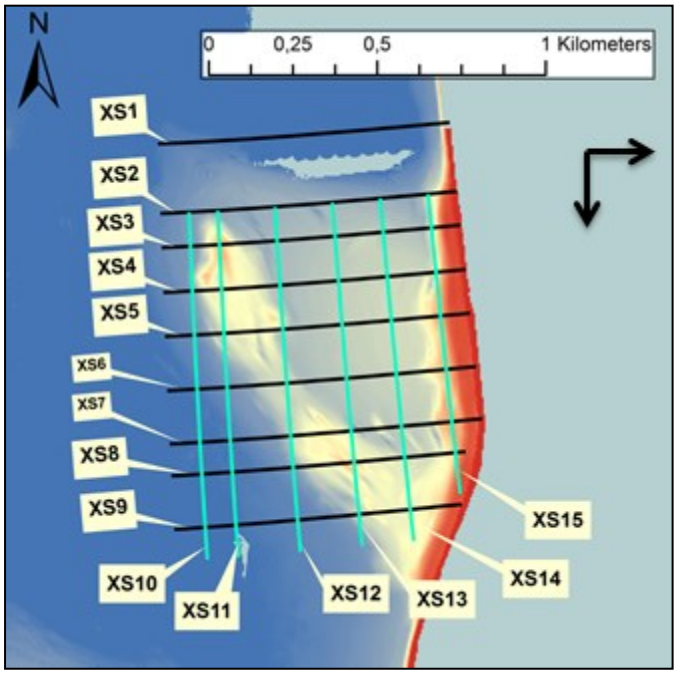

FIGURE 28: DEFINITION OF CROSS-SECTIONS. ORIENTATION OF CROSS-SECTIONS IS DEFINED BY BLACK ARROWS.

5.1 Hydrodynamic impact

The nourishment is a disturbance in the system and therefore affects hydrodynamics. This section will elaborate on the behaviour of flow, waves and sediment transport after construction of the nourishment. As hydrodynamics are affected by the nourishment on a small time scale, the dynamics during one tidal cycle are discussed.

5.1.1 Flow patterns and velocities

The tidal flat floods and dries every tidal cycle. Water levels therefore significantly change during a period of 1 day. A water level gradient then exists, which drives currents. In the next section, the change in water level and current velocities during a tidal cycle on February 14 2014 using case A.1 is discussed.

The left side of Figure 29 shows the flow pattern in the autonomous situation during flood tide. The size of the arrows represents the magnitude of the flow velocities. The location of the nourishment is plotted as a reference; however the 2013 bathymetry without nourishment was used in this simulation. The water level is 1.75 m +NAP, and maximum occurring flood velocities are plotted. The flat is flooded and flow is directed towards the east. The flow pattern is uniform as flow is not restricted by distinct features.

The flow pattern when the nourishment is present is shown in the right part of Figure 29. Two observations can be made. First, the magnitude of the velocities is not significantly different than the autonomous situation except north of the hook. Second, flow is restricted by the top of the hook and is diverted towards the south-east. The flow pattern in the sheltered area does not differ much from the flow in the autonomous situation.

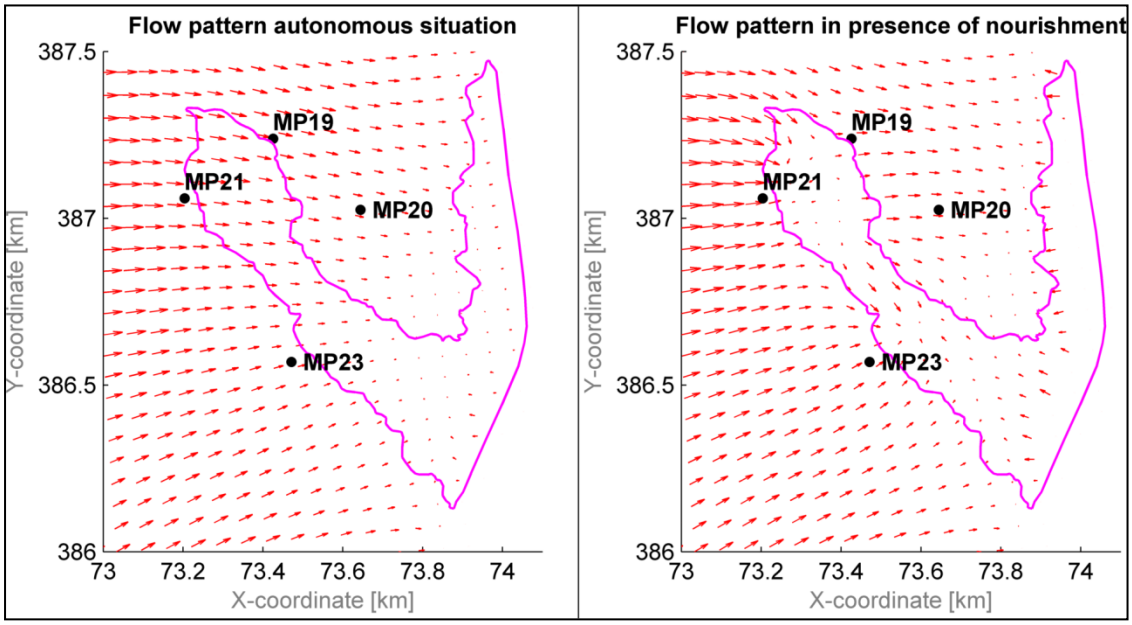

FIGURE 29: FLOW PATTERNS DURING FLOOD TIDE IN: (LEFT) AUTONOMOUS SITUATION (RIGHT) IN PRESENCE OF NOURISHMENT. PINK SHAPE REPRESENT NOURISHMENT BORDER, POINTS REPRESENT MEASURING LOCATIONS.

The left side of Figure 30 shows the situation in presence of the nourishment during ebb tide. Again, the maximum occurring velocities are plotted. The water level is -0.50 m +NAP. Water levels have dropped after high tide and the tidal flat is draining towards the deeper channels in the basin. The flow patterns clearly reflect the height differences on the tidal flat. The most elevated part is in the north-east, while the southern part is lower. Again, flow patterns are uniformly distributed.

The situation in presence of the nourishment can be seen in the right part of Figure 30. The water levels are lower than the nourishment height, therefore the nourishment becomes dry. No flow is observed on top of the nourishment. Flow inside the sheltered area concentrates near MP19, relative large velocities can be observed here.

Figure 31 shows the flow velocities that occur at different measuring locations, which are visualized in Figure 29 and Figure 30. It was concluded in section 4.3.1 that the Eastern Scheldt basin is ebb-dominated, while in section 4.3.2 it was concluded that the Oesterdam area is mainly flood-dominated. According to Figure 31, the Oesterdam tidal flat was indeed flood-dominated before construction of the nourishment as can be seen in the left part of the figure. Maximum flood velocities varied between 0.16 and 0.25 m/s and were larger than the ebb-velocities that varied between 0.15 and 0.21 m/s, see Table 10. The length of ebb-tide is however much larger than the flood tide.

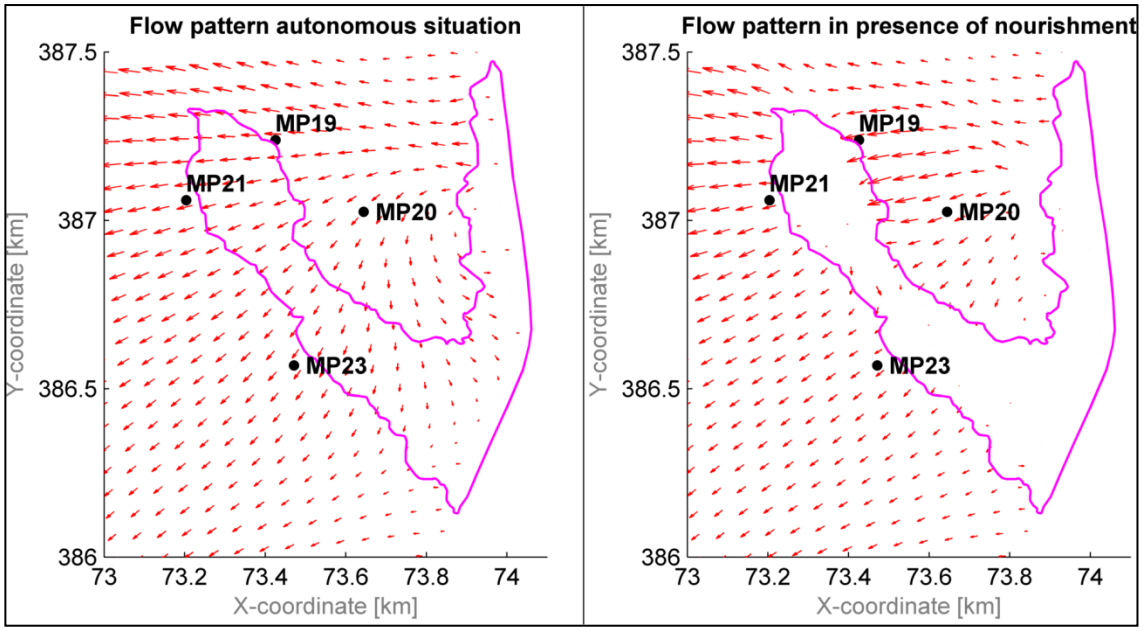

FIGURE 30: FLOW PATTERNS DURING EBB TIDE IN: (LEFT) AUTONOMOUS SITUATION (RIGHT) IN PRESENCE OF NOURISHMENT. PINK SHAPE REPRESENT NOURISHMENT BORDER, POINTS REPRESENT MEASURING LOCATIONS.

The construction of the nourishment significantly affected flow velocities near MP19, where ebb-tidal velocities are twice as large as in the autonomous situation. The large peak in the right part of Figure 31 however only occurs at the end of ebb tide (around 09:00 AM). Before this moment in time, water is still able to flow over the hook of the nourishment. Then, the hook forces the flow towards the north. The flow then converges, resulting in the large velocities. These large velocities also significantly increase sediment transport east of the hook. The ebb-flow is strong enough to transport the sediment outside the nourishment area, leaving a small but deep channel behind.

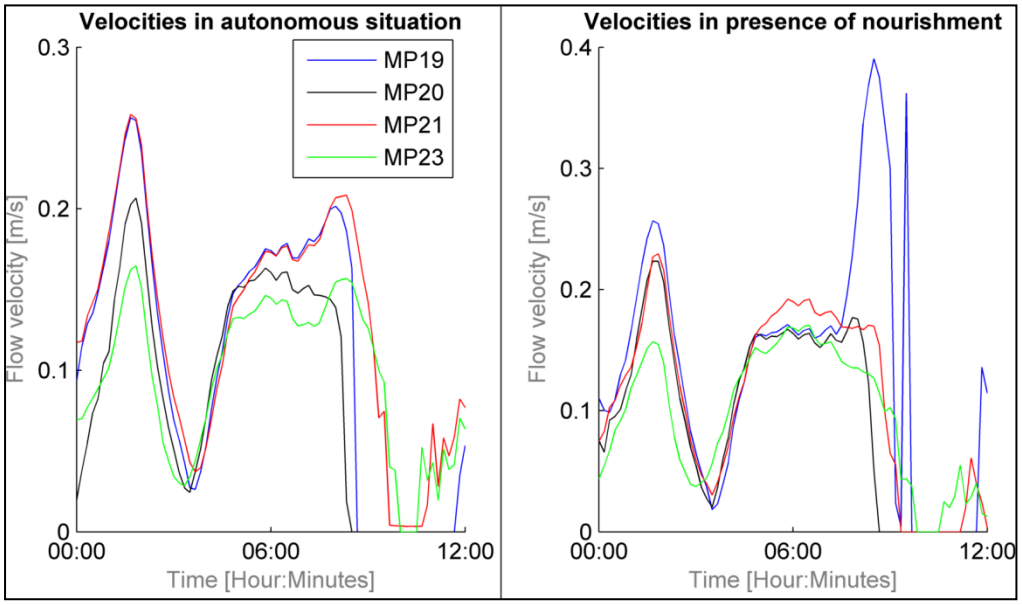

FIGURE 31: FLOW VELOCITIES AT MEASURING LOCATION DURING TIDAL CYCLE.

It is remarkable that the flow velocities near the other measuring locations are quite similar compared with the autonomous situation, although there are some changes, see Table 10. The peak during ebb-flow is not present near MP21 and MP23, as the nourishment restricts water during ebb-tide to flow directly from MP19 towards MP21 and from MP20 to MP23. Also, a new peak is observed at the end of

ebb-tide near MP20. This has probably a direct relation with the flow convergence near MP19. It seems that the tidal flat tends to become ebb-dominant.

TABLE 10: MAXIMUM FLOW VELOCITIES AT MEASURING STATIONS.

Measuring location	Maximum velocities autonomous situation [m/s]		Maximum velocities in presence of nourishment [m/s]	
	Flood tide	Ebb tide	Flood tide	Ebb tide
MP19	0.25	0.20	0.26	0.39
MP20	0.21	0.14	0.23	0.18
MP21	0.25	0.21	0.23	0.18
MP23	0.16	0.15	0.15	0.12

5.1.2 Waves

The behaviour of waves is discussed in this section. Only waves originating from approximately the north-west to south-west are important, as waves originating from other directions do not have large fetch lengths and thus cannot develop large wave heights. Also, the nourishment hook mainly protects the tidal flat from waves originating from the west. Case A.1 is discussed in this subsection.

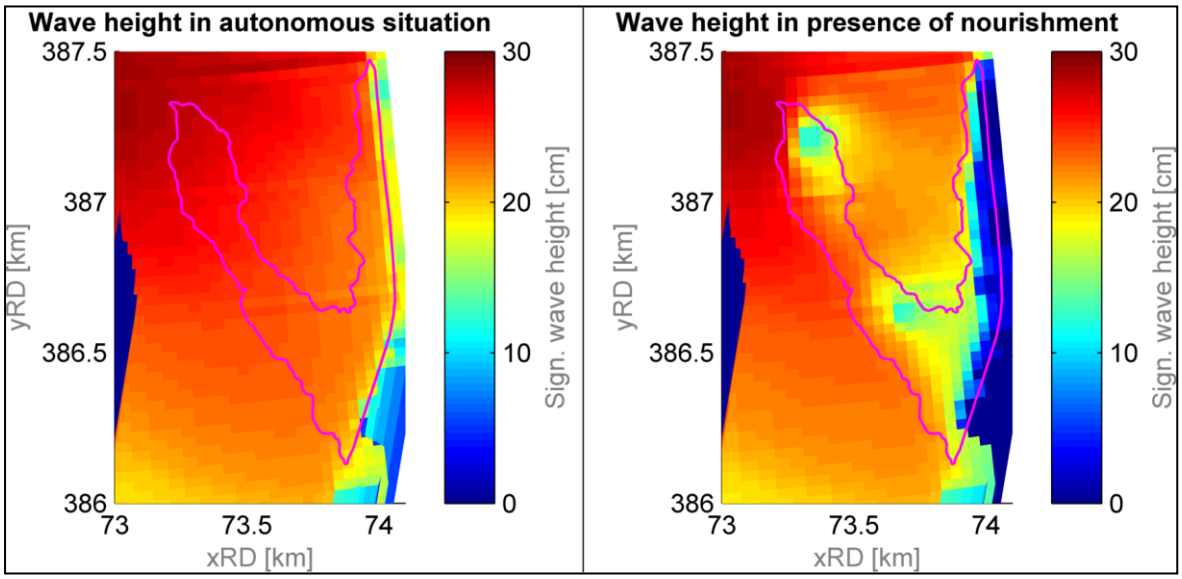

FIGURE 32: SIGNIFICANT WAVE HEIGHT NEAR TIDAL FLAT ON FEBRUARY 14 2014 01:00 PM AT THE BEGIN OF EBB TIDE: AUTONOMOUS SITUATION (LEFT) PRESENCE OF NOURISHMENT (RIGHT). PINK LINE REPRESENTS NOURISHMENT. NOTE THAT NOURISHMENT LOCATION IS ALSO VISUALIZED IN AUTONOMOUS SITUATION TO ALLOW COMPARISON OF BOTH FIGURES.

The wave direction on February 14 2014 at 01:00 PM was west (268 degrees with respect to the north). A top-down view of the area can be seen in Figure 32. The left part of the figure shows that in the autonomous situation, wave height gradually decreases towards the Oesterdam (near xRD = 74 km). The presence of the nourishment shows a different pattern; see the right side of Figure 32. Wave heights are lower near the elevated area of the nourishment hook. Also near the Oesterdam, wave heights are lower.

Figure 33 shows the change of significant wave height and water depth along cross-sections halfway ebb tide. The location of these cross-sections can be found in Figure 28. Water depth is also plotted in the figure as depth is important for the development of waves. The situation at high water is not shown, as water depths are too large for the waves to be affected by the bottom of the tidal flat. The situation at low water is also not shown, as water depths are too small for waves to reach the tidal flat.

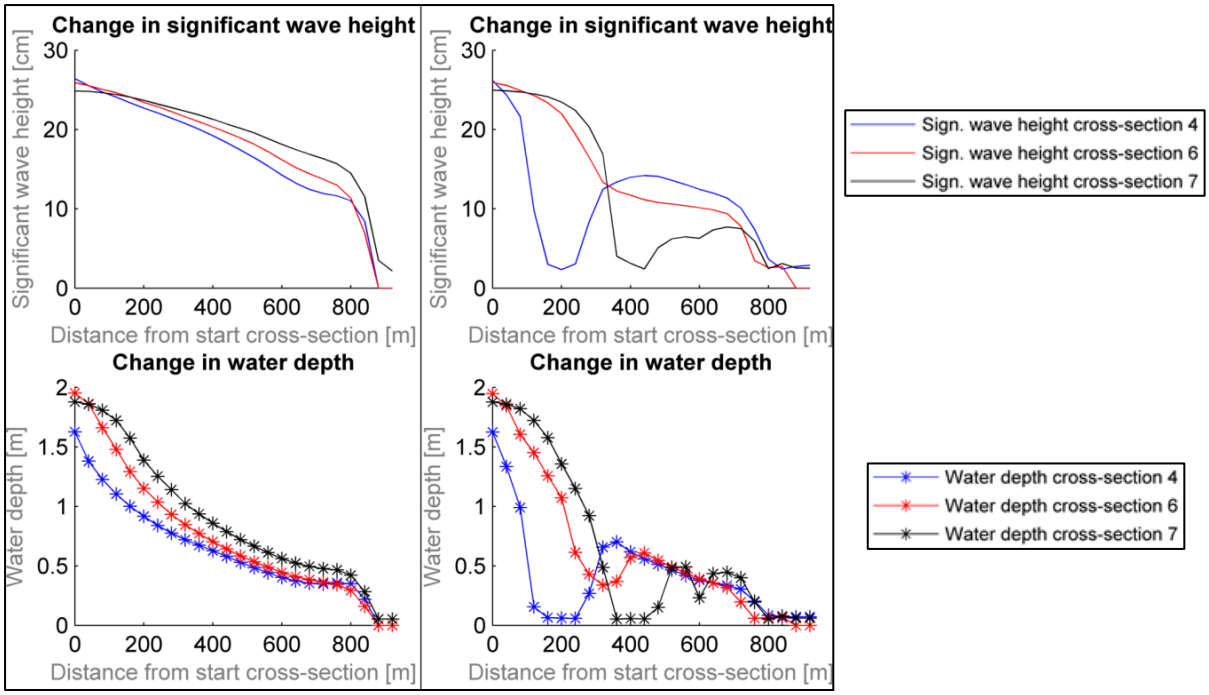

FIGURE 33: SIGNIFICANT WAVE HEIGHTS AND WATER DEPTH ON FEBRUARY 14 2014 01:00 PM AT THE BEGIN OF EBB TIDE: AUTONOMOUS SITUATION (LEFT) PRESENCE OF NOURISHMENT (RIGHT).

Cross-sections 4, 6 and 7 describe the change of wave height on the intertidal area from west to east. Cross-sections 4 and 6 cover the more elevated parts of the nourishment, while cross-section 6 covers the gap in the hook of the nourishment. The spatial layout of these cross-sections can be found in Figure 28.

The left part of Figure 33 shows the wave behaviour in a situation without nourishment. It should be noted that the entire tidal flat is flooded, as water depths are larger than zero. The wave-damping function of the tidal flat can be clearly seen. Wave height is decreasing after x = 100 m in the autonomous situation. At this moment, the waves are affected by the bed of the tidal flat and partly break, hereby dissipating their energy. The wave height suddenly becomes much smaller at x = 800 m. This is due to the rapidly decreasing water depth at this location, which leads to breaking of all waves and wave energy dissipation. Energy is thus dissipated on the entire intertidal area. Because the magnitude of energy dissipation by wave breaking depends on the local water depth, it is undesirable that the tidal flat erodes, as water depth increases in that case and less energy will be dissipated.

The change in wave height looks different after construction of the nourishment; see the right part of Figure 33. The wave height along the same cross-sections is shown at the same moment in time. When compared to the autonomous situation, two observations can be made. The first one is that near the top of the nourishment, wave heights decrease significantly, for example near x = 200 m for cross-section 4 and x = 400 m for cross-section 7. The second is that the gap in the nourishment (cross-section 6) does not break the waves to the same extent as higher elevated sections of the nourishment.

The relatively large decrease in wave height due to decreased water depth is caused by the nourishment. Waves break on the nourishment, leading to wave energy dissipation. Van Duin et al. (2004) indicate that this effect is known as the lee effect and is often observed for near-shore nourishments. The nourishment thus causes a considerable amount of wave damping. However, wave height is able to develop again east of the nourishment. This can be clearly observed for cross section 4 between x = 300 m and x = 800 m. Partly, this is caused by the depth profile that does not linearly decrease. The

phenomenon can also be explained by the following mechanism: wind exerts a stress on the water surface, leading to wave height growth. The longer this fetch length, the more waves will grow. Wind stresses acted in the direction of wave propagation for this case.

A manual calculation using the Brettschneider method as described in appendix V.4 for cross-section 4 shows that waves should be able reach wave heights of approximately 10 cm between x = 200 m and x = 400. It is therefore plausible that wind stresses cause the additional wave growth. A wind speed of 10 m/s, a water depth of 1 m and a fetch length of 250 m were assumed to be representative values for this calculation. Although this fetch effect occurs, wave heights just before breaking (x = 800-850 m) are lower than for the autonomous situation (order of 5-10 cm). The nourishment thus leads to smaller wave heights near the Oesterdam. At x = 800, wave energy is completely dissipated because of the elevated section of the nourishment close to the dam.

The water depth plot shows the location of the nourishment along the cross-sections; depth is suddenly decreasing at x = 200 m for cross-section 4, x = 300 m for cross-section 6 and x = 400 m for cross-section 7. It can be seen that water depths near the hook of the nourishment are approximately 50 cm larger along the gap than along the more elevated areas (cross-section 6 versus sections 4 and 7). The larger depth leads to less wave breaking, which is why cross-section 6 experiences less wave damping.

5.1.3 Sediment transport

The various hydrodynamic phenomena lead to the movement of sediment and consequently to morphological changes. Sediment transport due to flow and waves can only occur when the bed is flooded. The intertidal area is not always flooded during a tidal cycle. The flooding- and drying cycle plays an import role in sediment transport patterns. This is investigated in this section using case A.2.

Bed shear stresses

An important indicator for sediment transport is the bed shear stress, which is described in appendix VI.1. Sediment transport is initiated when a critical value is reached. The Oesterdam-model uses two different grain sizes; critical bed shear stresses are approximately 0.145-0.194 N/m^2 for the tidal flat and 0.194-0.27 N/m^2 for the nourishment area.

The magnitude of the maximum bed shear stresses during flood tide in the autonomous situation can be found in the left part of Figure 34, its direction in the left part of Figure 35. Critical bed shear stresses are exceeded in the deeper channel northwest of the flat and locally on the flat itself. The shear stresses are directed uniformly towards the east. Sediment transport then occurs from the deeper parts of the basin towards the tidal flat. This is the 'shoal-building'-force as was explained in chapter 2. However, the stresses tend to become smaller (0.1 N/m^2) than the critical values near the edges of the tidal flat. The flow is thus not strong enough to transport sediment towards the intertidal area

The right parts of Figure 34 and Figure 35 show the magnitude and direction of the maximum bed shear stresses occurring during flood tide in presence of the nourishment. Bed shear stresses are approximately 0.1 N/m^2 in the sheltered area, which is also observed in the autonomous situation. Bed shear stresses vary from 0.3 to 0.5 N/m^2 on top of the hook, thereby exceeding critical bed shears stresses. Water is able to flow over the nourishment and the direction of the shear stresses is not uniform anymore. On top of the nourishment, they are directed towards the northwest.

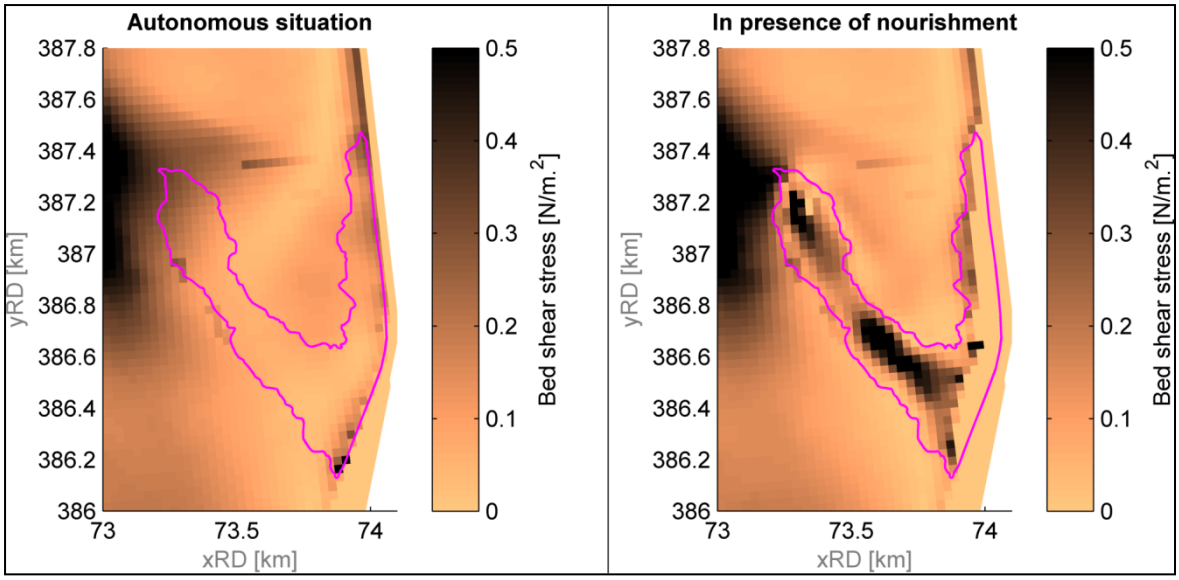

FIGURE 34: MAGNITUDE OF BED SHEAR STRESSES DURING FLOOD TIDE IN (LEFT) AUTONOMOUS SITUATION (RIGHT) PRESENCE OF NOURISHMENT.

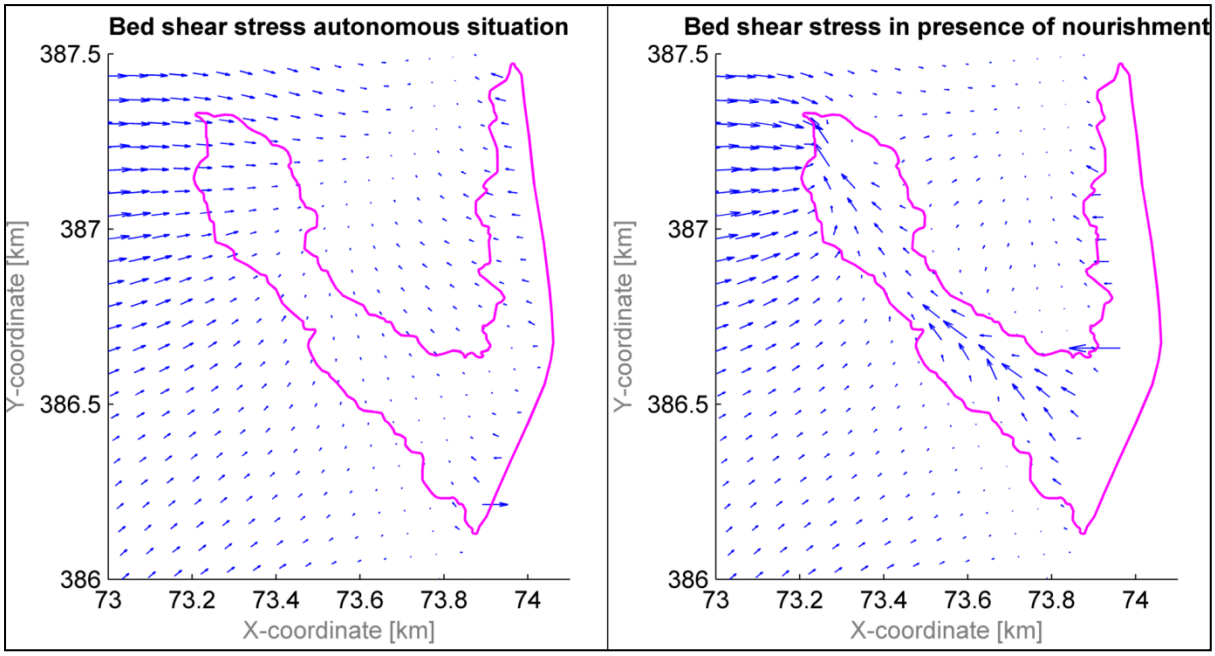

FIGURE 35: DIRECTION OF BED SHEAR STRESSES DURING FLOOD TIDE IN: (LEFT) AUTONOMOUS SITUATION (RIGHT) IN PRESENCE OF NOURISHMENT.

During ebb tide in the autonomous situation, maximum bed shear stresses are uniformly distributed, although the stresses in the northern parts of the tidal flat are larger than in the southern parts, see the left part of Figure 36. Critical bed shear stresses are exceeded in the entire north-western part of the area. The left part of Figure 37 shows the direction of these bed shear stresses during ebb tide in the autonomous behaviour. Because the stresses act towards the west, erosion of the tidal flat will occur. It was observed that during flood tide, bed shear stresses were hardly exceeded in the north-western part of the flat. Hardly any sediment is therefore transported from the deeper channels towards the intertidal area, while simultaneously sand is exported from the tidal flat towards the deeper areas. This phenomenon was already introduced in chapter 2.

In section 5.1.1 it was found that the nourishment constricts flow, which locally leads to flow convergence and significantly larger velocities than was observed in the autonomous situation. The right

parts of Figure 36 and Figure 37 visualize that the constriction of flow leads to large bed shear stresses. The stresses in the sheltered area are directed towards the nourishment hook and become larger as they reach the location of flow convergence. Relatively large amounts of sediment transport can be observed here during ebb tide. The bed shear stresses on top of the hook are close to zero, as the hook is not submerged at this moment in time.

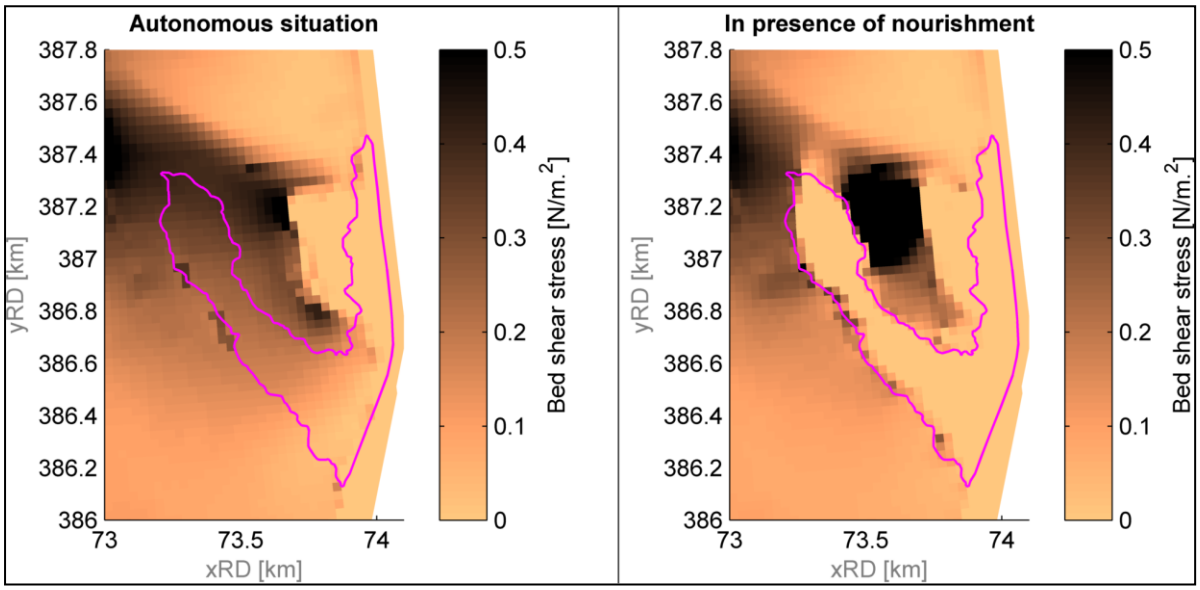

FIGURE 36: MAGNITUDE OF BED SHEAR STRESSES DURING EBB TIDE IN: (LEFT) AUTONOMOUS SITUATION (RIGHT) PRESENCE OF NOURISHMENT.

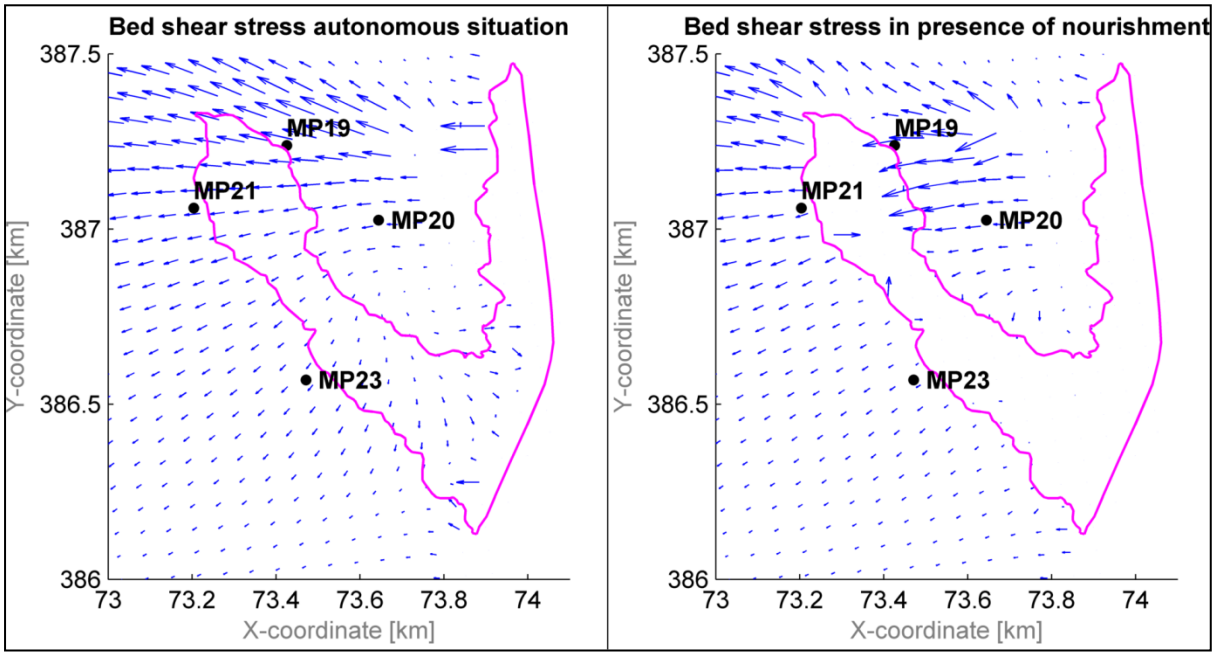

FIGURE 37: DIRECTION OF BED SHEAR STRESSES DURING EBB TIDE IN: (LEFT) AUTONOMOUS SITUATION (RIGHT) PRESENCE OF NOURISHMENT.

The behaviour of the bed shear stresses correlates with the flow velocity patterns observed in section 5.1.1. This can be expected, as bed shear stresses are quadratically related to velocities near the bed. The Oesterdam-model uses a 2DH-approach; therefore only depth-averaged velocities are investigated. However, depth-averaged velocities strongly correlate with velocities near the bed.

Concluding, the distribution of bed shear stresses has changed significantly after construction of the nourishment. Critical bed shear stresses are exceeded on top of the hook in the case of flood tide and large bed shear stresses occur directly east of the nourishment during ebb tide which is the result of large flow velocities, as explained in section 5.1.1.

Transport through cross-sections

Next, the transport through cross-sections will be discussed. The location of these sections can be found in Figure 60 of appendix VI.2. A lot of sections are defined, the most distinct and representative sections are discussed in this work. These are cross-sections 3 and 7, describing respectively sediment transport in the sheltered area behind the nourishment and sediment transport on top of the nourishment hook. The transport through these sections in the autonomous situation and in presence of the nourishment is found in Figure 38.

A distinction is made between bed load, suspended load and total transport. The plots show the cumulative transport in m^3 per running meter. A positive cumulative transport rate indicates transport towards the south and west. The cumulative transport does not start at zero in each cross-section due to model initialization. The model simulates 12 hours of hydrodynamics before it allows bed level updates. This initial contribution to the cumulative transport is thus not caused by erosion or accretion of the bed and therefore does not affect the analyses in this section.

Suspended sediment transport is dominant in the autonomous situation; approximately 80 to 100% of total transport is suspended transport, as can be seen in the left part of Figure 38. Negative cumulative transport indicates sediment transport towards the north. Net sediment transport is then directed from the tidal flat towards the deeper parts of the basin. Furthermore, total transport is twice as large in the northern part than in the southern part of the tidal flat. This corresponds with the observation that the largest bed shear stresses occur in the north-western part of the intertidal area.

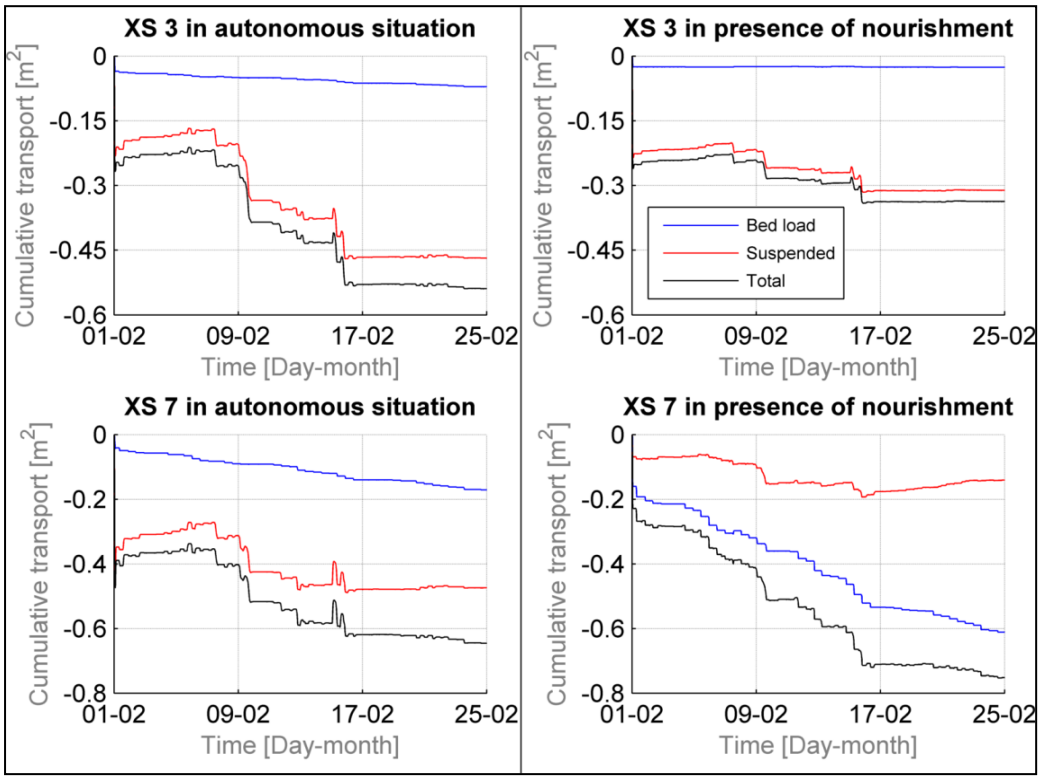

FIGURE 38: CUMULATIVE SEDIMENT TRANSPORT THROUGH CROSS-SECTIONS (XS) 3 AND 7 IN: (LEFT) AUTONOMOUS SITUATION (RIGHT) IN PRESENCE OF NOURISHMENT.

The cumulative transport in presence of the nourishment can be seen in the right part of Figure 38. When compared to the autonomous situation, some remarkable observations can be made. It can be seen that the total transport in cross-section 3 has decreased by approximately 35%. The nourishment thus reduces sediment transport towards the northern edge of the sheltered area. This does not hold for the transport in the small channel east of the hook. Suspended sediment is still dominant for this cross-section.

Furthermore, sediment transport patterns at the location of the hook changed significantly. The right part of Figure 38 also shows the sediment transport through cross-section 7 in presence of the nourishment. Not only has the total sediment transport slightly increased, bed load transport has become the dominant transport type. The increase in transport can be explained by the fact that the nourishment is a disturbance to the system. As each natural system tends to develop to an equilibrium situation, a disturbance will lead to a response of the system. Because the bed is elevated at the location of the nourishment, erosive forces like tidal currents and waves have more influence on the bed. More remarkable is the fact that bed load transport has become dominant on top of the nourishment. This can be observed for most of the cross-sections that are situated on top of the hook. This can be explained by the fact that the nourishment consists of coarser grains than the tidal flat in the autonomous situation. Probably, the flow is strong enough to initiate bed load transport of those grains, but is not able to take the sediment into suspension.

It should be noted that no cyclic behaviour can be observed in both the autonomous situation and when the nourishment is present. If the tidal dynamics are responsible for sediment transport, a daily variation should be visible. Now, the transport seems random. Relatively long periods without transport can be observed, while large peaks occur occasionally. The behaviour can be observed for the entire tidal flat. This indicates that tidal dynamics are not responsible for sediment transport from the tidal flat. Cross-section 7 however shows a more gradually distribution of sediment transport in presence of the nourishment than in the autonomous situation. It could therefore be argued that the importance of tidal dynamics increased for the sheltered area after construction of the nourishment.

Concluding, suspended sediment is still dominant in the sheltered area east of the nourishment. Approximately 80% of the total transport in this area is suspended sediment transport. This percentage is similar to the percentage as observed for the autonomous situation. Near the nourishment, bed load becomes much more important. Also, total sediment transport rates on top of the nourishment increased, while total sediment transport rates in the sheltered area has decreased significantly. Therefore, sediment transport patterns differ significantly from the autonomous situation.

The impact of the nourishment on the hydrodynamic processes in the system was investigated in this section. The short-term morphological behaviour will be discussed in the following section.

5.2 Morphodynamic impact

So flow velocities, wave behaviour and sediment transport are affected by the nourishment. The next question is what the morphodynamic impact of the nourishment is. This will be discussed in this section.

5.2.1 Initial response of the bed

This section considers the initial response of the bed using case A.1. However, the morphological changes in one tidal cycle are not large; therefore the simulation period was extended to the first spring-neap tidal cycle. The corresponding sedimentation-erosion-patterns can be found in Figure 39.

In general, the same morphological changes as observed for a simulation of 3 months of morphological developments can be found. This was already discussed in section 4.3.2, where the results of case A.2 were studied. Generally, the middle part of the nourishment is eroding while accretion is seen near the

lower elevated edges. The tip of the hook is the most dynamic area where erosion alternates with accretion. The sheltered area hardly experiences any morphological changes. The part of the nourishment close to the dam is mainly moving towards the west. However, the observed morphological changes are smaller than at the hook of the nourishment.

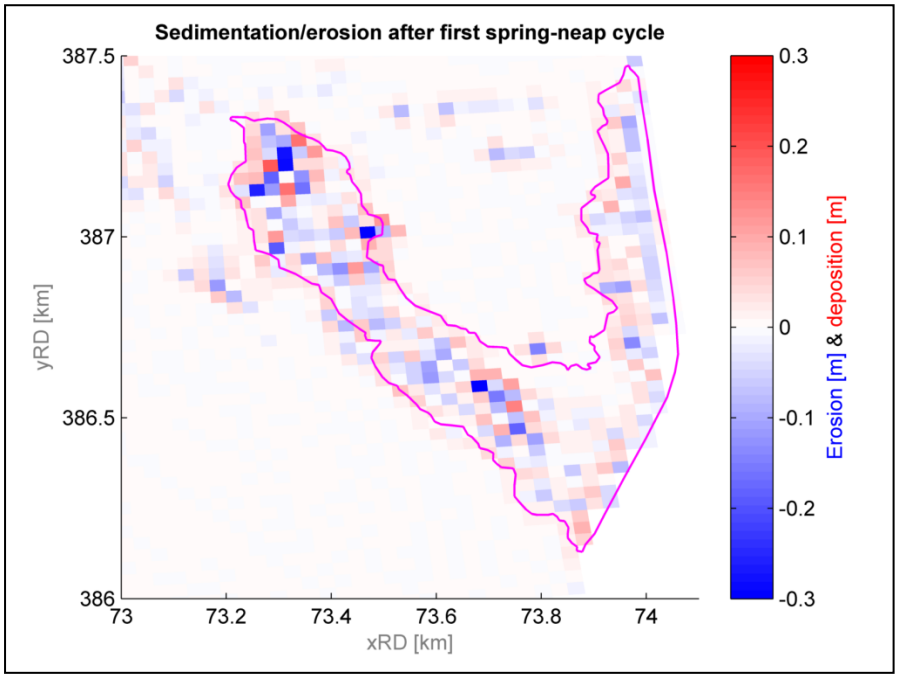

FIGURE 39: SEDIMENTATION/EROSION PATTERNS IN PRESENCE OF NOURISHMENT FOR A SPRING-NEAP TIDAL CYCLE.

5.2.2 Long-term response of the bed

Case A.3 includes long-term simulations of 6 months using a MorFac of 6. The first simulation used the 2013 bathymetry of the area as it was before construction of the nourishment. This simulation is used to show the need for measures near the tidal flats in the Eastern Scheldt. The second simulation included the nourishment in its bathymetry. Boersema et al. (2015) observe significant changes in hydro- and morphodynamics on and near the tidal flat in a period of three months. A long-term simulation of 6 months could support this statement.

Autonomous situation

A long-term simulation was performed using the 2013 bathymetry as it was before construction of the nourishment. The sedimentation/erosion-patterns of this simulation can be found in Figure 40. The morphological simulation period was December 1 2013 to June 1 2014.

Large-scale erosion can be observed on the tidal flat. Almost the entire area is eroding while deposition can be observed near its edges. The largest erosion rates (5-10 cm) can be observed in the north-western part of the area. In the middle of the tidal flat, erosion rates vary between 0-5 cm. Probably, sand is transported from the tidal flat towards its edges. West of where the hook is located in the future nourishment, a large area with deposition can be observed. The water depth is larger here during ebb tide, leading to sediment transport from the flat towards this area. The simulated erosion rates are larger than observed rates. The Oesterdam tidal flat has eroded by 25-50 cm in the period 1990-2010 as can been in Figure 49 in appendix II. The model thus overestimates bed level considerably as already 5-10 cm is eroded in 6 months.

Remarkable is the large amount of deposition close to the Oesterdam. Erosion rates exceed 10 cm. It is possible that during flood tide sediment is transported towards the east and accumulates close to the

dam. This cannot be validated, as there are no LIDAR or vaklodingen observations of bed level changes available from before the construction of the nourishment. However, there are also some locations visible near the Oesterdam where large erosion occurs. These patterns probably occur due to modelling inaccuracies. The Brier Skill Scores already indicated that this area is simulated badly.

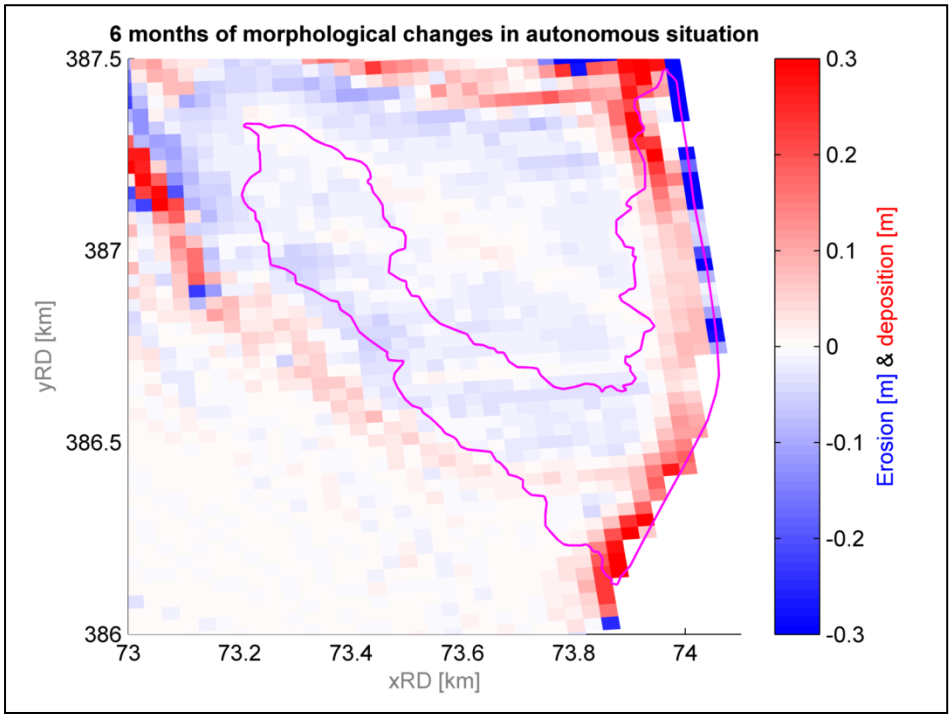

FIGURE 40: SEDIMENTATION/EROSION-PATTERNS AUTONOMOUS SITUATION LONG-TERM SIMULATION OF 6 MONTHS.

Adjustment period

Next, the long-term simulation including the nourishment is discussed. It was stated in chapter 2 that an adjustment period (approximately three months) has been identified, after which no significant bed level changes are observed. A long-term simulation of 6 months should indicate if the morphological activity became less. The corresponding sedimentation-erosion patterns are found in the left part of Figure 41.

The same patterns continue to control the morphodynamic development of the area; erosion on top of the nourishment and accretion near its edges. Also, erosion of the tidal flat continues north of the hook, as the hook does not protect this area. The tidal flat therefore becomes smaller in width. The sheltered area behind the hook is stable as hardly any bed level changes are observed. Also, erosion can be observed near the oyster reefs. They cause both local accumulation and erosion of sediment near their edges. The difference between the simulations of three and six months is plotted in the right part of Figure 41. Indeed, the process of erosion on top of the nourishment and deposition near its edges continues. The sheltered area still experiences erosion, although close to the hook accretion is observed. The magnitude of morphological changes near the oyster reefs however is much smaller.

So, according to the model, significant morphological changes continue to occur after the adjustment period of three months. However, it should be noted that the model considerably overestimates bed level changes. Therefore, no statements can be made about the durability of the nourishment in the long-term. It is not possible to fully ascribe this to model (in-) accuracy. The usability of MorFac depends on whether the representative tide and waves correctly describes the hydrodynamics occurring in the morphological simulation period. It is possible that the representative tide consists of hydrodynamics which are much stronger than in reality. This will lead to large morphological changes during a simulation, while in reality much calmer conditions occurred, leading to much less morphological activity.

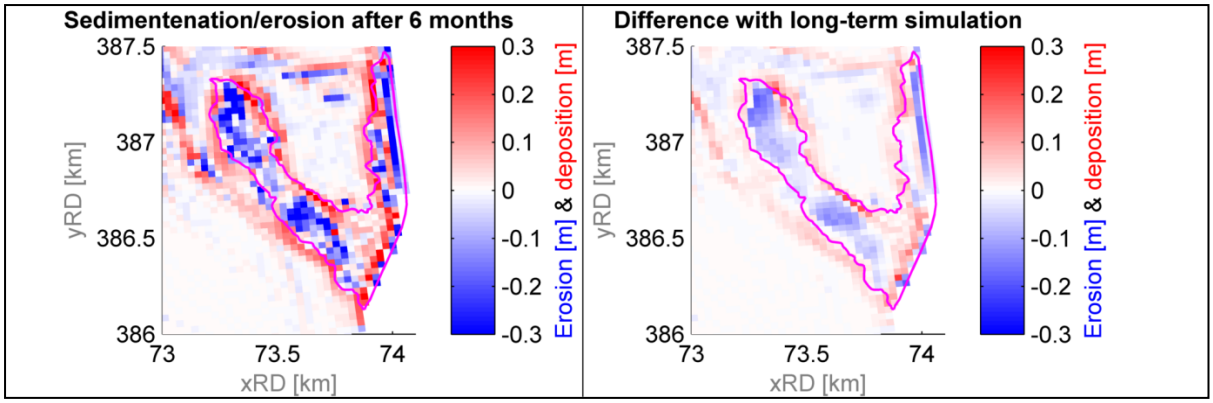

FIGURE 41: (LEFT) SEDIMENTATION-EROSION PATTERNS IN PRESENCE OF NOURISHMENT AFTER 6 MONTHS (RIGHT) DIFFERENCE BETWEEN SIMULATION OF 3 AND 6 MONTHS.

5.3 Synthesis

This chapter investigated the change in hydro- and morphodynamics of the Oesterdam tidal flat after construction of the nourishment in November 2013. It can be concluded that flow velocity, wave and sediment transport patterns significantly differ from the patterns observed in the autonomous situation.

Flow is constricted by the nourishment. This results in large velocities directly east of the nourishment hook. It was found that the Oesterdam tidal flat was flood-dominant before construction of the nourishment, but tends to become more ebb-dominant in the sheltered area.

Wave breaking and growth can be observed when looking at wave behaviour. First, waves partly break when they are affected by the bed of the intertidal area, dissipating their energy. On the tidal flat wave growth can be observed, as wave height tends to become larger again. Overall, the nourishment leads to an increase in wave damping as smaller wave heights are observed near the Oesterdam.

Sediment transport shows patterns similar to the flow velocities. Both the shoal-building and shoal-eroding forces have been identified by looking at bed shear stresses. It was found that the shoal-building force is not strong enough to bring sediment towards the tidal flat, while the nourishment is effective in decreasing the erosive forces. Cumulative plots of sediment transport show that due to the presence of the nourishment, sediment transport rates in the sheltered area east of the nourishment decrease. Sediment transport rates on top of the nourishment have increased. Suspended sediment transport is dominant except for the nourishment hook, where bed load transport is dominant. Also, cumulative sediment transport plots indicate that tidal forcing is not an important contributor to sediment transport as no daily patterns could be observed. This statement will be investigated in the next chapter.

If the nourishment was not constructed, the intertidal area would continue to erode and sand will be transported towards the deeper parts of the Eastern Scheldt. A simulation showed that after 6 months the tidal flat would have been eroded by approximately 5-10 cm. The model however overestimates the morphological changes. The model is therefore not able to assess the durability of the nourishment.

Finally, the largest morphological changes can be observed near the hook of the nourishment, where sediment is transported from the more elevated areas towards the shallower edges of the hook where it is deposited. Local sedimentation-erosion patterns could be observed near the oyster reefs and the sheltered area is relatively stable as hardly any morphological changes are observed.

The next chapter will focus on the drivers behind the processes discussed in this chapter. The influence of tides, waves and wind will be investigated.

6 Drivers of morphological changes

Next, the processes that are responsible for the morphological changes are identified, including tides, waves and wind. Different model cases are created to study these drivers, see Table 11. Case B.1 should give insight in the sensitivity of morphological changes to tidal dynamics. Furthermore, the importance of waves is investigated using case B.2. Last, the effect of wind to morphological changes is studied using case B.3. It was found that a simulation with tides and waves, but without wind forcing, is equal to case B.2. Without wind, no waves will be generated in the model. Therefore, case B.3 does include wind in the WAVE-module.

TABLE 11: MODEL CASES USED TO STUDY DRIVERS OF MORPHOLOGICAL CHANGES.

Case	Tides	Waves	Wind
B.1	X		
B.2	X		X
B.3	X	X	

First, the influence of tidal forcing is presented. Then, the impact of waves on morphological developments in the area is investigated. Subsequently, the importance of wind is discussed.

6.1 Influence of tides

Analysis of the sediment transport patterns in chapter 5 indicated that the tidal dynamics are not responsible for initiation sediment transport near the intertidal area. Therefore the importance of tidal forcing is discussed in this section. Case B.1 only considers tidal forcing. Figure 42 shows the sedimentation-erosion-patterns when waves and wind are not included in a simulation of three months of morphological changes.

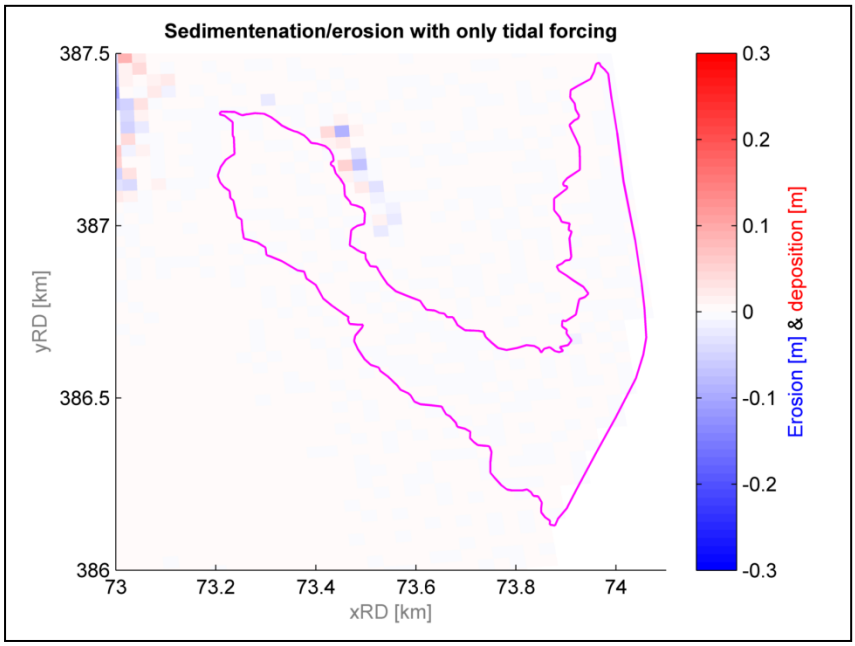

FIGURE 42: SEDIMENTATION-EROSION-PATTERNS FOR A SIMULATION WITHOUT WAVES AND WIND.

The main observation is that hardly any morphological changes occur. The tidal flat and the nourishment are both stable. Tidal currents are indeed not strong enough to transport sand towards the tidal flat. This 'shoal-building'-capacity of the tide has decreased due to the construction of the storm surge barrier. Also, no erosion of the bed is observed. Tidal currents are not able to move sediment from the nourishment.

Some developments are visible near locations with large flow velocities; to the east of the nourishment a zone with both erosion and sedimentation can be found. It was already found in section 5.1.1 that large flow velocities occur here during ebb tide. These velocities thus lead to bed shear stresses large enough to enable sediment transport. The currents are caused by tidal flow. So, the development of the nourishment and the tidal flat cannot be explained by looking at tidal dynamics. Next, the influence of waves is investigated.

6.2 Influence of waves

Boersema et al. (2015) assume that waves are mainly responsible for sediment transport. Figure 42 in the previous section showed that tidal forcing is not able to initiate sediment transport. In this section, it is investigated using case B.2 whether waves are the main drivers of sediment transport. Therefore, three months of morphological changes are simulated without the influence of waves. The effect of wind on flow is included. Corresponding sedimentation-erosion patterns can be found in Figure 43.

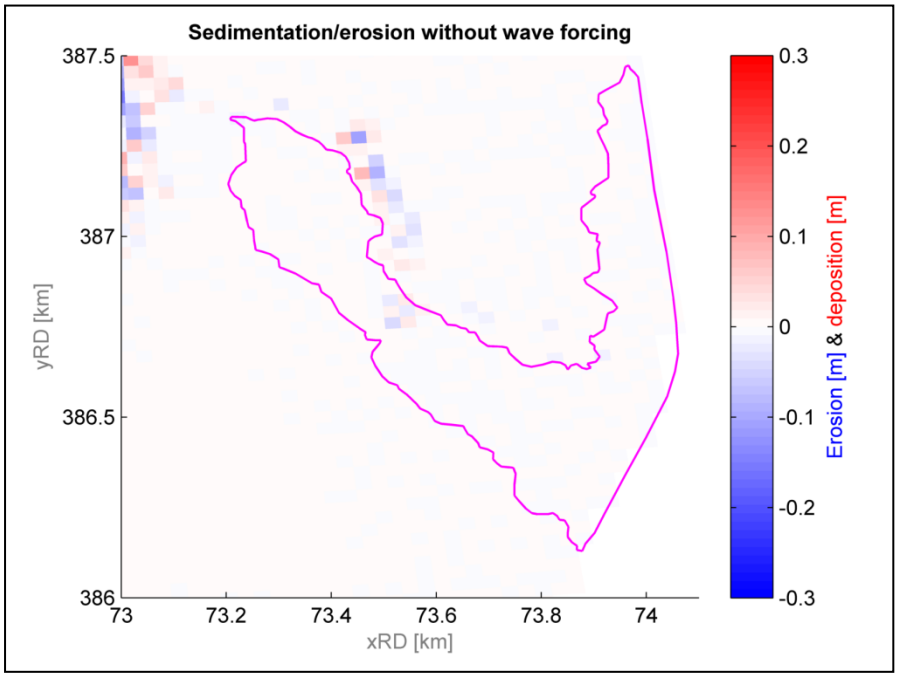

FIGURE 43: SEDIMENTATION-EROSION PATTERN FOR A SIMULATION WITHOUT WAVES.

Again, no significant morphological changes can be observed. So, hardly any sediment transport occurs when wave forcing is not included in the simulations. The initiation of sediment transport is thus dominated by wave behaviour. Wave breaking generally leads to stirring of sediment, thereby taking it into suspension. Figure 44 shows that sediment transport on top of the nourishment is larger when wave heights are larger (and more wave energy is dissipated by breaking). Importantly, sediment transport tends to become very small when wave height is lower than 20 cm. Therefore, the impact of waves on the nourishment is significant. Breaking of waves on the nourishment leads to suspended sediment transport. Flow due to tidal currents is only able to transport sediment east of the nourishment hook. In previous sections, it was already identified that large velocities occur at this location.

The morphological changes observed in Figure 42 are slightly smaller than the changes observed in Figure 43. Wind-driven flow was included in the simulation of the latter and probably causes sediment transport. Therefore, the influence of wind is discussed in the next section.

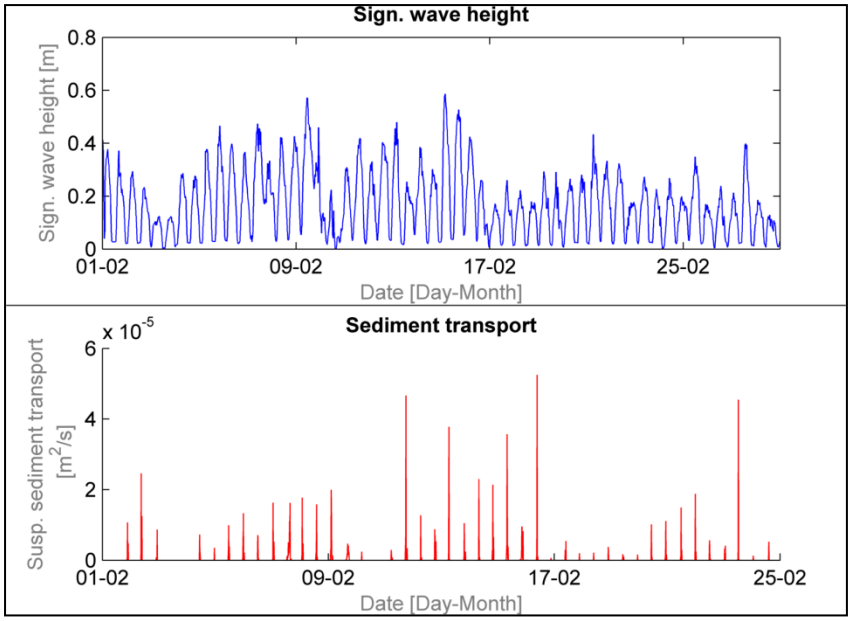

FIGURE 44: SIGNIFICANT WAVE HEIGHT VERSUS SEDIMENT TRANSPORT ON TOP OF THE NOURISHMENT.

6.3 Influence of wind

During the development of the Scaloost-model, it was already found that the simulation of wave behaviour strongly depends on the choice of which wind field is used as input (appendix III.2). Measuring station Marollegat is located in the middle of the 'Kom'-area, where the Oesterdam is situated. As this is the only station in the region, wind data from this station was used as input for the Oesterdam-model.

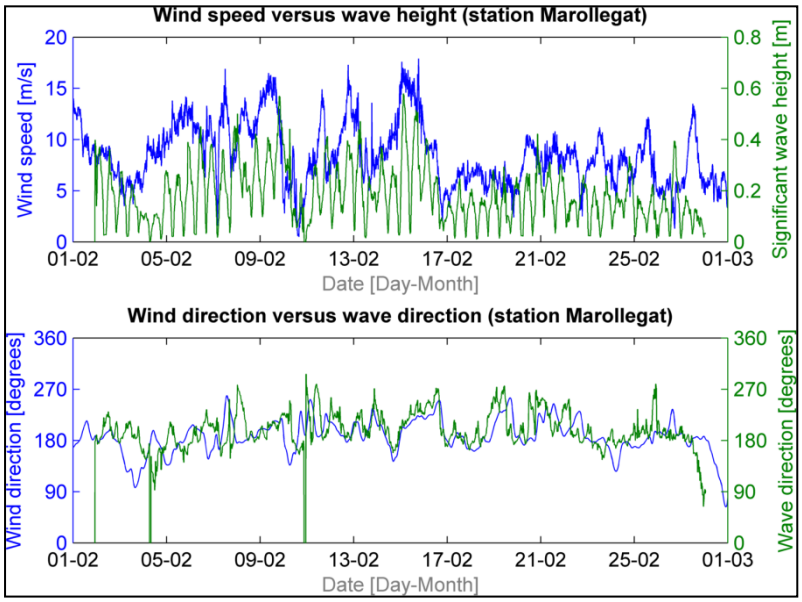

FIGURE 45: WIND SPEED AND DIRECTION VERSUS WAVE HEIGHT AND DIRECTION.

Figure 45 shows plots of wind speed and direction as well as wave height and direction near the Marollegat station. It can be observed that large wind speeds often lead to larger wave heights; also the wave direction is often similar to the wind direction.

Wind speed and direction are plotted against simulated wave height and direction in Figure 46. It can be seen that a correlation exists between wind speed and significant wave height and especially between wind direction and wave direction. The direction of the wind is very important for the direction of waves. A northern directed wind will result in northern directed waves. The correlation between wind speed and

significant wave height is less distinct, because depth, fetch and duration of wind stresses also play important roles (see Brettschneider method). However, generally large wind speeds generally result in large wave heights.

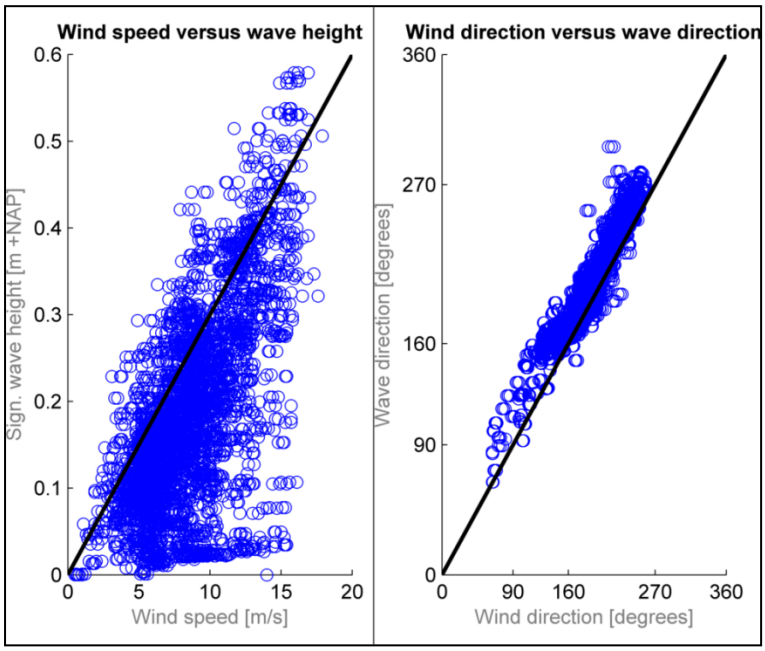

FIGURE 46: CORRELATION BETWEEN WIND AND WAVE CHARACTERISTICS. BLACK LINE REPRESENTS THE 1:1 RELATION.

Besides the generation of waves, wind stresses can also lead to currents. This wind-driven flow might be important. Le Hir et al. (2000) identify wind-driven flow as a main driver of sediment transport near intertidal areas. Therefore a simulation was performed including waves but without wind-driven currents (case B.3). The corresponding sedimentation-erosion-patterns can be found in Figure 47. 3 months of morphological developments are simulated.

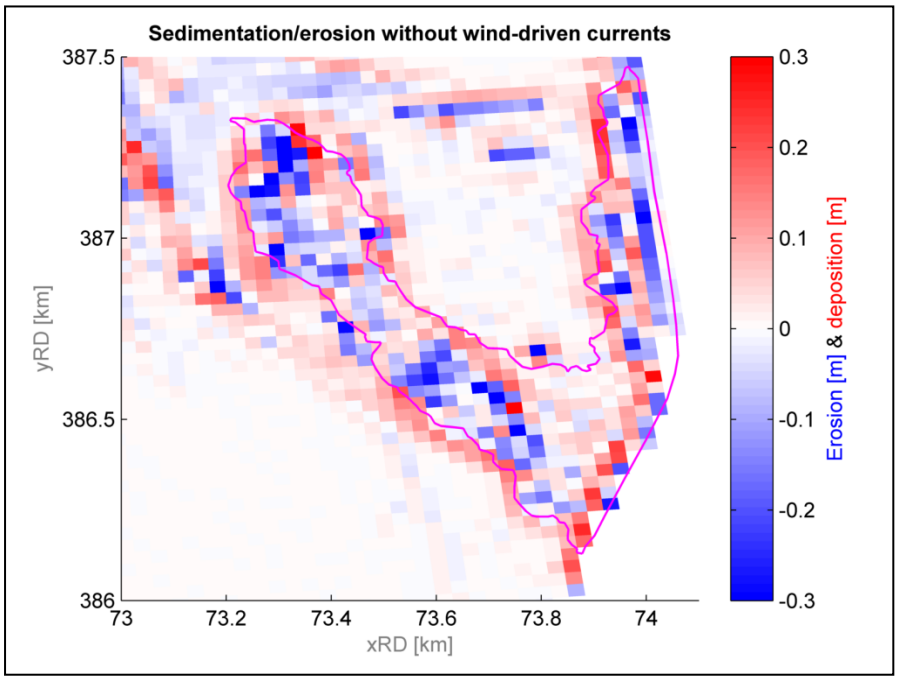

FIGURE 47: SEDIMENTATION-EROSION PATTERN FOR A SIMULATION WITHOUT WIND-DRIVEN CURRENTS.

When looking at these patterns, no distinct deviations can be seen with respect to the results from the simulation using tides, waves and winds (for example Figure 27). This suggests that wind-driven currents are not important. However, plots of cumulative sediment transport (Figure 48) show that the direction of sediment movement has changed in cross-section 3. While Figure 38 showed that sediment is transport out of the sheltered area, Figure 48 shows that sediment is imported in the sheltered area. It seems therefore that wind-driven currents are responsible for transporting sediment from the sheltered area towards the northern edge of the tidal flat. However, in a situation with tides and wind but without waves (section 6.2), hardly any transport is observed in the sheltered area. Probably, wind-driven flow only leads to transport if waves have brought the sediment into suspension. The wind-driven flow is thus partially responsible for the sediment transport on the tidal flat.

The behaviour observed in cross-section 7 is similar to the behaviour observed when the simulation includes all types of forcing, although total transport is slightly lower. Wind-driven currents are thus not very important for considering changes on the nourishment hook.

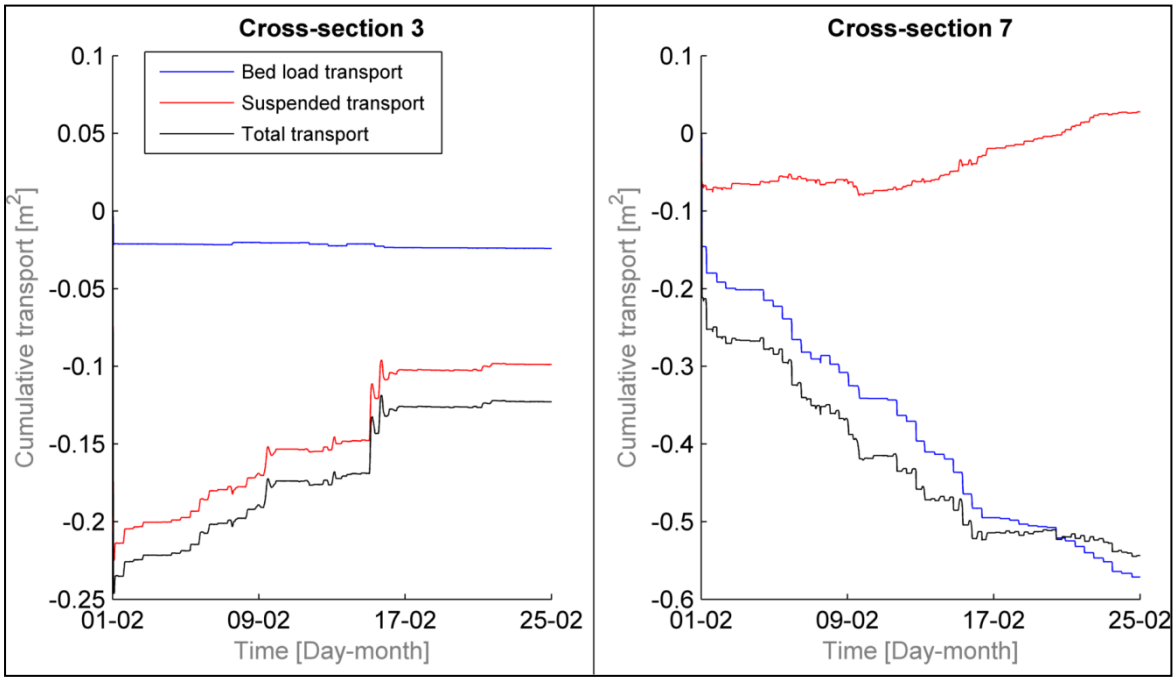

FIGURE 48: CUMULATIVE SEDIMENT TRANSPORT THROUGH CROSS-SECTIONS WITHOUT WIND-DRIVEN CURRENTS.

Last, wave-induced currents are important for the transportation of sediment stirred up by the breaking of waves. This statement is supported by Figure 47. The sediment that is eroded from the top of the nourishment is deposited directly near its edge. The main wave direction in these simulations is west. The movement of sediment towards the western edges of the nourishment is then partially caused by wave-induced currents, because tidal-driven and wind-driven currents cannot move large volumes of sediment.

6.4 Synthesis

Concluding, the morphological development of the Oesterdam nourishment is mainly controlled by wave behaviour, as was already identified by Das (2010) and Eelkema (2013). The nourishment has the tendency to erode on the top and transport the sand towards its edges. The sand on top of the nourishment is brought into motion by wave breaking and is transported towards the edges of the nourishment by tidal, wind-driven and wave-induced currents. This is a diffusive effect and shows that the system searches for a dynamic equilibrium situation. Wave breaking leads to initiation of sediment transport as sediment is stirred up. Sediment transport due to tidal- and wind-driven currents has a much smaller influence, although the area directly east of the nourishment experiences some erosion and

accretion. Tidal currents hardly influence the nourishment, while wind-driven currents account for a considerable part of the observed sediment transport on the tidal flat.

Tidal currents are however important directly east of the hook, where relatively large flow velocities cause transport of sediment towards the north. Measurements of the bed show the emergence of a small 'ebb-tidal delta' north of the tidal flat. The suspended material is not able to settle due to the large velocities and is transported to the north due to large velocities observed during ebb tide. A small but deep channel is therefore developing directly east of the nourishment. This channel is not observed in the model results; therefore its dynamics cannot be extensively discussed in this work. Chapter 4 already elaborated on the inaccuracy of the model to simulate the formation of this channel.

Besides the generation of currents, it was found that wind behaviour has a significant impact on the morphological developments. A strong correlation was found between wave direction and wind direction. A less distinct correlation was found between wave height and wind speed. However, as wind conditions vary throughout the year, the development of the nourishment strongly depends on the strength and direction of the wind.

7 Discussion

Previous chapter identified the main drivers of morphological changes near the Oesterdam nourishment. The findings of present work are discussed and reflected in this chapter.

Model assumptions

First, the validation shows that a small but constant underestimation of water levels can be observed, which could not be corrected during calibration. It is possible that this underestimation is already included in the boundary conditions of the Scaloost-model which are obtained from the extensively calibrated model DCSMv6-ZUNOv4. However, this model is only accurate at specific locations in the model. Some tricks were applied by the developers of this model to achieve a large accuracy at these locations. Therefore, the simulation of water levels at open sea (where the boundary of the Scaloost-model is situated) could be less accurate. Unfortunately, no validation data is available to assess the quality of the boundary conditions of the Scaloost-model.

Secondly, the use of a depth-averaged model does not affect the capabilities of the model. Water levels and flow velocities are simulated accurate, although a large underestimation was found for measuring location MP19. This is however caused by the resolution of the grid. A depth-averaged approach is thus valid for modelling hydrodynamics in basins with the same characteristics as the Eastern Scheldt.

Furthermore, it is assumed that the roughness is constant in the Scaloost- and Oesterdam-models. However, bed roughness is variable in both space and time. Especially for the Scaloost-model the assumption of a constant roughness is rather crude; bed roughness is likely to vary offshore and on the basin-side of the model. The implementation of a variable roughness should enlarge model accuracy. Also near intertidal areas the assumption of a uniform roughness field is possibly too strict. Ecological features like mussels and oysters as well as bed form features contribute locally to flow resistance (Walles, 2015). The same can be stated for the use of a uniform wind field. It was found that especially wave behaviour strongly depends on the wind field. Small deviations in wind input thus can lead to large deviations in wave simulation.

Next, only two sediment fractions were considered. There is however a considerable spatial variation in grain size distribution near the tidal flat as shown by the grain sizes measurements near the oyster reefs. Also, only non-cohesive sediment is included. Mulder & Louters (1994) state that mud flats exists in the Eastern Scheldt. It is unlikely that mud is important for the evolution of the nourishment as the nourishment consists of fine to medium grained sand. The absence of mud was confirmed during a field trip. However, mud can play a role when considering other flats in the Eastern Scheldt, as the properties of mud are different than the properties of non-cohesive materials such as sand.

In addition, according to the model, significant morphological changes continue to occur after the observed adjustment period of three months. It is too strict to fully ascribe this to model accuracy. As stated before, the usability of a MorFac depends on whether the representative tide correctly describes the hydrodynamics occurring in the morphological simulation period. Besides, other non-linear forces are not correctly summarized using MorFac. It is possible that the representative wind and wave fields consist of dynamics that are much stronger than in reality. This will lead to large morphological changes during a simulation, while in reality dynamics were much calmer in the same period.

Finally, large overestimations of bed level changes can be observed. The morphological developments within the model are much faster than observed in the field. While the large-scale morphodynamic processes are simulated in a correct way, the magnitude of erosion and deposition is largely overestimated. Therefore, the Oesterdam-model is not capable to answer questions concerning the durability of the nourishment. Different model settings and MorFacs were tested to decrease the

overestimation. However, the overestimation still occurred in all simulations. Therefore, a comparison between the developments of an autonomous situation and a situation with the nourishment is valid.

Simulation of wave height near intertidal areas

It was concluded that waves originating from the North Sea are not important when looking at hydro- and morphodynamic processes in the back of the Eastern Scheldt. Simulation of waves directly after the barrier cannot be validated, because there are no measuring stations in that area. For the present work this is not a problem. However, the Roggenplaat is another tidal flat that is going to be nourished (NOS, 2014). This flat is situated near the barrier. It is not known whether waves from the North Sea are important near for example the Roggenplaat. Therefore, when this nourishment is going to be monitored, it is important to focus on the measurement of both the magnitude and direction of the significant wave height near and on the tidal flat. These data are valuable for a validating a potential numerical model that covers the Roggenplaat.

Also, because the dataset with observed wave heights is questionable, it would be good to pay attention to the measurement instruments. It might be possible to calibrate the current equipment. The measurements near the Oesterdam were performed using pressure boxes. According to a study of Deltares (2014), those boxes have to be positioned high enough in the water column to keep the impact of the pressure limitation small. At the same time, they have to be positioned low enough to prevent the measuring instrument from surfacing. A compromise has to be found between these elements. Another conclusion was that the possible consequences of pressure limitation should be taken into account during data processing, as the consequence on measured wave heights and wave periods can be significant.

Furthermore, new state-of-the-art equipment can be used. Although expensive, it would increase the credibility of field data analyses and model results. For example, Boshenyatov et al. (2011) describe a method for measuring small-amplitude waves on a water surface. They reach a measurement accuracy of ±0.01 mm by using a device that makes use of a resistive sensor.

Resolution of grid

Some of the physical phenomena that were observed in the field could not be properly simulated using the Oesterdam-model. For example, the model is not able to recreate conditions that lead to the development of the channel east of the nourishment hook. This channel has a width of a few meters; a grid cell size of 30 m is thus too coarse to properly represent the depth of the channel. Therefore, a finer gridded model should be used when considering features of this dimension. However, computational capacity limits the use of fine gridded models as calculation time exceeds desired levels. Also, the structure of grids used in Delft3D does not allow for large spatial differences in grid resolution.

The use of a domain decomposition approach was tested. This method enables different grid resolutions in a model domain and is described in appendix VII. It was however not possible to implement this method for the models used in this work. Wave behaviour was simulated incorrectly and caused model instabilities. Deltares (2014) states that a domain decomposition approach might lead to instabilities due to dry cells. This is probably the case for the Oesterdam-model, as there are large intertidal areas present in the model domain. Therefore, it is not advised to use a domain decomposition approach for such an application.

8 Conclusions and recommendations

This chapter contains the conclusions of the present work in which the research questions are answered. Furthermore, recommendations are given.

8.1 Conclusions

Goal of present work was to identify the mechanisms that control the morphodynamic impact of the 2013 Oesterdam nourishment near an intertidal area in the Eastern Scheldt.

> *Q1: How well can Delft3D simulate the hydrodynamic processes and morphological developments near the nourishment?*

The Scaloost- and Oesterdam-models simulates the hydro- and morphodynamic processes accurately. When looking at water levels, the bias of the models ranges from 4 to 11 cm and unbiased Root Mean Square Errors varies between 8 and 12 cm. A small but constant overestimation of low tide leads to deviations in flow velocity simulation, although these deviations are acceptable. Wave heights are simulated accurately as the bias ranged between 3 and 12 cm, while the scatter index varies between 0.01 and 0.11 [-]; however there is a large discrepancy between the local measurements of wave height and the Oesterdam-model results. An overestimation of 20-25 cm can be observed. A manual calculation using the Brettschneider method indicates that the simulated wave heights show realistic behaviour. Therefore, the quality of the measurements is questionable. Also, flow velocities in a channel east of the hook are underestimated. The grid size is the origin of this discrepancy. The channel has a width of a few meters, while the grid size of one cell is 30 m. It is thus impossible to correctly represent the depth of the channel.

The morphological changes simulated in the Oesterdam are consistent with observations to a certain extent. The observed large-scale sedimentation-erosion-patterns can be identified in the model results, such as erosion of the top of the nourishment and accretion near the edges of the nourishment. More detailed features like the occurrence of a channel close to the nourishment hook are however simulated incorrectly. Also, the model overestimates bed level changes; 5-10 cm of the bed eroded in 6 months according to a long-term simulation, while in reality, the flat has eroded by 25 to 50 cm in the last 20 years. Therefore, it is not possible to make statements about the durability of the nourishment.

The hydrodynamics and the large-scale morphological patterns are thus well represented by the model. It can be concluded that the Scaloost- and Oesterdam-models are suitable to study the hydro- and morphodynamic processes near the Oesterdam nourishment.

> *Q2: What are the flow, wave, sediment transport and morphodynamic patterns in the area before and after construction of the nourishment?*

The processes that control the erosion of tidal flats in the Eastern Scheldt are identified. Tidal currents are not able to bring sediment towards the flat while the erosive processes did not change in magnitude. The spatial variation of flow velocities before construction of the nourishment is not large, as there are not distinct features on the tidal flat that restricts flow. Wave breaking and wind growth can be observed near the intertidal area. Waves partly break due to the sudden change in depth. Wind stresses can lead to wave growth on the tidal flat itself. Waves break at the Oesterdam, thereby dissipating all energy.

The effect of the Oesterdam nourishment on water levels, waves, flow velocities and sediment transport patterns is significant. Flow patterns changed, creating an area with large velocities east of the nourishment hook. These velocities occur because the elevated hook constricts water movement and leads to convergence of flow. Without taking this area in account, flow velocities near the nourishment

are largest during flood tide, which makes the area flood-dominated. The maximum observed flow velocity is 0.26 m/s. However, the small channel east of the nourishment is ebb-dominant and the maximum observed ebb flow velocity is 0.39 m/s. Furthermore, wave damping increased, as breaking of waves on the elevated parts of the nourishment leads to more energy dissipation. The nourishment protects the sheltered area behind the hook against wave attack.

Sediment transport patterns also changed considerably. Not only did the spatial distribution of bed shear stresses change (as they correlate with currents and waves), also a decrease in sediment transport was found in the sheltered area behind the hook of the nourishment. The increased wave breaking on top of the nourishment is responsible, since less wave energy reaches the sheltered area of the tidal flat and less sediment is taken into motion. Because of the additional wave damping, sediment transport rates on top of the hook increased. Consequently, gradients in the sediment transport rates leads to significant morphological changes on top of the nourishment. Suspended sediment transport is dominant in the area, except for the top of the nourishment hook where bed load is transport. This is explained by the much larger grain size of the nourishment.

If the nourishment was not constructed, the intertidal area would have continued to erode. In that case, sand will be transported towards the deeper parts of the Eastern Scheldt, leading to degradation of the intertidal area and larger wave attacks on the Oesterdam. The largest morphological changes after construction of the nourishment can be observed near its hook. Sediment is transported from the top of the hook towards the edges of the nourishment. This has a diffusive effect as the top of the nourishment is eroding, while deposition near its edges causes an expansion. Furthermore, a channel with locally high flow velocities causes sediment transport from the tidal flat towards its northern edge where an ebb-tidal delta is emerging. The sediment that is deposited near the edges by the diffusive effect is thus transported from the nourishment. The sheltered area behind the hook is relatively stable as hardly any morphological changes can be observed after the construction of the nourishment. The artificial oyster reefs show local sedimentation-erosion-patterns. Their influence however is limited.

Q3: What processes drive the morphodynamics of the nourished Oesterdam tidal flat?

The morphodynamics of the nourished Oesterdam tidal flat are mainly controlled by waves and indirectly by wind. Waves are identified as important contributors to sediment transport. Breaking of waves on top of the nourishment causes sediment stirring, which consequently results in initiation of motion. Wind conditions have a significant impact on the morphological developments. Correlations were found between wave direction and wind direction and between wave height and wind speed.

Wind-driven, wave-induced and to a lesser extent tidal currents transport the sand from the top of the nourishment towards its edges. Wind-driven currents are especially important for the sheltered area. If they were not present, sediment towards the more elevated areas of the tidal flat can be observed. This is however only observed when waves bring sediment into suspension. Currents due to tidal flow also affect the morphodynamics. Their impact is nevertheless smaller in comparison with wind-driven and wave-induced currents. Tidal currents are however important for the development of the channel east of the nourishment hook, as this channel drains the tidal flat after high tide.

Concluding, the morphological development of the nourishment depends largely on waves, as they are the main initiator of sediment transport. Sediment is spread from the more elevated parts of the nourishment towards the lower tidal flat. Indirectly, wave behaviour highly depends on the meteorological conditions occurring close to the Oesterdam as strong correlations were found between the existing wind conditions and wave height and direction. The importance of the tide has significantly reduced due to the construction of the storm surge barrier. Since the meteorological conditions cannot

be controlled, it will be difficult to predict the durability of the nourishment. However, it seems that nourishments are a promising measure, as the erosion rate of the tidal flat has decreased and the wave attack on the Oesterdam has reduced. However, still a lot of knowledge has to be obtained about the long-term effects of such interferences in coastal systems.

8.2 Recommendations

The local measurements of significant wave heights cannot be used to validate the Oesterdam-model because they are of insufficient quality. More attention should be paid towards measurement campaigns in the future. The usability of measurement instruments should be assessed. Calibration can improve the credibility of the measurements. The best solution is probably to purchase new and more accurate measurement instruments. Also, it is important that the measurements are performed simultaneously and the value of metadata should not be underestimated.

Furthermore, although the quality of the dataset is questionable, it is still possible that the simulation of wave behaviour near intertidal areas is not accurate. As waves are important drivers of sediment transport and morphodynamics in these regions, it is important to known whether the wave model is able to simulate the behaviour of waves correctly. Therefore, a study should be initiated that investigates the simulation of waves in intertidal areas using SWAN.

Next, the resolution of the Oesterdam-model grid was too coarse to simulate the evolution of distinct features near the nourishment. In future studies, the grid size should be adapted on basis of the smallest features that are to be modelled. Deltares is developing a new software package for hydrodynamic simulations that uses unstructured grids. This model (D-Flow Flexible Mesh) is able to spatially vary the resolution of the grid. Computational times would decrease significantly as fine grid sizes only have to be defined close to the area of interest.

Last, because certain phenomena are not well represented, the long-term development of the Oesterdam nourishment and tidal flat cannot be extensively studied using the Oesterdam-model. Knowledge about the durability of such nourishments is still too little and further research is recommended. Also, the influence of the nourishment configuration is unknown. For this nourishment, flow converges near the hook which leads to sediment transport towards the edge of the tidal flat, thereby creating an ebb-tidal delta. More nourishment projects are considered to mitigate the large-scale erosion in the Eastern Scheldt. The knowledge about the influence of nourishment location and size should be increased in order to optimize the effectiveness of those projects. Such studies should focus on finding representative conditions concerning tides and waves, as long-term modelling will involve some kind of method to accelerate morphological changes.

9 References

Berenbrock, C., & Tranmer, A.W. (2008). *Simulation of Flow, Sediment Transport, and Sediment Mobility of the Lower Coeur d'Alene River, Idaho.* Reston, Virginia: United States Geological Survey.

Boersema, M., De Vries, M.B., Bouma, T.J., Salvador de Paiva, J., Pesch, C., Van den Brink, A.M., et al. (2014). *Projectplan zandhonger suppletieprojecten: Deelproject: Monitoring veiligheidsbuffer Oesterdam.* Vlissingen: Centre of Expertise Delta Technology.

Boersema, M., Ysebaert, T., Bouma, T.J., Paree, E., Van der Werf, J.J., Salvador de Paiva, J., et al. (2015). *Zandhonger suppletieprojecten: Deelproject: Evaluatie monitoring veiligheidsbuffer Oesterdam eerste jaar na aanleg.* Vlissingen/Yerseke/Delft: Centre of Expertise Delta Technology.

Booij, N., Ris, R.C., & Holthuijsen, L.H. (1999). A third-generation wave model for coastal regions, Part I, Model description and validation. *Journal of Geophysical Research, C4*(104), 7649-7666.

Borsje, B.W., De Vries, M.B., Hulscher, S.J.M.H., & De Boer, G.J. (2008). Modeling large-scale cohesive sediment transport affected by small-scale biological activity. *Estuarine, Coastal and Shelf Science, 78*, 468-480.

Bosboom, J., & Stive, M.J.F. (2015). *Coastal Dynamics I.* Delft: Delft Academic Press.

Boshenyatov, B.V., Levin, Y.K., Popov, V.V., & Semyanistyi, A.V. (2011). A Method for Measuring Small-Amplitude Waves On a Water Surface. *Instruments and Experimental Techniques, 54*(2), 254-255.

Chow, V.T. (1959). *Open Channel Hydraulics.* New York: McGraw-Hill Book Co.

Clancy, R.M., Kaitala, J.E., & Zambresky, L.F. (1986). The Fleet Numerical Oceanography Center Global Spectral Ocean Wave Model. *Bulletin American Meteorological Society, 67*(5), 498-512.

Das, I.L.L.. (2010). *Msc thesis: Morphodynamic modelling of the Galgeplaat.* Delft: Delft University of Technology.

Davies, L. J. (1964). A morphogenic approach to world shorelines. *Zeitschrift Fur Geomorphologie, 8*(127), 127-142.

De Bok, C. (2001). *Long-term morphology of the Eastern Scheldt.* Rijkswaterstaat RIKZ, RIKZ/2002.108x.

De Bruijn, R.A. (2012). *Msc thesis: The future of the Oosterschelde with a new inlet channel.* Delft: Delft University of Technology.

De Ronde, J.G., Mulder, J.P.M., Van Duren, L.A., & Ysebaert, T. (2013). *Eindadvies ANT Oosterschelde. 1207722-000-ZKS-0010.* Delft: Deltares.

De Vriend, H.J., & Van Koningsveld, M. (2012). *Building with Nature: Thinking, acting and interacting differently.* Dordrecht: Ecoshape, Buidling with Nature.

Deltares. (2012). *Modelling of morphologic effects of a nourishment on the Galgeplaat in the Eastern Scheldt. 1002333-000-ZKS-0009.* Delft: Deltares.

Deltares. (2014). *Delft3D-FLOW. Simulation of multi-dimensional hydrodynamic flows and transport phenomena, including sediments. User Manual. Hydro-Morphodynamics.* Delft: Deltares.

Deltares. (2014). *Delft3D-WAVE. Simulation of short-crested waves with SWAN. User Manual. Hydro-Morphodynamics.* Delft: Deltares.

Deltares. (2014). *Nauwkeurigheid golfmetingen Petten. 1209433-011-HYE-0004.* Delft: Deltares.

Dissanayake, D.M.P.K., Wurpts, A., Miani, M., Knaack, H, Niemeyer, H.D., & Roelvink, J.A. (2012). Modelling morphodynamic response of a tidal basin to an anthropogenic effect: Ley Bay, East Frisian Wadden Sea - applying tidal forcing only and different sediment fractions. *Coastal Engineering, 67*, 14-28.

Eelkema, M. (2013). *Doctoral thesis: Eastern Scheldt Inlet Morphodynamics.* Delft: Delft University of Technology.

Fletcher, M. (2012, 8 23). *Oosterscheldekering Sluice Gates - 1st section.* Opgehaald van Flickr: https://www.flickr.com/photos/mustangmark/7881753122

Friedrichs, C., & Aubrey, D. (1988). Non-linear tidal distortion in shallow well-mixed estuaries: a synthesis. *Estuarine, Coastal and Shelf Science, 27*(5), 521-545.

Google Earth. (2013, October 4). *Eastern Scheldt*. Opgeroepen op April 14, 2015, van Google Earth: http://www.earth.google.com

Hoogduin, L. (2009). *MSc. thesis: Sediment transport through the Eastern Scheldt storm surge barrier.* Delft: Delft University of Technology.

Howard, K.L., Zarillo, G., Splitt, M., Lazarus, S., Chiao, S., Santos, P., et al. (2009). The impact of atmospheric model resolution on a coupled wind/wave forecast system. *The 16th Conference on Air-Sea Interaction.* Phoenix, AZ, January 11-15, 2009.

Huisman, B.J.A., & Luijendijk, A.P. (2009). *Sand demand of the Eastern Scheldt: morphology around the barrier.* Delft: Deltares.

Ikeya, V.K. (2014). *Internship report: morphodynamics and sediment transport at the Oesterdam sand nourishment.* Vlissingen: Delta Academy, HZ University of Applied Science.

Jacobse, J.J. (2005). *Zandhonger Oosterschelde. Rode draad uit de workshop van 29 oktober 2005.* Rotterdam: Royal Haskoning.

Kohsiek, L.H.M., Mulder, J.P.M., Louters, T., & Berben, F. (1987). *De Oosterschelde naar een nieuw onderwaterlandschap. Eindrapport project GEOMOR, Nota GWAO-87.029.* Den Haag: RWS Dienst Getijdewateren.

Le Hir, P., Roberts, W., Cazaillet, O., Christie, M., Bassoullet, P., & Bacher, C. (2000). Characterization of intertidal flat hydrodynamics. *Continental Shelf Research, 20*(12-13), 1433-1459.

Lesser, G.R., Roelvink, J.A., Van Kester, J., & Stelling, G.S. (2004). Development and validation of a three-dimensional morphological model. *Coastal Engineering, 51*(8-9), 883-916.

Louters, T., Van den Berg, J.H., & Mulder, J.P.M. (1998). Geomorphological Changes of the Oosterschelde Tidal System during and after the Implementation of the Delta Project. *Journal of Coastal Research, 14*(3), 1134-1151.

Mulder, J.P.M., & Louters, T. (1994). Changes in basin geomorphology after implementation of the Oosterschelde estuary project. *Hydrobiologia, 282/283*, 29-39.

Nash, J.E., & Sutcliffe, J.V. (1970). River flow forecasting through conceptual models part I - A discussion of principles. *Journal of Hydrology, 10*(3), 282-290.

Nederpel, A., & Van Balen, W. (2012). *Bureaustudie ter validatie van golfgroeiformules voor gelimiteerde strijklengte. Voor veiligheidstoetsing van regionale keringen. Concept. PR2160.20.* Delft: HKV Lijn in Water.

NOS. (2014, 11 18). *Roggenplaat bij Oosterschelde gered*. Opgeroepen op July 25, 2015, van NOS.nl: http://nos.nl/artikel/2004369-roggenplaat-bij-oosterschelde-gered.html

Pawlowicz, R., Beardsley, B., & Lentz, S. (2002). Classical tidal harmonic analysis including error estimates in MATLAB using T_TIDE. *Computers & Geosciences, 28*, 929-937.

Pritchard, D.W. (1967). *"What is an estuary: physical viewpoint" 83.* Washington D.C.: American Association for the Advancement of Science.

Pugh, D.T. (1987). *Tides, Surges and Mean Sea-Level: a handbook for engineers and scientists.* Chichester: Wiley.

Rijkswaterstaat. (2013). *Oosterschelde: aanpak zandhonger.* Opgehaald van Rijkswaterstaat: http://www.rijkswaterstaat.nl/water/plannen_en_projecten/vaarwegen/oosterschelde/oosterschelde_zandhonger/index.aspx

Rijkswaterstaat. (2015, April 22). *Dataleveringen*. Opgeroepen op April 22, 2015, van Waterberichtgeving: http://waterberichtgeving.rws.nl/nl/water-en-weer_dataleveringen.htm

Rogers, K., & Woodroffe, C.D.(2012). Incorporating estuaries as a source or sink of sediment within assessments of coastline risk and adaptation to climate change. *21st NSW Coastal Conference Papers* (pp. 1-16). Australia: ACS.

Shields, A.F. (1936). Application of similarity principles and turbulence research to bed-load movement, vol 26. *Mitteilungen der Preussischen Versuchsanstalt für Wasserbau und Schiffbau, Berlin, Germany*, 5-24.

Sumihar, J.H. (2013). *Integratie van metingen en modellen voor de waterstandsmonitoring in Zeeland: het frequenter draaien van RWsOS Noordzee.* Delft: Deltares.

Sutherland, J., Peet, A.H., & Soulsby, R.L. (2004). Evaluating the performance of morphological models. *Coastel Engineering, 51*(8-9), 917-939.

Van der Werf, J.J., Reinders, J., & Van Rooijen, A.A. (2013). *Evaluatie Galgeplaat proefsuppletie 2008-2012.* Delft: 1206994-000, Deltares.

Van der Werf, J.J., Reinders, J., Van Rooijen, A.A., Holzhauer, H., & Ysebaert, T. (2015). Evaluation of a tidal flat sediment nourishment as estuarine management measure. *Ocean & Coastal Management, 114*, 77-87.

Van der Westhuysen, A. J.(2011). Improved modelling of wave-current interaction in SWAN. *Coastal Engineering Proceedings, 1*(32), waves.45.

Van Duin, M..J.P., Wiersma, N.R., Walstra, D.J.R., Van Rijn, L.C., & Stive, M.J.F. (2004). Nourishing the shoreface: observations and hindcasting of the Egmond case, The Netherlands. *Coastal Engineering, 51*(8-9), 813-837.

Van Rijn, L.C. (1993). *Principles of Sediment Transport in Rivers, Estuaries and Coastal Seas, Part 1 .* Amsterdam: Aqua Publications.

Van Rijn, L.C. (2001). *General view on sand transport by currents and waves: data analysis and engineering modelling for uniform and graded sand (TRANSPOR 2000 and CROSMOR 2000 models. Z2899.29/Z2099.30/Z2824.30.* Delft, The Netherlands: WL | Delft Hydraulics.

Van Rijn, L.C. (2007). Unified view of sediment transport by currents and waves. 1. Initiation of motion, bed roughness and bed-load transport. *Journal of Hydraulic Engineering, 133*(6), 649-667.

Van Rijn, L.C., Roelvink, J.A., & Horst, W. (2000). *Approximation formulae for sand transport by currents and waves and implementation in DELFT-MOR.* Tech. Rep. Z3054.40, Delft, The Netherlands: WL | Delft Hydraulics.

Van Rijn, L.C., Walstra, D.J.R., Grasmeijer, B., Sutherland, J., Pan, S., & Sierra, J.P. (2003). The predictability of cross-shore bed evolution of sandy beaches at the time scale of storms and seasons using process-based profile models. *Coastal Engineering, 47*(3), 295-327.

Van Zanten, E., & Adriaanse, L.A. (2008). *Verminderd getij: Verkenning naar mogelijke maatregelen om het verlies van platen, slikken en schorren in de Oosterschelde te beperken.* Middelburg: Rijkswaterstaat Zeeland.

Van Zanten, E., & Provoost, Y. (2013). *Memo: effect zandhonger op de steenbekledingen van de dijken van de Oosterschelde.* Middelburg: Rijkswaterstaat Zeeland.

Van Zanten, E., & Schaap, J. (2012). *Monitoringsplan Zandhongerproeven 2013-2018.* Middelburg: Rijkswaterstaat Zeeland.

Vroon, J. (1994). Hydrodynamic characteristics of the Oosterschelde in recent decades. *Hydrobiologia* 282-283 (1), 17-27.

Walles, B. (2015). *PhD Thesis: The role of ecosystem engineers in the ecomorphological development of intertidal habitats.* Wageningen, NL: Wageningen University.

Wang, Z.B., De Ronde, J.G., Van der Spek, A.J.F., & Elias, E.P.L. (2009). Response of the Dutch coastal system to (semi-) closures of tidal basins. *Proceedings of ICEC 2009*, *Vol. 1*, pp. 203-210. Sendai, Japan.

Wiegmann, N., Perluka, R., Oude Elberink, S.J., & Vogelzang, J. (2005). *Vaklodingen: de inwintechnieken en hun combinaties. Vergelijking tussen verschillende inwintechnieken en de combinaties ervan. Technical Report.* Delft: AGI-2005-GSMH-012. Adviesdienst Geo-Informatica en ICT (AGI).

Willems, A., & Webbers, P.B. (2003). Modelling a probabilistic safety management system for the Eastern-Scheldt storm-surge barrier, the basin and the surrounding dikes. In T. Bedford, & P. Van Gelder, *Safety and Reliability Vol. 2* (pp. 1713-1719). Lisse: Swets & Zeitlinger.

Wright, L.D., Gammisch, R.A., & Byrne, R.J. (1990). Hydraulic Roughness and Mobility of Three Oyster-Bed Artificial Substrate Materials. *Journal of Coastal Research, 6*(4), 867-878.

Zhang, X. (2012). *MSc Thesis: Modelling of nourishment strategies and impact of barrier closure on the Galgeplaat and Dortsman morphodynamics in the Eastern Scheldt.* Delft: UNESCO-IHE.

Zijl, F., Verlaan, M., & Gerritsen, H. (2013). Improved water-level forecasting for the Northwest European Shelf and North Sea through direct modelling of tide, surge and non-linear interaction. *Ocean Dynamics, 63(7)*, 823-847.

Appendices

Appendix I: Sources used

The following websites were used as data source:

- www.scopus.com
- www.sciencedirect.com
- www.scholar.google.com
- www.google.com (for example Rijkswaterstaat reports)
- http://kennisbank.deltares.nl

Furthermore, the following persons supplied data and literature:

- Jebbe van der Werf
- Lodewijk de Vet
- Meinard Tiessen
- Remco Plieger
- Caroline Gautier
- Matthijs Boersema
- Joao Salvador de Paiva
- Niels Alferink

Appendix II: Erosion and increased wave attack Eastern Scheldt

The figures in this appendix describe the erosion of the tidal flats in the Eastern Scheldt and the increase of wave attack after construction of the storm surge barrier.

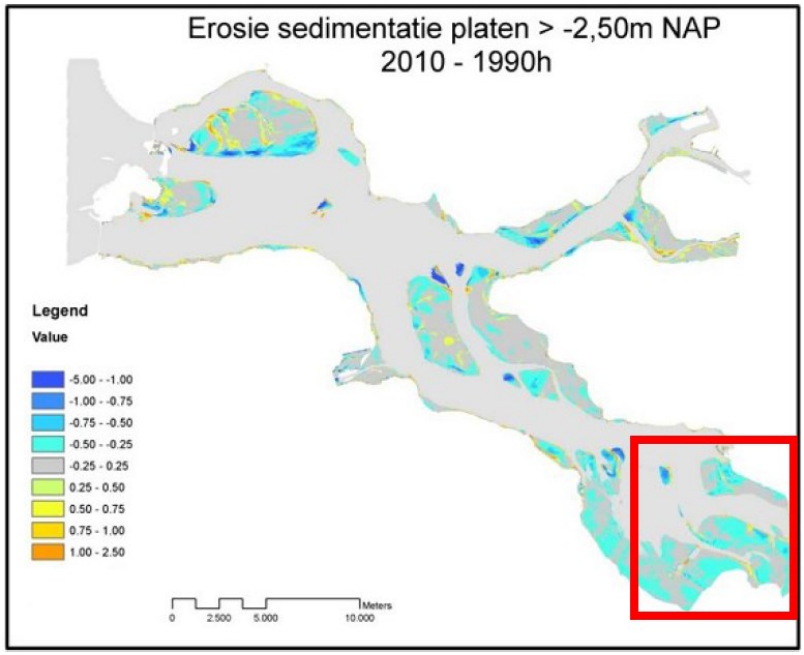

FIGURE 49: DEVELOPMENT OF INTERTIDAL AREAS IN THE EASTERN SCHELDT IN THE PERIOD 1990-2010 (DE RONDE ET AL., 2013). BLUE COLOURS INDICATE EROSION, RED AND YELLOW COLOURS INDICATE ACCRETION. RED BOX INDICATES OESTERDAM TIDAL FLAT AREA.

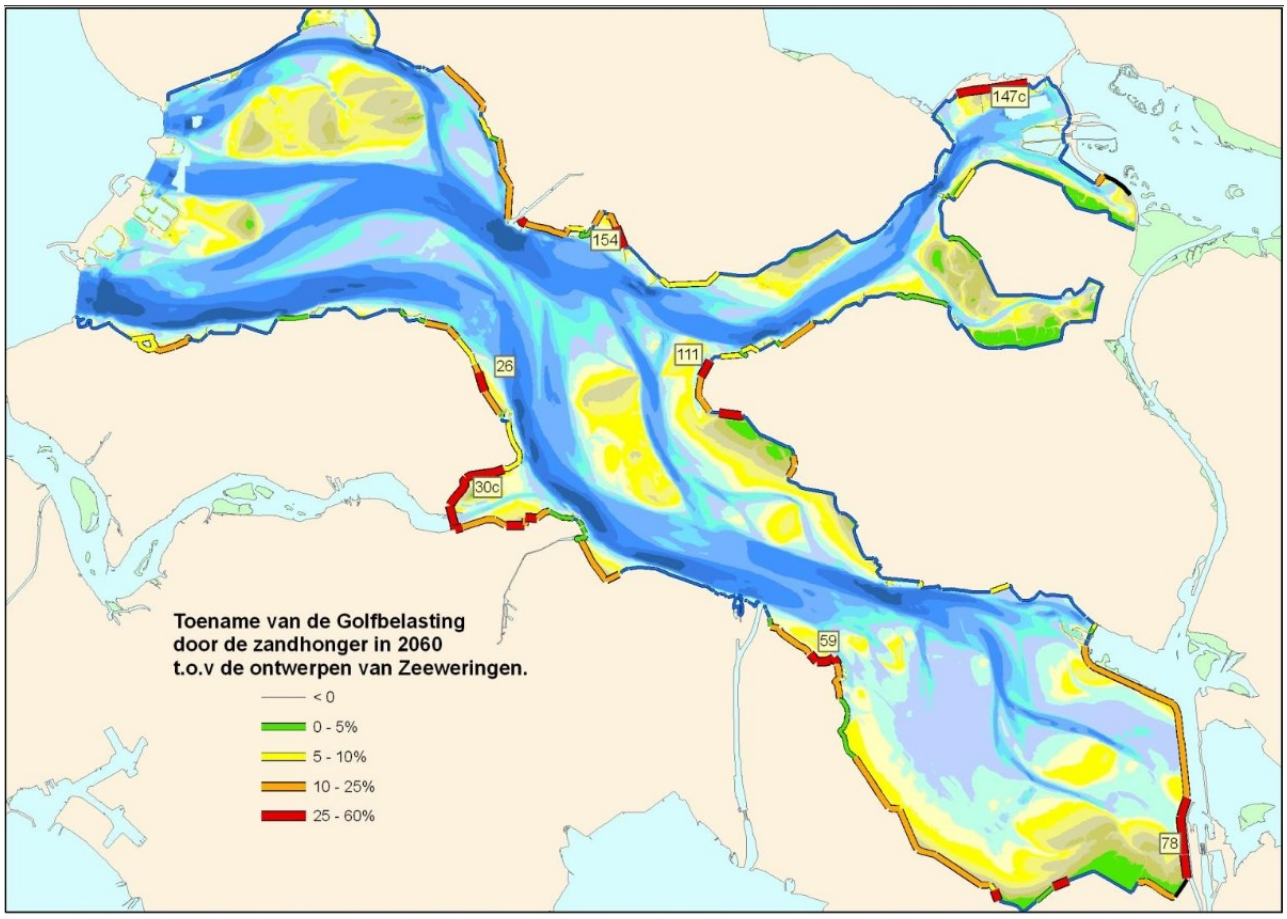

FIGURE 50: INCREASE OF WAVE ATTACK DUE TO THE SAND HUNGER IN 2060 (VAN ZANTEN & PROVOOST, 2013)

Appendix III: Detailed description of models

This appendix includes a more detailed description of Delft3D and elaborates on the model settings of the Scaloost- and Oesterdam models.

III.1 Description of Delft3D

Delft3D is a numerical process-based model that solves the non-linear shallow water equations derived from the three-dimensional Navier-Stokes equations for incompressible free surface flow. A finite-differences method is used in combination with a staggered grid, where water levels and flow velocities are defined at different locations; see Figure 51 for an example of such a grid.

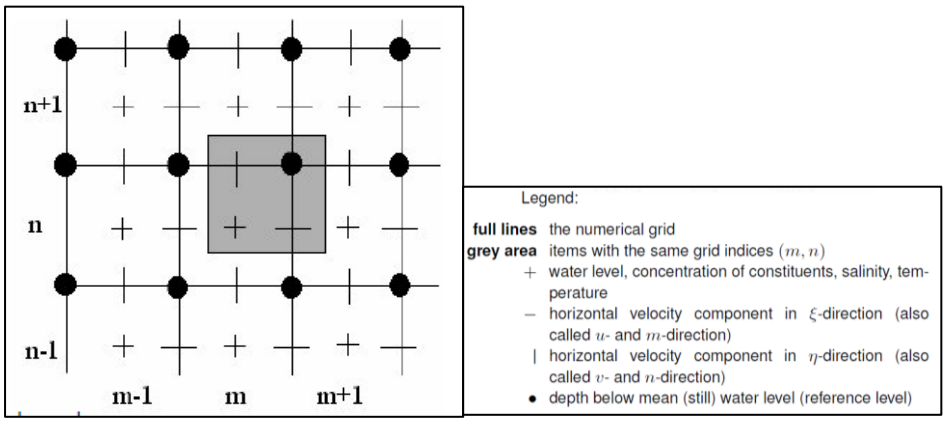

FIGURE 51: STAGGERED GRID IN DELFT3D (DELTARES, 2014).

Several modules are included in the package. The FLOW- and WAVE-modules are used in this work. The FLOW-module simulates non-steady flow and sediment transport resulting from tidal and meteorological forcing. (Deltares, 2014). The WAVE-module uses the SWAN-model to simulate the behaviour of waves (Deltares, 2014). It is possible to perform an online coupling. A feedback mechanism then exists between the two modules. A more detailed description of Delft3D can be found in Lesser et al. (2004) and Deltares (2014).

Motion of water is simulated by solving the depth-averaged unsteady shallow water equations. The following equations are included: the horizontal momentum equations, a continuity equation, a turbulence closure model (κ-ε), a sediment transport equation and a sediment continuity equation. The vertical momentum equation can be reduced to the hydrostatic pressure gradient relation; it is assumed that vertical accelerations are small compared to the gravitational acceleration. Therefore the FLOW-module of Delft3D is suitable for predicting flow in shallow seas, coastal areas and estuaries (Deltares, 2014).

The FLOW-module simulates a large number of processes, including tidal forcing at the open boundaries, wind shear stresses at the surface, wind-driven currents, wave effects on bed shear stresses, turbulence-induced mass and momentum fluxes, spatially varying bed shear stresses, drying and flooding of intertidal areas and flow through hydraulic structures. Also Coriolis forces are considered, although the effects of these forces are probably minor in the Eastern Scheldt basin (Das, 2010).

Wave behavior is simulated using the SWAN-model. A description of this model can be found in Booij et al. (1999). Important processes are among others wave breaking due to rapidly decreasing water depth that can lead to sediment transport and wave-induced mass fluxes. Wave breaking is modeled as a shear stress at the water surface. Furthermore enhanced bed shear stresses influence the flow simulation.

Wave-induced mass fluxes causing net onshore sediment transport are also included as additional turbulence production due to dissipation in the bottom wave boundary layer. White-capping is added as an extra production term in the κ-ε turbulence model. Wave growth is included, as are refraction and frequency shifts. Also, non-linear triad interactions are taken into consideration. Last, the occurrence of a wave-induced current in the direction of wave propagation is modeled as an additional shear stress in the bottom wave boundary layer.

III.2 Model settings

This section discusses more briefly the set-up of the Scaloost- and Oesterdam-models. Among others boundary and initial conditions, wind input is given.

Boundary conditions Scaloost-model

The open boundaries of the Scaloost-model can be found in Figure 52 (blue lines). The north-western boundary is represented by water levels; the other two boundaries are represented by current velocities. This approach is necessary, because using only water levels led to ill-posed boundaries and instability of the model. A small over- or underestimation of water levels results then in continuity problems that have to be compensated by an unrealistically large response of flow velocities (Deltares, 2014). In order to avoid the formation of artificial boundary layers near the boundaries of the grid, the keyword 'Cstbnd' is used in Delft3D. The advection terms near the boundaries that contain normal gradients are then switched off.

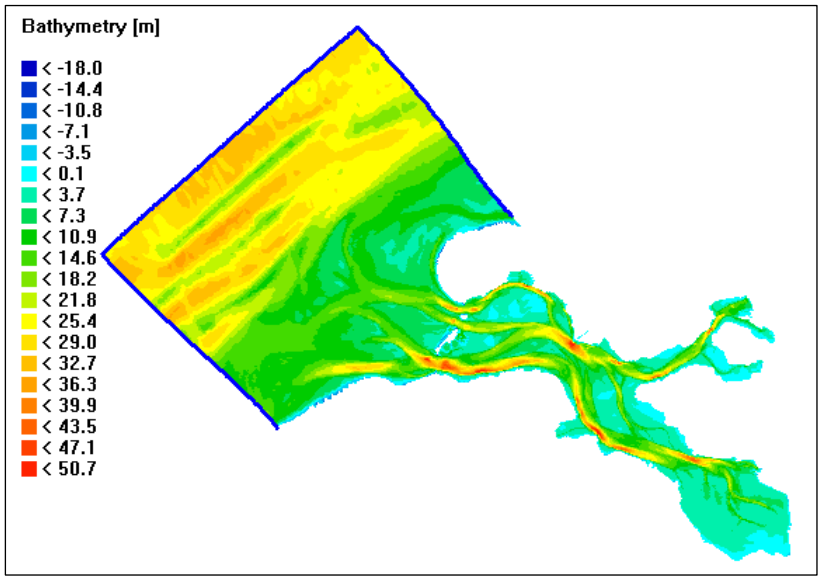

FIGURE 52: BATHYMETRY AND OPEN BOUNDARIES (BLUE LINES) OF SCALOOST-MODEL.

As stated earlier in this work, water levels and current velocities are retrieved from an overall North Sea-model: DCSMv6-ZUNOv4. Zijl et al. (2013) describe this model. This 2DH-model is actually a combination of the Dutch Continental Shelf Model version 6 (DCSMv6) and the ZUidelijke NOordzee model version 4 (ZUNOv4). This allows an increased grid resolution by means of domain decomposition. This approach is used to better match local spatial scales in the Dutch estuaries and Wadden Sea.

DCSMv6 has a grid size of 1.5'x1.0', which is approximately 2 km. The grid has a dimension of 1120x260 cells. ZUNOv4 has a variable grid size up to 200 to 400 m. The domain can be seen in Figure 53. The bathymetry is based on a NOOS (North West Shelf Operational Oceanographic System) gridded data set, supplemented by the ETOPO2 dataset and data from the Dutch hydrographical office. The boundary forcing is divided in two parts, tides and surges. 22 tidal constituents from a global tidal model (GOT00.2) are imposed at the open boundaries, including 8 main constituents, 6 smaller diurnal, semi-diurnal

constituents and an annual constituent Sa. Also surges are included as an inverse barometer correction based on temporal- and spatial-varying pressure fields. The meteorological forcing consists of wind speed and air pressure data obtained from the HIRLAM model provided by the KNMI. The Charnock-relation is used for calculating sea surface roughness.

DCSMv6-ZUNOv4 has a computational time step of 1 minute. The water level simulations are accurate with a Root Mean Square Error of 5 to 10 cm using data from the Dutch estuarine measuring stations. The simulated current velocities are not validated against observations.

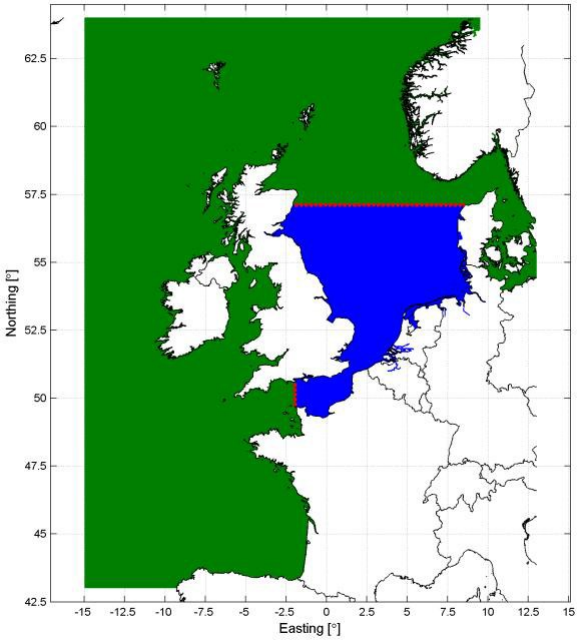

FIGURE 53: DOMAIN OF DCSMV6 (GREEN) AND ZUNOV4 (BLUE). RED DASHED LINE INDICATES INTERNAL BOUNDARY COUPLING (SUMIHAR, 2013).

Wave information obtained from wave measuring stations at sea is imposed on the boundaries of the Scaloost-model by means of a so-called wavecon-file (Deltares, 2014). Per time step, the significant wave height, the peak period and the wave direction are specified in this file.

The measuring station Schouwenbank offshore of the barrier provides a dataset that contains long time series of significant wave height, wave direction and peak period data. A uniform wave field is imposed at the boundaries each time step. Although this is not the most realistic approach and gives not the most accurate simulation quality, it significantly reduces calculation time. Also, the simulation of wind waves in the Eastern Scheldt basin itself will not be affected, as most sea waves are blocked by the barrier.

The spectrum ranges from 0.05 to 1 Hz and includes 24 frequency bins. The directional space consists of 36 directions. The spectra are specified as a JONSWAP-shape with a peak enhancement factor of 3.3 where the peak period is used and a cosine power defines the directional spreading.

Boundary conditions Oesterdam-model

The Oesterdam-model is nested in the Scaloost-model. Concretely this means that water levels retrieved from the Scaloost-model are imposed on the open boundary of the Oesterdam-model. The choice for imposing water levels instead of for example flow velocities is based on the ability of validation. The measuring station Yerseke is situated close to the open boundary. This station measures only water levels, so the correctness of the boundary conditions could be verified.

Besides hydrodynamic conditions, the open boundary also requires sediment transport conditions. The conditions that should be imposed are sediment concentrations. No data are available concerning sediment concentrations near this boundary. Therefore, Neumann boundary conditions were implemented. In this case, the flow enters the open boundary carrying sediment at their equilibrium concentration profiles. A zero sedimentation concentration gradient thus exists at the boundary. The use of this kind of boundary should prevent unrealistic large-scale deposition and erosion near the open boundaries (Deltares, 2014).

The WAVE-module uses the same open boundary as the FLOW-module. Wave conditions are imposed at this boundary using a wavecon-file. Furthermore, the same settings are used as in the WAVE-module of the Scaloost-model.

Initial conditions

Deltares (2014) states that for complicated bathymetries with large drying and flooding areas it is suggested to start simulations at high water. In this way, discrepancies between initial values and boundary conditions will be washed out of the system instead of propagating inward. Therefore, simulations are started at 1.5 m +NAP.

Wind

Wind is implemented in both Scaloost- and Oesterdam-models as a spatially uniform wind field that varies in time. The wind speed and direction measured at an elevation of 10 m above the free surface is used as suggested by Deltares (2014). The use of both wind data measured at the free surface and at 10 m above surface was investigated. The wind data measured at 10 m above the free surface indeed led to the best model behaviour. Wind data is retrieved from the measuring stations described in section 4.1.

Data retrieved from measuring station Stavenisse (STAV) proved to represent average values for the Scaloost-model. The accuracy of the wave simulation depends largely on which data source is used. The representative wind rose can be observed in the left part of Figure 54. The most important wind direction is southeast, while wind speeds vary between 2.5 and 10 m/s and peaks of maximum 15 m/s can be observed.

Wind data obtained from the Marollegat measuring station is representative for the Oesterdam-model. The corresponding wind rose can be found in the right part of Figure 54. The wind data of this station led to good simulation of wave behaviour in the area of interest. Again, the most important wind direction is southwest, while wind speeds vary approximately between 2.5 and 10 m/s. Larger maximum wind speeds are observed than for the Stavenisse data.

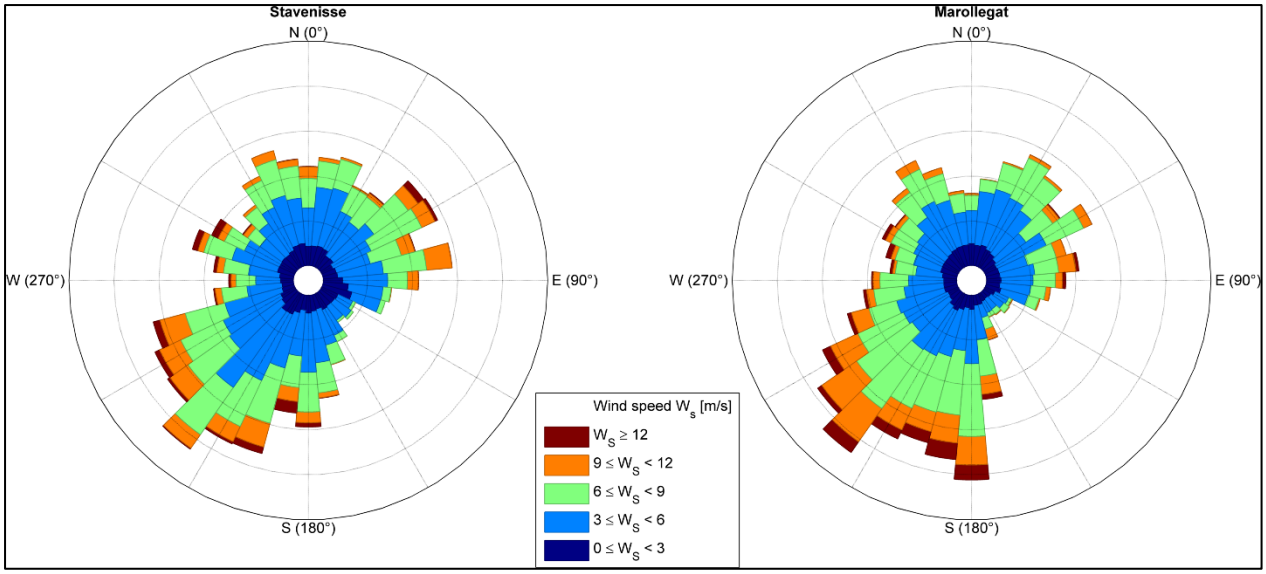

FIGURE 54: WIND SPEED AND DIRECTION AT MEASURING STATIONS: STAVENISSE (LEFT) AND MAROLLEGAT (RIGHT) (RIJKSWATERSTAAT, 2015).

Sediment transport and morphology

Sediment transport is enabled in both the Scaloost-and Oesterdam-models, while bed level updates are only enabled in the Oesterdam-model. The elevation of the bed is updated each half time step. Thus hydrodynamic flow calculations are performed using the correct bathymetry. A spin-up period of 12 hours is required. During this period, the hydrodynamic behaviour of the simulation can be initialized. After these 12 hours, the model is allowed to update its bathymetry. The formulations of Van Rijn (1993) for non-cohesive sediment are used. Both bed-load and suspended transport is included. Aeolian and cohesive sediment transports are not considered in this work.

A distinction is made between the following types of transport: bed load transport due to currents and waves as well as suspended load transport due to waves. Sediment below a reference height is treated as bed load and above the reference height as suspended load. Sediment is entrained in the water column by imposing a reference concentration at the reference height (Deltares, 2014). Van Rijn et al. (2003) states that the magnitude of the bed load transport can be calculated using equation 6:

$$|S_b| = 0.006\rho_s w_s D_{50} M^{0.5} M_e^{0.7} \quad (6)$$

With:

TABLE 12: EXPLANATION BED EQUATION 6 (DELTARES, 2014).

Parameter	Description
ρ_s	Density of sediment [kg/m^3]
w_s	Fall velocity of grains [m/s]
D_{50}	Median diameter of grains [m]
S_b	Bed load transport [kg/m/s]
M	Sediment mobility number due to waves and currents [-]
M_e	Excess sediment mobility number [-]

The calculation of the bed load transport direction assumes that it is composed of a part due to currents ($S_{b,c}$) and a part due to waves ($S_{b,w}$). The first acts in the direction of the flow and the latter in the direction of wave propagation (Deltares, 2014). These components are computed according to:

$$S_{b,c} = \frac{S_b}{\sqrt{1 + r^2 + 2|r|cos\varphi}} \quad (7)$$

$$|S_{b,w}| = r|S_{b,c}| \quad (8)$$

$$r = \frac{(|U_{on}| - v_{cr})^3}{(|v_R| - v_{cr})^3} \quad (9)$$

Equation 7 calculates the direction of bed load transport due to currents, equation 8 calculates the direction of bed load transport due to waves.

TABLE 13: EXPLANATION EQUATIONS 7, 8 AND 9 (DELTARES, 2014).

Parameter	Description
U_{on}	Near-bed peak orbital velocity in direction of wave propagation [m/s]
v_{cr}	Critical depth-averaged velocity for initiation of motion [m/s]
v_R	Magnitude of an equivalent depth-averaged velocity computed from the velocity in the bottom computational layer, assuming a logarithmic velocity profile [m/s]
φ	The angle between current and wave direction [◦]

Suspended sediment transport is modeled using equation 10 (Van Rijn, 2001):

$$S_{s,w} = f_{SUSW}\gamma U_A L_T \quad (10)$$

TABLE 14: EXPLANATION EQUATION 10 (DELTARES, 2014).

Parameter	Description
$S_{s,w}$	Wave-related suspended transport [kg/(ms)]
f_{SUSW}	User-defined tuning parameter [-]
γ	Phase lag coefficient (= 0.2) [-]
U_A	Velocity asymmetry value [m/s]
L_T	Suspended sediment load [kg/m^2]

Oyster reefs and other bathymetric features

The oyster reefs are placed because of their possible function to hinder sediment transport. Therefore the reefs are modelled as un-erodible objects that locally heighten the bathymetry and increase bed roughness. The roughness is calculated as follows: According to Wright et al. (1990), the Nikuradse roughness height (k_s) of such a reef is approximately 0.3 m. This roughness height is converted to the roughness coefficient used in the present work. K_s is equal to a Manning's n coefficient of:

$$n = 0.04 k_s^{\frac{1}{6}} = 0.04 * 0.3^{\frac{1}{6}} = 0.032\ m^{\frac{1}{3}}/s \quad (11)$$

Equation 11 is known as the Strickler formula (Chow, 1959). A spatially varying roughness field is implemented in the Oesterdam-model. Locations with oyster reefs thus have a roughness of 0.032 s/m$^{1/3}$, whereas the rest of the grid cells have a roughness of 0.029 s/m$^{1/3}$ as was found during calibration of the Scaloost-model.

Furthermore, part of the nourishment situated within a couple of meters near the dam was re-profiled at the start of 2014, as already pointed out in section 2.4.1. Sand has been moved towards the west over a width of 1 m. This was done because a lot of sand was transported on top of the Oesterdam by the wind. This area however does not actively contribute to sediment transport processes near the hook. Therefore the re-profiling was not included in the Oesterdam-model, because of availability of time.

Morphological acceleration factor

Because morphodynamic time scales are much larger than hydrodynamic time scales, the MORFAC-method is implemented. This MORphological time scale FActor speeds up the morphological changes (Deltares, 2014). It is implemented by multiplying the erosion and deposition rates by the so-called MorFac. A MorFac of 1 results in the most realistic simulation. A MorFac of 2 accelerates the morphological simulation with a factor 2. So, if the hydrodynamic changes within one tidal cycle are simulated in the model, the morphological changes of 2 tidal cycles will be simulated. Zhang (2012) investigated the use of the MorFac-method when simulating morphodynamics near the Galgeplaat in the Eastern Scheldt. It was concluded that a MorFac of 48 or smaller gives acceptable results.

The MorFac should be used with caution. The hydrodynamic period must represent conditions that occur during the morphological time scale. For example, a stormy period of a month cannot be used to simulate morphological behavior throughout the year, as there are also calmer periods in a year. This problem is solved as follows. First, the full morphological time series of hydrodynamics is plotted, see Figure 55. Now this series is cut into pieces of a month. The statistical data of each month (median, 1st quartile and 3rd quartile) are compared. The month that represents the full time series the best is used as the hydrodynamic simulation period. This is known as the representative tide. For this case, the period December 1 2013 to June 1 2014 is the full time series. The month February has the best match and is thus chosen as the representative tide.

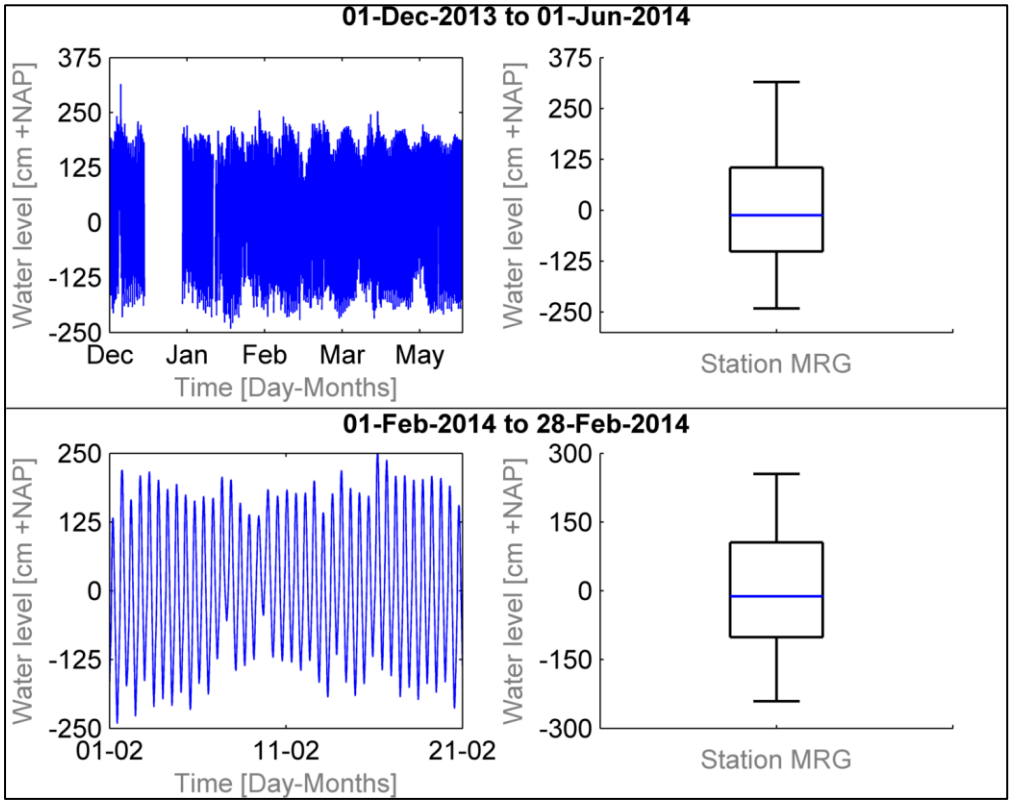

FIGURE 55: TIME SERIES WATER LEVEL AND BOX PLOTS.

Appendix IV: Measuring stations

The location of the measurement stations can be found in this appendix. Also, the type of variable they measure is given.

TABLE 15: DATA CONCERNING MEASURING LOCATIONS.

Name	Code	X-coord. (RD)	Y-coord.(RD)	water level	wind	wave
Brouwershavensegat 02	BG2	33140	421239	x	x	x
Domburger Rassen	DORA	17325	405275			x
Kats (Zandkreeksluis buiten)	KATS	49430	396103	x	x	
Marollegat (Oosterschelde)	MRG	71992	388510	x	x	x
Oosterschelde 4	OS4	37837	408813	x	x	x
Oosterschelde 11	OS11	23021	407778	x		
Oosterschelde 14	OS14	36827	415974	x		
Roompot (binnen) (SVKO)	RPBI	37226	404731	x		
Roompot (buiten) (SVKO)	RPBU	36931	404793	x		
Schouwenbank	SCHB	11332	419605			x
Stavenisse	STAV	59300	401630	x	x	
Yerseke (Oosterschelde)	YE	63701	391850	x		
Bergsediepsluis West	BDSL	69930	392386	x		

Appendix V: Validation

This appendix describes the calibration of the Scaloost-model, the re-calibration of the WAVE-module, the Brettschneider method, assessment of the simulation of flow velocities and the morphodynamic validation.

V.1 Calibration

The model is calibrated in such a way that the accuracy of the water level prediction is largest at the location of the Yerseke observation station. The boundary of the Oesterdam-model is situated close to this station. The calibration period is September 1 2013 to September 30 2013. The Root Mean Square Error and Nash-Sutcliffe coefficient are used as indicators of model accuracy. The energy loss coefficient and the bed roughness coefficient have to be calibrated.

Energy loss coefficient

First the concept of the energy loss coefficient is introduced. As stated before, the storm surge barrier is modelled in the FLOW-module as porous plates. The plates add a quadratic loss term (M_ξ or M_η) to the local momentum balance. The amount of mass and momentum exchanged through the plates is controlled by the so-called dimensionless energy loss coefficient. This relation is defined in x- and y-direction (equations 12 and 13):

$$M_\xi = -\frac{c_{loss,u}}{\Delta x} u\sqrt{u^2+v^2} \tag{12}$$

$$M_\eta = -\frac{c_{loss,v}}{\Delta y} v\sqrt{u^2+v^2} \tag{13}$$

With c_{loss} is the energy loss coefficient and u and v respectively the flow velocities in x- and y-directions. De Bruijn (2012) used a coefficient of 1.5 [-] for a detailed implementation of the storm surge barrier, while Hoogduin (2009) and Das (2010) used an energy loss coefficient of 2.3 [-] for a simpler implementation of the barrier. The latter is used as a first estimate for calibration. It was found that a coefficient of 2.6 results in the most optimal loss of mass and momentum near the barrier, see Figure 56.

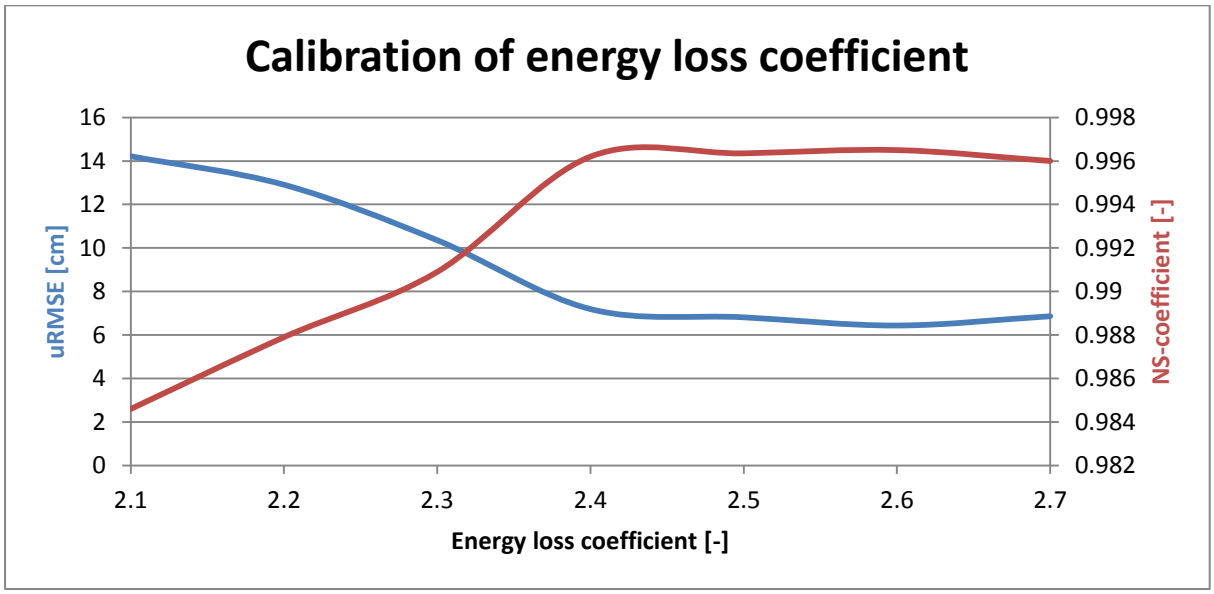

FIGURE 56: CALIBRATION OF ENERGY LOSS COEFFICIENT USING URMSE AND NS-COEFFICIENT.

Bed roughness

The bed roughness coefficient is also used as calibration parameter. Hoogduin (2009), Das (2010), De Bruijn (2012) and Eelkema (2013) used a Manning friction coefficient (n) of 0.025 $s/m^{1/3}$ for their

implementation of the Eastern Scheldt in Delft3D. Therefore, this parameter value was a good starting point for calibration. It was found that a value of 0.029 s/m$^{1/3}$ leads to the most representative simulation of flow for the Scaloost-model, see Figure 57.

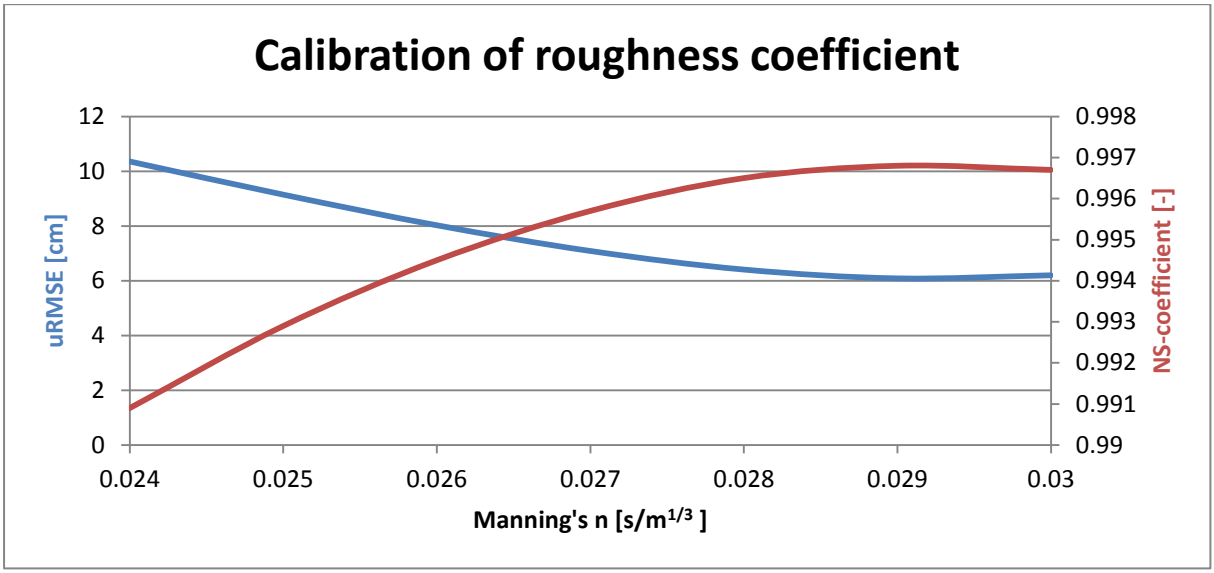

FIGURE 57: CALIBRATION OF ROUGHNESS COEFFICIENT USING URMSE AND NS-COEFFICIENT.

V.2 Definition of tidal amplitude and phase

Equation 14 describes the change of the water level at a specific location in time (Pugh, 1987):

$$\zeta_P(t) = \hat{\zeta}_n \cos(\sigma t - \phi) \tag{14}$$

With:

TABLE 16: EXPLANATION EQUATION 14.

Parameter	Description
ζ_P	Height of tidal wave at time t [m]
$\hat{\zeta}_n$	Amplitude of tidal component [m]
σ	Angular frequency of tidal component [rad/s]
ϕ	Phase of tidal component [rad]

V.3 Re-calibration of Delft3D-WAVE

Several options were considered to improve the simulation of waves near the tidal flat. For example, the frequency domain of SWAN was extended to include waves with a frequency of 2 Hz (SWAN has a default maximum frequency of 1 Hz). Also, the parameters that control depth-induced breaking and bottom friction for waves were varied without result.

Last, another formulation for white-capping was used. Instead of the default formulation in SWAN (Komen), the Van der Westhuysen-formulation was used. This formulation should lead to better behaviour in shallow regions like intertidal areas. The Komen-formulation overestimates wave heights under strong opposing currents due to insufficient steepness dissipation of waves on an opposing current gradient (Van der Westhuysen, 2011). The Van der Westhuysen-formulation uses another method of accounting for dissipation of waves on a counter-current gradient. The use of this formulation lead to small a decrease in wave height simulation, although the simulation of wave heights near the Oesterdam intertidal area still shows a discrepancy of 20-25 cm when compared to observed values.

V.4 Brettschneider method

The large overestimation of wave heights near the intertidal area could not be solved within the time limits of the present work. A manual calculation of wave height was performed to check the validitiy of the wave simulation. The Brettschneider method is used for this calculation (Nederpel & Van Balen, 2012). This method requires knowledge about the fetch length, water depth and wind speed. Three important parameters are considered, the dimensionless wave height, the dimensionless fetch length and the dimensionless water depth:

$$Dimensionless\ wave\ height = \frac{gH_s}{{U_{10}}^2}\ [-] \tag{15}$$

$$Dimensionless\ fetch\ length = \frac{Fg}{{U_{10}}^2}\ [-] \tag{16}$$

$$Dimensionless\ depth\ \delta = \frac{dg}{{U_{10}}^2} = [-] \tag{17}$$

With:

TABLE 17: DESCRIPTION BRETTSCHNEIDER METHOD (EQUATIONS 15, 16 AND 17).

Parameter	Description
g	Acceleration of gravity constant [m/s^2]
H_S	Significant wave height [m]
U_{10}	Wind speed at 10 m above the surface [m/s]
F	Fetch length [m]
d	Water depth [m]

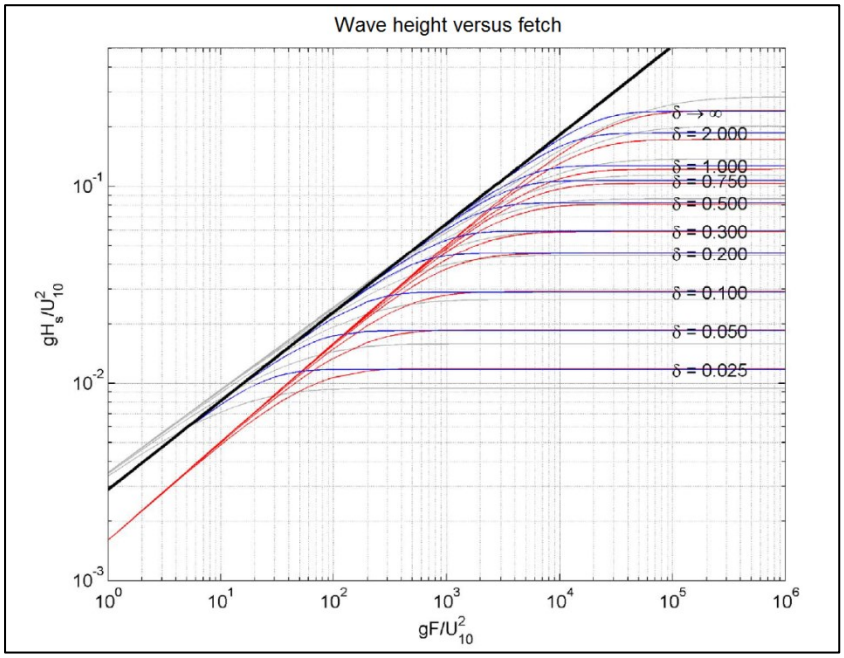

FIGURE 58: CURVES REPRESENTING THE RELATION BETWEEN DIMENSIONLESS WAVE HEIGHT AND DIMENSIONLESS FETCH. THICK BLACK LINE IS BRETTSCHNEIDER METHOD, BLUE AND RED LINES ARE OTHER METHODS (NEDERPEL & VAN BALEN, 2012).

The relation between the dimensionless wave height, fetch length and depth can be found in Figure 58. When fetch length, water depth and wind speed are known, significant wave heights can be approximated. This was done for three different conditions, with wind from three different directions

(west, east, south). Wind from the north does not occur very often, see Figure 54 in Appendix III.2. The input values (fetch length, water depth and wind speed) were retrieved from the Oesterdam-model input. The results can be found in Table 18. The table shows the wave height approximated by the Brettschneider method and wave height as simulated in the model. As can be seen, the magnitude of the wave heights is comparable. Although the Brettschneider is an approximation, it generally gives a good impression of the magnitude of the wave heights. Therefore, it can be concluded that the wave height measurements are questionable, as they never exceed values of 10-15 cm.

TABLE 18: RESULTS BRETTSCHNEIDER METHOD.

	Direction	**Fetch length [m]**	**Water depth [m]**	**Wind speed [m/s]**	**Wave height Brettschneider [cm]**	**Simulated wave height [cm]**
March 3 2014 06:00	South	1400	3.5	11.4	32	31
February 28 2014 13:00	West	900	2	4.6	9	12
February 25 201416:30	East	800	1	9.5	19	14

V.5 Results validation of flow velocities

This section contains information about the validation of the flow velocities near the local measuring points.

TABLE 19: RESULTS VALIDATION OF FLOW VELOCITY SIMULATION.

Measuring location	**uRMSE [m/s]**	**Bias [m/s]**	**NS [-]**
MP18	0.06	-0.03	0.11
MP19	-0.1	0.02	0.03
MP20	0.06	-0.06	0.43
MP21	-0.13	-0.03	-0.37
MP23	-0.08	-0.03	-0.70
MP24	-0.06	-0.04	-0.73

V.6 Quantitative validation of bed level simulation: Brier skill scores

Although the sedimentation/erosion patterns are visually compared in chapter 4, the similarities between two figures are not easy visible by the eye. Also, some features are not simulated in an acceptable way. Therefore, a quantitative way of validating bed level changes is introduced: the Brier Skill Score (BSS). This coefficient is used by Sutherland et al. (2004). It is defined as:

$$BSS = 1 - \frac{< \left(|z_{b,c} - z_{b,m}| - \Delta z_{b,m} \right)^2 >}{< \left(z_{b,0} - z_{b,m} \right)^2 >} \tag{18}$$

With:

TABLE 20: DESCRIPTION EQUATION (18

Parameter	Description
$z_{b,c}$	Calculated bed level [m +NAP]
$z_{b,m}$	Measured bed level [m +NAP]
$\Delta z_{b,m}$	Error of measured bed level [m]
$z_{b,0}$	Initial bed level [m +NAP]

The qualification of whether bed level changes are simulated in a reasonable way can be found in Table 21. A perfect simulation of bed level changes leads to a BSS of 1, while a BSS of 0 or lower indicates bad model performance. The BSS shows some similarities with the NS-coefficient used in this work. However, the BSS also includes a measurements error.

TABLE 21: QUALIFICATION OF ERROR RANGES BSS (VAN RIJN ET AL. (2003)).

Qualification	BSS
Excellent	1-0.8
Good	0.8-0.6
Reasonable/fair	0.6-0.3
Poor	0.3-0
Bad	<0

The measurement error of the dataset with bed level observations is 10 cm. Only bed level changes in the area around the nourishment are considered. In RD-coordinates, this area is situated from x = 73.2 km to x =74.2 km and from y = 386 km to y = 387.5 km. The Brier Skill Score of simulated bed level changes in the area is 0.01. This qualifies as a poor model simulation. However, the Brier Skill Score does not give information about the spatial variation of the discrepancy between simulated and observed values.

Therefore, the accuracy of simulated bed level changes is investigated for three different areas (Figure 26). These areas are the hook of the nourishment (area I), the sheltered tidal flat (area II), and the part of the nourishment close to the dam. Brier Skill Scores are respectively 0.22, 0.34, and -0.03. The part of the tidal flat close to the Oesterdam is simulated inaccurate. The Skill Score is below zero, which indicates that the baseline (the initial bed) is a better predictor of bed level changes. Skill Scores of the tidal flat itself (the hook and the sheltered area) show better values, although the prediction is still qualified as poor to reasonable. The Brier Skill Score of the entire area however does not fully represent the accuracy of the model as spatial variations are not taken into account.

Change of bed level along cross-sections

The bed level development along cross-sections is discussed in the next sections. The location of these cross-sections can be found in Figure 28 of chapter 5. Characteristic sections are 3 and 11, which overlap the most dynamic part of the nourishment, cross-section 6, which overlaps the gap in the nourishment and an oyster reef, and cross section 13, that overlaps the intertidal area. It is important to notice that cross-sections 1 to 9 start in the west and cross-sections 10-15 start in the north.

The changes in these sections can be seen in Figure 59. Cross-section 3 is situated on the top of the hook and cross-section 6 in the gap of the hook. It can be seen that significant changes are visible in cross-section 3 both in the simulation and observations. Part of the sediment has moved towards the edges of the nourishment (x = 100 m and x = 300 m). Cross-section 6 is relatively stable and hardly any deposition and erosion is observed in both the observed and simulated section.

Figure 59 also shows the bed level changes in cross-section 11. Especially at x = 100, some major deviations can be observed between observed and simulated bed level changes. While both bed levels decrease with respect to the initial situation (T0), the simulated bed level shows a much stronger erosion rate (20 versus 50 cm). Also an accreting area can be found at x = 200 m when looking at the simulated cross-section. The nourishment thus shows diffusive behaviour in the model.

The change of bed levels in the sheltered region behind the nourishment can be seen in cross-section 13. The bed level of the tidal flat itself (x = 100 m to x = 600 m) is stable in both simulated and observed cross-sections. Again, the nourishment is mainly eroding (x = 800 m), although its erosion rate is overestimated by 20 cm. Concluding, the model roughly identifies the regions with large-scale erosion and deposition rates in a correct way, although their magnitude is overestimated by approximately 20 cm.

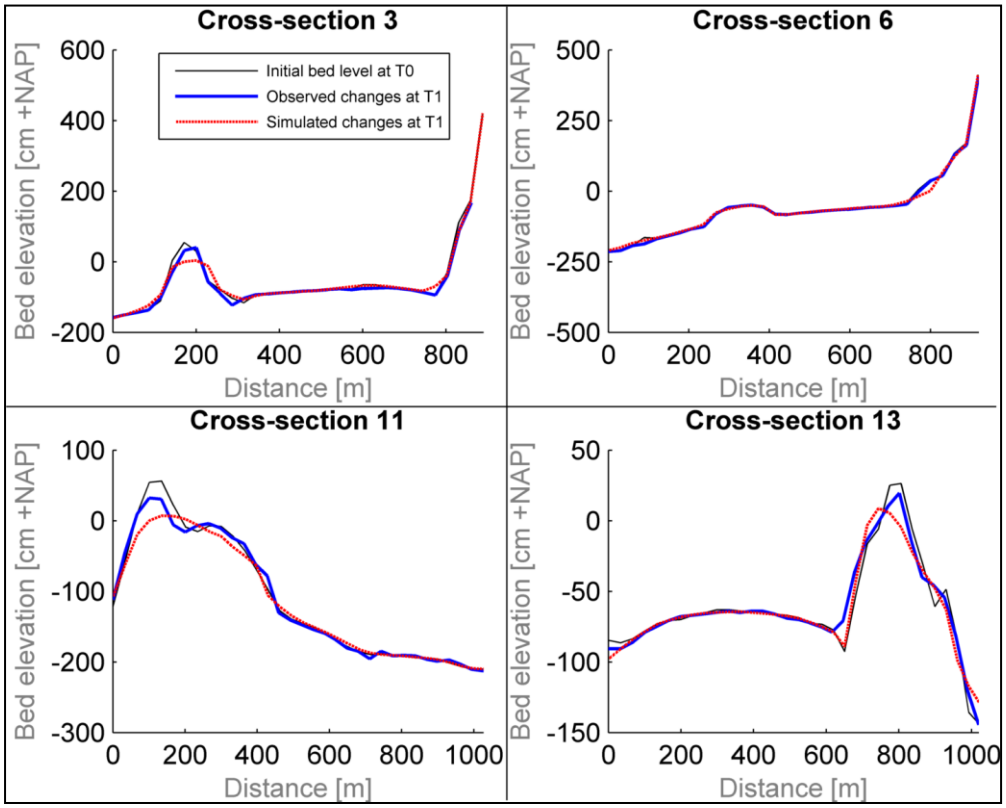

FIGURE 59: BED LEVEL CHANGES ALONG CROSS-SECTIONS IN PERIOD DECEMBER 1 2013 (T0) – FEBRUARY 18 2014 (T1).

Appendix VI: Definition of initiation of sediment transport and cross-sections

This appendix gives an introduction to the initiation of sediment transport and defines cross-sections that are used for sediment transport analyses.

VI.1 Initiation of sediment transport

A coefficient that plays an important role when calculating the initiation of motion for sediment is the Shields parameter (Shields, 1936). This parameter shows the relation between the flow and gravity forces working on a grain. It is defined as equation 19:

$$\theta = \frac{\tau}{(\rho_s - \rho) g D_{50}} \tag{19}$$

The terms in this equation are explained in Table 22:

TABLE 22: DESCRIPTION EQUATION 19.

Parameter	Description
θ	Dimensionless Shields parameter for specific grain [-]
τ	Bed shear stress [N/m^2]
ρ_s	Density of sediment [kg/m^3]
ρ	Density of water [kg/m^3]
g	Acceleration of gravity constant [m/s^2]
D_{50}	Median grain size [m]

Sediment transport is initiated when bed shear stresses exceed a specific critical value. This critical bed shear stress varies for different grain sizes and the flow pattern near the bed. An overview of values for the critical bed shear stress can be found in Table 23. Note that these are case-specific values and can vary in other situations due to for example the presence of bed forms. The median grain size of the Oesterdam-area is approximately 0.18 mm, leading to a critical shear stress of 0.145-0.194 N/m^2.

TABLE 23: CRITICAL BED SHEAR STRESS BY GRAIN SIZE CLASSIFICATION (BERENBROCK & TRANMER, 2008).

Particle	Diameter [mm]	Shields Parameter [-]	Critical bed shear stress [N/m2]
Coarse sand	0.5-1	0.033-0.029	0.27-0.47
Medium sand	0.25-0.5	0.048-0.033	0.194-0.27
Fine sand	0.125-0.25	0.072-0.048	0.145-0.194
Very fine sand	0.0625-0.125	0.109-0.072	0.110-0.145

VI.2 Definition of cross-sections used for sediment transport calculations

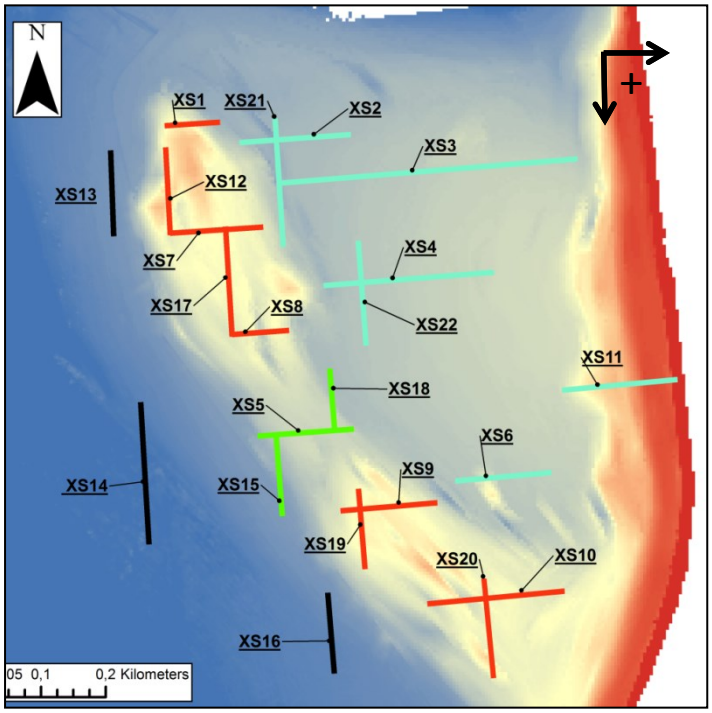

FIGURE 60: CROSS-SECTIONS USED FOR DETERMINING SEDIMENT TRANSPORT. BLACK SECTIONS REPRESENT THE DEEPER PART OF THE TIDAL FLAT, RED SECTIONS THE NOURISHMENT ITSELF, GREEN SECTIONS THE GAP IN THE NOURISHMENT AND BLUE SECTIONS THE SHELTERED AREA. POSITIVE SEDIMENT TRANSPORT INDICATES TRANSPORT TOWARDS THE WEST AND SOUTH.

Appendix VII: Domain decomposition method

Initially, a domain decomposition approach was tested for Oesterdam model. This technique is used to divide a model into smaller model domains. Communication between the domains takes place along the so-called domain-decomposition boundaries (Deltares, 2014). This allows for a local refinement of a grid. One important requirement is that grid lines in the coarse domain should be continued in the fine domain. The computation is then carried out separately on each of those domains. The advantages of a multi-domain modelling approach are the possibility of coupling different models, increase the accuracy of the model in the area of interest and increase the modelling efficiency by a parallel execution of the computations on different domains. The 'Domain Decomposition toolbox' is only available for Delft3D-FLOW, not for WAVE. For more information, one is referred to the Delft3D-FLOW manual (Deltares, 2014).

The grids of the different domains can be found in Figure 61. The coarse grid (Oesterdam A) has a resolution of 70x30 m in the western parts and 50x45 m in the eastern parts. The finer grid (Oesterdam B) has a resolution of 15x15 m in the entire domain. Unfortunately, this approach led to model instabilities. Especially the simulation of waves became very instable. Therefore, this approach was not implemented in the Oesterdam-model used in this work.

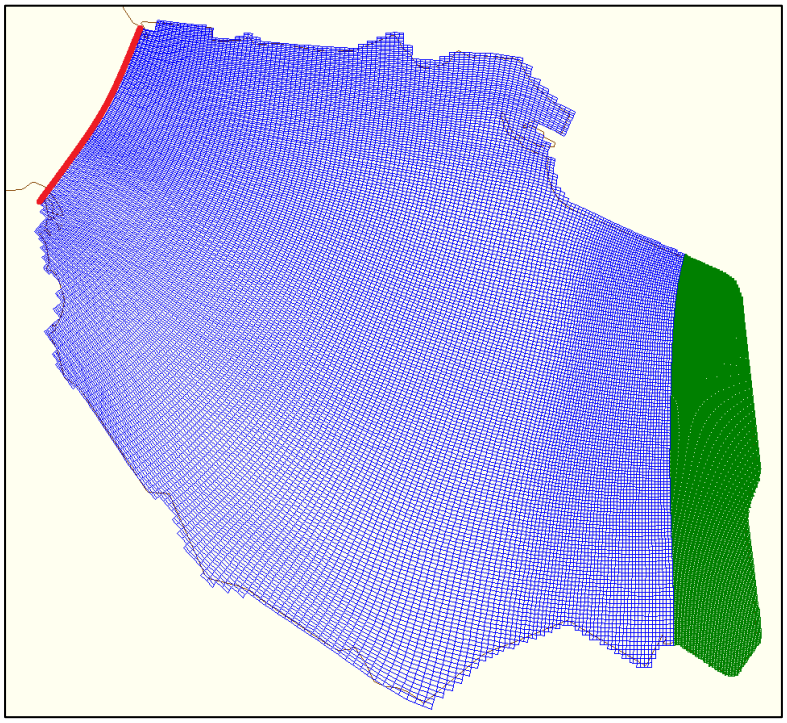

FIGURE 61: COMPUTATIONAL GRIDS OF OESTERDAM MODEL (BLUE: OESTERDAM A; GREEN: OESTERDAM B); THE OPEN BOUNDARY OF OESTERDAM A IS SHOWN AS A RED LINE.